THE EVOLUTIONARY LINKS BETWEEN THE ISOLATED NEUTRON STAR POPULATIONS

by
ALİ ARDA GENÇALİ

**Submitted to the Graduate School of Engineering and Natural Sciences
in partial fulfilment of
the requirements for the degree of Doctor of Philosophy**

**Sabancı University
July 2023**

ALİ ARDA GENÇALİ 2023 ©

All Rights Reserved

ABSTRACT

THE EVOLUTIONARY LINKS BETWEEN THE ISOLATED NEUTRON STAR POPULATIONS

ALİ ARDA GENÇALİ

PHYSICS Ph.D DISSERTATION, July 2023

Dissertation Supervisor: Prof. Ünal Ertan

Keywords: Accretion, Accretion Discs, Neutron Stars

In this thesis, we have investigated the long-term evolutions and evolutionary connections of the isolated neutron star populations namely ordinary radio pulsars, anomalous X-ray pulsars (AXPs), soft gamma repeaters (SGRs), dim isolated neutron stars (XDINs), high magnetic field radio pulsars (HBRPs), central compact objects (CCOs), rotating radio transients (RRATs), and long-period pulsars (LPPs), with the fallback disc model. Among these families, the highest birth rate is estimated for RRATs followed by XDINs and radio pulsars. The total birth rate of these populations exceeds the estimated galactic core-collapse supernova rate, commonly known as the birth-rate problem. The presence of evolutionary connections between these populations, particularly between RRATs, XDINs, and radio pulsars, as proposed earlier could potentially solve this problem. Our investigation in this thesis together with earlier work show that neutron stars with fallback discs can evolve into the properties of all different neutron star populations as a natural outcome of differences in their initial conditions: the initial period, the disc mass, and the dipole moment of the neutron star. These results are obtained with a continuous dipole-moment distribution ranging from a few $10^{27} - 10^{31}$ G cm^3. Our results indicate that each of these systems are evolutionarily connected to at least one of the other populations. RRATs have evolutionary connections with almost all the other isolated neutron star populations, except for persistent AXP/SGRs and LPPs. Furthermore, our results imply that AXP/SGRs are the progenitors of LPPs. In the early phases of the evolution, RRATs could be observed as ordinary radio pulsars, and/or HBRPs, while during the late phases, they could exhibit XDIN behaviour. These evolutionary links predicted in our model provide the most comprehensive quantitative support to the early ideas proposed to account for the birth-rate problem of these neutron star families.

ÖZET

İZOLE NÖTRON YILDIZ POPÜLASYONLARI ARASINDAKİ EVRİMSEL BAĞLAR

ALİ ARDA GENÇALİ

FİZİK DOKTORA TEZİ, TEMMUZ 2023

Tez Danışmanı: Prof. Dr. Ünal Ertan

Anahtar Kelimeler: Kütle Aktarımı, Kütle Aktarım Diskleri, Nötron Yıldızları

Bu tezde, izole nötron yıldızı popülasyonlarının; normal radyo pulsarları, anormal X-ışını pulsarları (AXPs), yumuşak gama ışını tekrarlayıcıları (SGRs), X-ray sönük izole nötron yıldızları (XDINs), yüksek manyetik alanlı radyo pulsarları (HBRPs), merkezi yoğun cisimler (CCOs), geçici dönen radyo kaynakları (RRATs) ve uzun periyotlu pulsarlar (LPPs) arasındaki uzun süreli evrimlerini ve evrimsel bağlarını kalıntı disk modeliyle inceledik. Bu aileler arasında en yüksek doğum oranı RRAT'lara ait olup, onları XDIN'ler ve radyo pulsarları takip etmektedir. Bu popülasyonların toplam doğum oranı, galaksideki çekirdek çökmesiyle oluşan süpernova oranını tahminini aşmaktadır. Bu genellikle doğum oranı problemi olarak literatürde geçer. Daha önceden de önerildiği gibi özellikle RRAT'lar, XDIN'ler ve radyo pulsarları arasındaki evrimsel bağların varlığı, bu problemi potansiyel olarak çözebilir. Bu tezdeki araştırmalarımız ve daha önceki çalışmalarımız, kalıntı disklere sahip nötron yıldızlarının başlangıç koşullarındaki farklılıkların (başlangıç periyodu, disk kütlesi ve nötron yıldızının dipol momenti) doğal bir sonucu olarak, kaynakların farklı nötron yıldızı popülasyonlarının özelliklerine evrilebileceğini göstermektedir. Bu sonuçlar, birkaç $10^{27} - 10^{31}$ G cm^3 aralığında sürekli bir dipol moment dağılımıyla elde edilmiştir. Sonuçlarımız, bu sistemlerin her birinin en az bir diğer popülasyonla evrimsel bağı olduğunu göstermektedir. RRAT'lar, sürekli AXP/SGR'ler ve LPP'ler dışında tüm diğer izole nötron yıldızı popülasyonlarıyla evrimsel bağlara sahiptir. Ayrıca, sonuçlarımız AXP/SGR'lerin LPP'lerin atası olduğunu göstermektedir. Evrimin erken evrelerinde, RRAT'lar sıradan radyo pulsarları ve/veya HBRP'ler olarak gözlemlenebilirken, geç evrelerde XDIN davranışı sergileyebilirler. Modelimizde tahmin edilen bu evrim ilişkileri, nötron yıldızı sistemlerinin doğum oranı problemine çözüm olarak önerilmiş önceki fikirlere kapsamlı bir nicel destek sağlamaktadır.

ACKNOWLEDGEMENTS

I am deeply grateful for the opportunity to complete this doctoral journey, and I owe a debt of gratitude to numerous individuals who have played pivotal roles in its realization.

Foremost, I extend my heartfelt appreciation to my advisor, Prof. Ünal Ertan, for his boundless patience, unwavering support and encouragement throughout this challenging yet rewarding PhD pursuit. His guidance and mentorship have not only enhanced my expertise in the field but also shaped my understanding of fundamental physics and critical thinking. His dedication to my growth as a researcher has been truly invaluable.

I would also like to express my sincere thanks to the distinguished members of my thesis jury, Prof. Kazım Yavuz Ekşi, Prof. Emrah Kalemci, Prof. Ersin Göğüş, and Assoc. Prof. Ebru Devlen, for their time, expertise, and valuable feedback during the evaluation of my work. Prof. Ekşi's guidance during my undergraduate studies left an indelible mark on my academic path, and Prof. Mehmet Ali Alpar's valuable comments on my thesis enriched its quality significantly.

My heartfelt gratitude extends to the Scientific and Technological Research Council of Turkey (TUBİTAK) for their support through grants 117F144 and 120F329, which have been instrumental in the successful execution of this research. I am also grateful to Sabancı University for providing me with a conducive study environment and scholarship, which contributed significantly to my academic journey.

To my beloved girlfriend, Serena Abudara, words cannot adequately convey the depth of my appreciation for your unwavering support, understanding, and love throughout this challenging chapter of my life. Your presence has been a constant source of joy and motivation, and I cherish every moment we've shared. Your encouragement during the difficult times has been a guiding light, and I am profoundly grateful for your love.

To my family, I extend my profound thanks for your unconditional support and love throughout all the stages of my educational and personal growth. Your encouragement and belief in my abilities have been a driving force behind my achievements, and I am forever grateful for your unwavering presence in my life.

Lastly, I would like to express my gratitude to Farzad Rokhsar Talabazar, Ali

Mürteza Altıngün, Ömer Faruk Çoban, Ndiogou Niang, Ozan Toyran, Bilal Cantürk, Ahmet Mert Bozkurt, Onur Akbal, Onur Benli, Ebru Çetin, Erçil Toyran, Beyza Özoğul, and all my other friends and colleagues who have been a source of inspiration and camaraderie during this journey. Your presence and encouragement have made this pursuit all the more rewarding.

This thesis is not just an academic achievement; it represents the collective efforts and support of all those who have touched my life in profound ways. Thank you for being an integral part of my journey and for making this achievement possible.

To my beloved family,
with endless love and gratitude

TABLE OF CONTENTS

LIST OF TABLES

LIST OF FIGURES

LIST OF ABBREVIATONS

ASD Accretion with Spin-down 13

AXPs Anomalous X-ray Pulsars 3

CCOs Central Compact Objects 3

CCSN Core Collapse Supernova 55

HBRPs High Magnetic Field Radio Pulsars 3

HMXBs High-mass X-ray Binaries 2

LMXBs Low-mass X-ray Binaries 2

LPPs Long-period Radio Pulsars 3

NS Neutron Star 1

RRATs Rotation Radio Transients 3

SGRs Soft Gamma Repeaters 3

SNR Supernova Remnant 1

SP Strong Propeller 14

SU Spin Up 37

tMSPs Transitional Millisecond Pulsars 38

WP Weak Propeller 13

XDINs Dim Isolated Neutron Stars 3

1. INTRODUCTION

Main-sequence stars sustain hydrostatic equilibrium through thermo-nuclear reactions, which counteract the gravitational forces. When the thermo-nuclear reactions terminate, the core of a massive main-sequence star undergoes a rapid collapse, leading to an immensely powerful explosion known as a "supernova". This explosive event expels the outer layers of the star, which forms an expanding, luminous shell called supernova remnant (SNR). Depending on the mass of the main-sequence star, a supernova can yield either a neutron star (NS) or a black hole. If the gravitational force is balanced by the neutron degeneracy pressure and repulsive strong interaction during the collapse, the core of the collapsing star becomes a NS. The mass of a typical NS is about one solar mass ($M_\odot = 1.99 \times 10^{33}$ g) compressed into a radius of ~ 10 km, which means an extraordinarily high average density of $\sim 10^{15}$ g cm^3. These systems are the most compact objects we can directly observe in the universe.

As a result of the conservation of angular momentum and magnetic flux during the core collapse, NSs are born with exceptionally high rotational rates with spin periods of milliseconds and intense magnetic dipole fields with strengths $B \sim 10^{12-13}$ G at their surfaces. With increasing radial distance, r, from the star, speed of the closed field lines increases, and approaches to the speed of light, c. This radius is called light cylinder radius, $r_{\rm LC} = c/\Omega_*$, where Ω_* is the angular spin frequency of the star. Since the speed of the field lines cannot exceed c, the field lines outside $r_{\rm LC}$ are open. These open field lines originate from the magnetic poles of the NS. Charged particles (electrons and positrons) accelerated to relativistic speeds along these open field lines generating electromagnetic radiation mostly in the radio band. This emission forms a geometry similar to a cone opening outward from the magnetic poles.

For most of the NSs, the axis of the magnetic dipole field is not aligned with the rotational axis. If the Earth is in the region of the sky traced by the rotating emission cone, we detect a radio pulse for each complete rotation of the star (Pacini, 1967). These sources are commonly called radio pulsars or simply pulsars. The first pulsar was detected by a PhD student Jocelyn Bell in 1967 (Hewish, Bell, Pilkington, Scott, & Collins, 1968). After some controversy, it has been understood that extremely

stable pulses with very short periods can only be produced by rotating NSs (Antony Hewish, 1974 Nobel Prize). After the first discovery, more than 2500 radio pulsars have been discovered. Observations showed that pulsars are not only radio sources; their emission spectrum span a broad range of wavelengths, from radio to gamma rays. NSs, with their extraordinary properties, are excellent laboratories for studying physics under extreme conditions (Ghosh, 2007).

These strong magnets rotating in vacuum lose angular momentum through magnetic dipole radiation and gradually slow down in time. The radio pulsation mechanism is estimated to cease when the rotational power of the source decreases below a critical value (Bhattacharya & van den Heuvel, 1991; Bhattacharya, Wijers, Hartman, & Verbunt, 1992; K. Chen & Ruderman, 1993). The lifetime of a radio pulsar is estimated to be $\sim 10^{7-8}$ yr (Faucher-Giguère & Kaspi, 2006; Keane & Kramer, 2008; Popov, Turolla, & Possenti, 2006).

There are many NSs in binary systems as well. These systems are classified depending on the mass of the companion star, $M_{\rm c}$: (i) high-mass X-ray binaries (HMXBs) if $M_{\rm c} >$ a few $M_{\odot}$, (ii) low-mass X-ray binaries (LMXBs) if $M_{\rm c} \lesssim M_{\odot}$. In both types of systems, depending on their evolutionary phase and binary separation, there could be mass transfer from the companion star to the compact object. In the case of HMXBs, mass transfer on to the NS occurs predominantly through winds from the massive companion. In LMXBs, the mass transfer starts when the Roche lobe of the companion star is filled. In this case, material from the companion star flows through the Lagrangian point into the Roche lobe of the NS. Due to the conservation of its angular momentum, the matter, cannot fall directly on to the NS. Instead, it forms an accretion disc around the NS (Frank, King, & Raine, 2002).

The matter in the disc rotates with Keplerian speeds, $v_{\rm K}$. By means of viscous dissipation, angular momentum is transferred outward, while the matter flows inward, towards the NS. The outer disc is cut by the strong tidal forces of the companion star. The inner disc is truncated at a radius, $r_{\rm in}$, depending on the mass inflow rate of the disc and the magnetic dipole moment, μ, of the NS. The radius at which the rotational speed of the closed field lines equals $v_{\rm K}$ is called co-rotation radius, $r_{\rm co}$. If $r_{\rm in} \leq r_{\rm co}$, the matter couples to the closed field lines at $r_{\rm in}$, and can flow along the field lines on to the NS. Due to extreme compactness, mass accretion on to a NS is approximately 30 times more efficient than hydrogen fusion reactions in conversion of rest-mass energy into radiation. The mass flow heats up the polar regions of the star to X-ray temperatures. The rotation of the star causes a periodic modulation of the observed X-ray flux, which is observed as a pulsed X-ray emission. These sources are called X-ray pulsars.

In the last a few decades, rapid developments in the observational techniques led to the discovery of new isolated NS populations. These systems are anomalous X-ray pulsars (AXPs), soft gamma-ray repeaters (SGRs), dim isolated neutron stars (XDINs), central compact objects (CCOs), high magnetic field radio pulsars (HBRPs), rotating radio transients (RRATs), and long-period radio pulsars (LPPs). These single NS families have properties rather different from those of ordinary radio pulsars (see Abdo et al., 2013; Pavlov, Kargaltsev, Sanwal, & Garmire, 2001, and references therein). The characteristic properties of these NS populations are summarised in Chapter 2.

Two basic models have been proposed to explain the emergence of these isolated NS systems with rather different characteristics: the magnetar model (Thompson & Duncan, 1995) and the fallback disc model (Alpar, 2001; Chatterjee, Hernquist, & Narayan, 2000; Ertan, Ekşi, Erkut, & Alpar, 2009a). In the magnetar model, sources spin down in vacuum through magnetic dipole torques. With this assumption, the dipole field strength, B_0, on the poles of the star is inferred to be greater than 10^{14} G for most AXP/SGRs and HBRPs, and $\sim 10^{13} - 10^{14}$ G for XDINs. For AXP/SGRs observed X-ray luminosities, $L_{\rm X}$, are greater than their rotational powers with few exceptions. In this model, the X-rays are assumed to be generated through magnetic field decay (Enoto, Kisaka, & Shibata, 2019; Harding, 2013; Kaspi & Beloborodov, 2017; Kaspi & Kramer, 2016).

After the supernova explosion, some of the ejected matter that is failed to reach escape velocity or that is decelerated by the reverse shocks eventually falls back (Chevalier, 1989; Colgate, 1971; Woosley, Heger, & Weaver, 2002; Zel'dovich, Ivanova, & Nadezhin, 1972). If this matter has sufficient angular momentum, a fallback disc could form around the newly born NS (Michel, 1988; Michel & Dessler, 1981; Mineshige, Nomura, Hirose, Nomoto, & Suzuki, 1997; Perna, Duffell, Cantiello, & MacFadyen, 2014). It was estimated by Perna et al. (2014) through numerical simulations that fallback discs around NSs are expected to form under special conditions of negligible magnetic torques and weak, highly anisotropic explosion.

The fallback discs have been invoked to explain various phenomena observed in pulsars such as those with braking indices $n < 3$ (Benli & Ertan, 2017; Çalışkan, Ertan, Alpar, Trümper, & Kylafis, 2013; W. C. Chen & Li, 2006; Fu & Li, 2013; Menou, Perna, & Hernquist, 2001a; Özsükan et al., 2014; Yan, Perna, & Soria, 2012), drifting sub-pulses, pulsar nulling (Cordes & Shannon, 2008), the lack of pulsations, pulsar jets (Blackman & Perna, 2004), the discrepancy between characteristic and supernova ages (Marsden, Lingenfelter, & Rothschild, 2001), enhanced X-ray luminosities of AXPs, rotational evolution of AXP/SGRs (Ekşi & Alpar, 2003; Ertan & Alpar,

2003; Ertan & Çalışkan, 2006; Ertan, Ekşi, Erkut, & Alpar, 2009b; Ertan & Erkut, 2008; Marsden, Lingenfelter, Rothschild, & Higdon, 2001), the distribution of the radio pulsars in the $P-\dot{P}$ diagram (Alpar, Ankay, & Yazgan, 2001), formation of planets around pulsars (Lin, Woosley, & Bodenheimer, 1991), and periodic timing variations of pulsars (Qiao, Xue, Xu, Wang, & Xiao, 2003).

It was proposed that the period clustering and the $L_{\rm X}$ levels of AXPs could be explained by the fallback disc model with conventional magnetic dipole fields (Chatterjee et al., 2000). Alpar (2001) suggested that the fallback disc properties, if included in the initial conditions (initial period, P_0, and B_0), could account for the properties of NS populations including AXPs.

Emission characteristics of fallback discs have been extensively investigated in a series of earlier work for different sources (Ertan & Çalışkan, 2006; Ertan, Çalışkan, & Alpar, 2017; Ertan, Erkut, Ekşi, & Alpar, 2007; Ertan, Göğüş, & Alpar, 2006; Özsükan et al., 2014; Perna, Hernquist, & Narayan, 2000; Posselt et al., 2018). Emission in the infrared band and at longer wavelengths is expected from the fallback discs around young NSs (Perna et al., 2000), and such emissions have been investigated (see Mignani et al., 2007; Tam, Kaspi, van Kerkwijk, & Durant, 2004, and references therein). It was shown that the observed excess emission of the pulsar PSR 0656+14 in the R and I bands can be attributed to the emission from a disc (Perna et al., 2000). Ertan and Çalışkan (2006) showed that the near-IR and optical emission observed from most of AXP/SGRs can be reproduced by active fallback discs. The first detection of a fallback disc around an AXP, 4U 0142+61, was reported by Z. Wang, Chakrabarty, and Kaplan (2006), showing that the observed mid-infrared emission can be modelled with an irradiated disc. Z. Wang et al. (2006) attributed the earlier detections in the near-IR and optical bands to the magnetospheric emission, while they proposed that the mid-IR data could be produced by an X-ray irradiated inactive disc. It was shown that the observed broadband emission of the source (from optical to mid-infrared; Hulleman, van Kerkwijk, & Kulkarni, 2000, 2004; Morii et al., 2005; Z. Wang et al., 2006) can be produced by an X-ray irradiated, active fallback disc (Ertan et al., 2007). Similarly, mid-infrared emission was detected from 1E 2259+58, indicating a similar emission mechanism operating in 4U 0142+61 (Kaplan, Chakrabarty, Wang, & Wachter, 2009). Detailed calculations show that mass transfer on to the NS can account for the observed soft and hard X-ray spectra of AXP/SGRs consistently with the energy-dependent pulse profiles (Guo et al., 2015; Kylafis, Trümper, & Ertan, 2014; Trümper, Dennerl, Kylafis, Ertan, & Zezas, 2013; Trümper, Zezas, Ertan, & Kylafis, 2010; Zezas, Trümper, & Kylafis, 2015). There is no companion star that feeds the fallback disc through mass transfer. The properties of sources (such as B_0) estimated in this model could

be significantly different from those estimated in the magnetar model. In the fallback disc model, the B_0 value for a particular source could be one to two orders of magnitude smaller than that predicted in the magnetar model.

The long-term evolutions of individual sources from all different isolated NS populations were investigated with the fallback disc model. These studies indicated that the rotational and X-ray emission properties of AXP/SGRs (Benli & Ertan, 2016), XDINs (Ertan, Çalışkan, Benli, & Alpar, 2014), HBRPs (Benli & Ertan, 2017, 2018b), CCOs (Benli & Ertan, 2018a), RRATs (Gençali & Ertan, 2018, 2021), and LPPs (Gençali, Ertan, & Alpar, 2022, 2023) could be attained by NSs evolving with fallback discs and conventional magnetic dipole fields. We discuss the details of the fallback disc model in Chapter 3.

The birth rates of individual NS families were estimated from the observed numbers and distributions in our galaxy. If it is assumed that each population evolves independently, the estimated total birth rate significantly exceeds the galactic supernova rate estimated to be $\sim 1.9 \pm 1.1$ century^{-1} (Diehl et al., 2006; Faucher-Giguère & Kaspi, 2006; Keane & Kramer, 2008; Popov et al., 2006; Rozwadowska, Vissani, & Cappellaro, 2021). From the statistical calculations, RRATs seem to have the highest birth rate among the isolated NSs. It is also estimated that XDINs and radio pulsars have birth rates similar to and smaller than that of RRATs (Keane & Kramer, 2008; Popov et al., 2006), and much greater than those of other populations. Since the total birth rate cannot exceed the galactic supernova rate, there are likely evolutionary links between some of these NS families (Faucher-Giguère & Kaspi, 2006; Keane & Kramer, 2008; Manchester et al., 2005; Popov et al., 2006). Possibility of evolutionary connections among these populations, particularly between radio pulsars, RRATs, and XDINs, has been proposed earlier (Beniamini, Hotokezaka, van der Horst, & Kouveliotou, 2019; Faucher-Giguère & Kaspi, 2006; Gullón, Miralles, Viganò, & Pons, 2014; Jawor & Tauris, 2022; Johnston & Karastergiou, 2017; Kaspi & Kramer, 2016; Keane & Kramer, 2008; Popov et al., 2006). Nevertheless, there is no systematic and comprehensive theoretical study to predict the details of these evolutionary links.

The results of our earlier work on the evolution of individual sources with fallback discs also imply evolutionary links between some of these populations (Benli & Ertan, 2016; Gençali & Ertan, 2018, 2021; Gençali et al., 2022, 2023), which motivates us for this comprehensive work. For instance, evolution of AXP/SGRs with relatively strong dipole fields to long periods was predicted before the discovery of LPPs (Benli & Ertan, 2016). Another work with the same model gave hints about the evolution of some RRATs approaching to the XDIN properties (Gençali & Ertan,

2018, 2021). In this thesis, we investigate all possible long-term evolutionary connections between the NS populations tracing the initial conditions in the frame of the fallback disc model.

In this thesis, we have investigated the long-term evolution and evolutionary connections of isolated NS populations. For the torque calculations and the critical conditions for the transitions between the rotational phases, we have used two models: (i) the simplified model applied earlier to individual isolated NSs (Model I), (ii) a more realistic analytical model (Model II) recently developed by (Ertan, 2017, 2018, 2021). The details of both models, along with their applications to different NS populations, have been described in the earlier work (Benli & Ertan, 2016; Çalışkan et al., 2013; Ertan et al., 2014, 2009a). These models and the differences between them are described in Chapter 3 summarising also their earlier applications to different NS populations.

In Chapter 2, we summarised the characteristic properties of the isolated NS populations. The details of the fallback disc models (Model I and II) are described in Chapter 3 and the results of the numerical simulations for the long-term evolution of different populations, and the estimated evolutionary connections between them are discussed in Chapter 4. We summarise our conclusions in Chapter 5.

2. ISOLATED NEUTRON STAR POPULATIONS

Different varieties of isolated (single) NSs have ages estimated to be less than a few million years. In addition to their striking distinguishing behaviours some populations also show similar characteristics. In the literature, the dipole field strengths of these sources are estimated with the assumption that they are rotating in vacuum, and slowing down purely by dipole torques. In this chapter, we will use "$B_{\rm df}$" to denote the field strength at the surface of the star deduced by this assumption. As discussed in Chapter 1, their actual field strength could be much smaller than $B_{\rm df}$ in the presence of fallback disc torques. Below, we summarise the observed characteristic properties of these single NS families.

2.1 AXP/SGRs

AXP/SGRs are the most intriguing class of NSs with unique observational properties. These systems are known for their sporadic soft gamma bursts with luminosities exceeding 10^{44} erg s^{-1} (Cline et al., 1980; Hurley et al., 1999; Palmer et al., 2005). These objects exhibit periodic X-ray pulsations, typically with $P \sim 2-12$ s and $\dot{P} \sim 10^{-15}$ to 10^{-10} s s^{-1} (Olausen & Kaspi, 2014)[1]. Observed $L_{\rm X}$ values of AXP/SGRs vary widely, spanning a range of $10^{30}-10^{36}$ erg s^{-1}. For most AXP/SGRs, the estimated $L_{\rm X}$ values are much beyond their rotational powers. The range of $B_{\rm df}$ for AXP/SGRs is estimated to be $\sim 10^{13}-10^{15}$ G. For most sources, these $B_{\rm df}$ values exceed the quantum critical value, beyond which ordinary radio pulsations are estimated to be quenched (Baring & Harding, 1998, 2001). Some of the AXP/SGRs show non-ordinary, transient radio pulsation epochs (Camilo, Ransom, Halpern, & Reynolds, 2007; Camilo et al., 2006; Camilo, Ransom, Peñalver, et al., 2007; Kaspi & Beloborodov, 2017). The mechanism generating these radio pulsations seem to be different from those operating in ordinary radio pulsars, and

are likely to be similar to that of LPPs (Hurley-Walker et al., 2022).

The super-Eddington soft gamma bursts of these sources require strong magnetar fields. Presence of strong, small-scale multipole fields close to the surface of the NS is compatible with the fallback disc model, since the rotational evolution of the star is governed by the interaction of the inner disc with the large-scale dipole field. In this model, individual source properties of AXP/SGRs can be reproduced only with conventional fields of young NSs with $B_0 \sim 10^{12} - 10^{13}$ G.

2.2 XDINs

XDINs constitute NSs that emit predominantly thermal soft X-rays at low $L_{\rm X}$ levels, typically in the range of $10^{30} - 10^{32}$ erg s^{-1} (Burwitz et al., 2003; Haberl et al., 2004; Kaplan et al., 2003; Rea et al., 2007; Schwope, Schwarz, & Greiner, 1999). The blackbody temperatures are found to be $\sim 50 - 100$ eV (Haberl, 2007; Turolla, 2009). The observed P range ($3 - 17$ s) is similar to that of AXP/SGRs while their $\dot{P}$ values ($10^{-15} - 10^{-12}$ s s^{-1}) are mostly smaller than those of AXP/SGRs (Haberl, 2004; Haberl et al., 2004; Hambaryan et al., 2017; Kaplan & van Kerkwijk, 2005, 2009a, 2009b, 2011; Tiengo & Mereghetti, 2007; van Kerkwijk & Kaplan, 2008). No radio pulsations have been observed from XDINs. Their characteristic ages are $(1 - 4) \times 10^6$ yr, a few times longer than the estimated kinematic ages (Mignani et al., 2013; Motch, Pires, Haberl, Schwope, & Zavlin, 2009; Tetzlaff, Neuhäuser, Hohle, & Maciejewski, 2010). So far, 7 XDIN sources have been identified, all of which have been observed within a distance of 500 pc. This indicates that these sources are highly common in the galaxy. For XDINs, the dipole-torque formula gives $B_{\rm df} = 10^{13} - 10^{14}$ G placing them above the pulsar death-line. The non-detection of radio pulsations from XDINs is attributed to their narrow emission cones (Haberl, 2005). In the fallback disc model, the estimated B_0 values for XDINs ($\lesssim 10^{12}$ G) are not sufficient to yield pulsed radio emission (Ertan et al., 2014).

[1] http://www.physics.mcgill.ca/~pulsar/magnetar/main.html

2.3 HBRPs

These sources exhibit ordinary radio pulsar behaviour with P ($\sim 0.1-10$ s) and $\dot{P}$ ($\sim 10^{-14}-10^{-12}$ s s^{-1}) values that give $B_{\rm df} \sim 10^{13}-10^{15}$ G, similar to those of AXP/SGRs (Kaspi & Beloborodov, 2017). This led to the identification of these systems as "high-magnetic-field radio pulsars" (Gavriil et al., 2008). Some HBRPs have measured braking indices, $n \sim 1-3$ (Antonopoulou et al., 2015; Archibald, Kaspi, Tendulkar, & Scholz, 2016; Camilo et al., 2000; Espinoza, Lyne, Kramer, Manchester, & Kaspi, 2011; Kaspi, Manchester, Siegman, Johnston, & Lyne, 1994; Weltevrede, Johnston, & Espinoza, 2011). The estimated $L_{\rm X}$ values of HBRPs are $\lesssim 10^{33}$ erg s^{-1}, which together with rotational properties give $B_0 \sim 10^{12}-10^{13}$ G in the fallback disc model (Benli & Ertan, 2017, 2018b). They often have strong and highly variable X-ray pulse profiles (e.g., Hu, Ng, Takata, Shannon, & Johnston, 2017; Parent et al., 2011) They exhibit transient behaviours, including outbursts, glitches and flares, indicating a dynamic and active nature. (Antonopoulou et al., 2015; Archibald et al., 2017, 2016; S. Dai et al., 2018; Göğüş et al., 2016; Kaspi & McLaughlin, 2005; Kuiper & Hermsen, 2009; Livingstone, Ng, Kaspi, Gavriil, & Gotthelf, 2011; Ng et al., 2012; Parent et al., 2011).

2.4 CCOs

CCOs are the X-ray pulsars located at the centres of SNRs, indicating that they are relatively young compared to other single NS populations. They exhibit predominantly thermal X-ray emission with $L_{\rm X} \sim 10^{33}$ erg s^{-1}. The observed X-ray spectra of CCOs are usually successfully modelled by two blackbodies with temperatures $\sim 0.2-0.5$ keV corresponding to emitting areas much smaller than their total surface areas (De Luca, 2017; Halpern & Gotthelf, 2010). These sources have not been detected in the optical, infrared, and radio bands so far. They have similar rotational behaviours with $P \sim 0.1-0.4$ s and $\dot{P} \sim 10^{-17}$ s s^{-1} (Gotthelf, Halpern, & Alford, 2013). Considering their low $\dot{P}$ values, the current periods of CCOs are likely to be close to their birth periods. Unlike AXP/SGRs, the rotational powers of these systems are about an order of magnitude smaller than the observed $L_{\rm X}$ levels. CCOs have relatively low $B_{\rm df} \sim 10^{10-11}$ G, placing a gap in the $B_{\rm df}$ distribution of

CCOs and other populations (AXP/SGRs, XDINs, HBRPs) in the magnetar model (Gotthelf et al., 2013; Halpern & Gotthelf, 2010).

2.5 RRATs

RRATs comprise a recently discovered NSs identified by sporadic and short ($0.5-$ 100 ms) radio bursts. They have rotational periods in the $0.1-10$ s range with very high flux densities in the $10^{-3}-10$ Jy range. Time separations between the short bursts vary from minutes to hours. The physical mechanism responsible for the radio bursts of RRATs has not been understood yet (McLaughlin et al., 2006). The sporadic nature of the radio bursts makes it difficult to measure the $\dot{P}$ values. Among more than 100 currently known RRATs, the $\dot{P}$ values were estimated only for ~ 40 sources, and found to be in the range of $10^{-16}-10^{-12}$ s s^{-1} (ATNF Pulsar Catalogue, version 1.70, Manchester et al., 2005)[2]. From the obtained range of P and $\dot{P}$, the characteristic ages of these sources can be calculated to be in the range of 10^5 to 10^8 years.

It is challenging to determine the correct positions, and therefore, X-ray emission properties of RRATs from their radio bursts (Kaplan, Esposito, et al., 2009). Out of more than 100 RRATs (Taylor et al., 2016), $L_{\rm X}$ ($\sim 4\times10^{33}$ erg s^{-1}) was estimated only for one source (PSR J1819-1458; McLaughlin et al., 2006; Rea et al., 2009). There are $L_{\rm X}$ upper limits for several RRATs (Kaplan, Esposito, et al., 2009; Keane et al., 2013; Rea & McLaughlin, 2008). They often exhibit a thermal X-ray spectrum, suggesting the presence of a heated surface. The physical mechanism yielding RRAT behaviour is relatively new and active area of research. Further detections in X-rays are needed to understand their physical and long-term evolutionary properties.

[2] https://www.atnf.csiro.au/research/pulsar/psrcat/

2.6 LPPs

LPPs are the radio pulsars characterised by their relatively long rotational periods and radio burst epochs during which they show pulsed radio emission. Recently, two LPPs have been identified, namely PSR J0901–4046 (hereafter J0901) and GLEAM-X J162759.5–523504.3 (hereafter as GLEAM-X). J0901 has $P \sim 76$ s and $\dot{P} \simeq 2.25 \times 10^{-13}$ s s^{-1} (Caleb et al., 2022). GLEAM-X has a longer P (~ 1091 s), and its $\dot{P}$ has an upper limit of 1.2×10^{-9} s s^{-1} (Hurley-Walker et al., 2022). Both LPPs exhibit varying pulse shapes during their transient radio-pulsar phases. Similarly, five AXP/SGR sources have been observed to exhibit radio pulsations with considerable variable pulse profiles (Esposito et al., 2020; Kaspi & Beloborodov, 2017) during transient epochs following X-ray outbursts (Kaspi & Beloborodov, 2017). Based on the similarities in their radio behaviour, it has been suggested that the radio pulses of GLEAM-X might be generated through a mechanism similar to that of radio emitting AXP/SGRs (Hurley-Walker et al., 2022). For J0901 and GLEAM-X, the $L_{\rm X}$ upper limits are $\sim 10^{30}$ erg s^{-1} and $\sim 10^{32}$ erg s^{-1} respectively. With these low $L_{\rm X}$ values, there could be many other LPPs with X-ray fluxes that remain below the detection limits. In other words, they are likely to be detected only during their radio burst epochs.

Most recently, one more LPP has been identified as a long-period radio transient, namely GPM J1839–10 (Hurley-Walker et al., 2023). GPM J1839–10 has a measured $P \simeq 1318.1957$ s ($\simeq 22$ min) with an upper limit on $\dot{P} < 3.6 \times 10^{-13}$ s s^{-1} (Hurley-Walker et al., 2023). The observed pulses exhibit significant variation in brightness, spanning two orders of magnitude. These pulsations have durations ranging from 30 to 300 seconds with maximum flux densities in the range of $0.1 - 10$ Jy and display quasi-periodic substructure. An investigation of the archival data revealed that the radio pulsations have been repeating since at least 1988 (Hurley-Walker et al., 2023). The estimated radio luminosity of the source is $\sim 10^{28}$ erg s^{-1}, which is larger than the rotational power of the source ($\lesssim 6.2 \times 10^{24}$ erg s^{-1}). The persistent $L_{\rm X}$ upper limit was estimated to be $\lesssim 1.5 \times 10^{32}$ erg s^{-1} (Hurley-Walker et al., 2023).

3. LONG-TERM EVOLUTION OF NEUTRON STARS WITH FALLBACK DISCS

In this chapter, we investigate the long-term evolution of RRATs and recently discovered LPPs with the model applied earlier to all the other isolated NS populations (Model I). For a detailed study of the evolutionary links between the populations, we will also use the recently developed more realistic model (Model II). In Section 3.3.1, we describe the Model II with a comparison to Model I, and its application to the torque reversals of LMXBs, providing a test for the model to be employed in the investigation of the evolutionary links between the single NS families (Chapter 4).

Sections 3.1.1 and 3.1.2 were published in Monthly Notices of the Royal Astronomical Society, January 2021, Volume 500, Issue 3, pp. 3281–3289. A. A. Gençali, Ü. Ertan

Section 3.1.3 was published in Monthly Notices of the Royal Astronomical Society Letters, June 2022, Volume 513, Issue 1, pp. L68–L71. A. A. Gençali, Ü. Ertan, and M. A. Alpar

Section 3.1.4 was published in Monthly Notices of the Royal Astronomical Society Letters, March 2023, Volume 520, Issue 1, pp. L11–L15. A. A. Gençali, Ü. Ertan, and M. A. Alpar

Some parts are modified to maintain continuity of definitions and discussions.

3.1.1 The Model I

We use the long-term evolution model for a neutron star with a fallback disc which is applied earlier to other young neutron star populations (Benli & Ertan, 2016, 2017, 2018a, 2018b; Çalışkan et al., 2013; Ertan et al., 2014, 2009b; Gençali & Ertan, 2018). Since the details of the model are given in these work, we briefly describe the model calculations below.

We solve the disc diffusion equation using the α-prescription for the kinematic viscosity, $\nu = \alpha c_{\rm s} h$, where α is the kinematic viscosity parameter, $c_{\rm s}$ is the sound speed, and h is the pressure scale-height of the disc (Shakura & Sunyaev, 1973). We start with a surface density profile for a steady, geometrically thin disc. In the accretion with spin-down (ASD or weak propeller, WP) phase, the matter coupling to the field lines from the co-rotation radius, $r_{\rm co}$, at which the speed of the field lines equals the Kepler speed, flows along the field lines on to the star. In this phase, we equate the accretion rate, $\dot{M}_*$, to the mass-inflow rate of the disc, $\dot{M}_{\rm in}$, which gives an X-ray luminosity $L_{\rm acc} = GM\dot{M}_*/R_*$ where G is the gravitational constant, M and R_* are the mass and the radius of the neutron star. We calculated the total X-ray luminosity, $L_{\rm X}$, including the contribution of the intrinsic cooling luminosity, $L_{\rm cool}$, of the star. We use the theoretical $L_{\rm cool}$ curve for neutron stars with conventional magnetic dipole fields (Page, 2009). In the calculation of $L_{\rm cool}$, we also include the internal heating by external torques (Alpar, 2007) which does not affect significantly the $L_{\rm X}$ evolution of young neutron stars with fallback discs. When the accretion is allowed, $L_{\rm acc}$ dominates $L_{\rm cool}$ in most cases.

In addition to viscous dissipation, the disc is heated by the X-rays emitted by the star. Effective temperature of the disc can be written as $T_{\rm eff} \simeq \left[(D + F_{\rm irr})/\sigma\right]^{1/4}$ where σ is the Stefan-Boltzmann constant, and D is the rate of viscous dissipation per unit area of the disc. The irradiation flux can be written as $F_{\rm irr} = 1.2\, C L_{\rm X}/(\pi r^2)$ where r is the radial distance from the star, and C is the irradiation parameter which depends on the albedo and geometry of the disc surfaces (Fukue, 1992). Outside a radius of about 10^9 cm, $F_{\rm irr}$ dominates D. There is a critical temperature, $T_{\rm p}$, below which the disc becomes viscously inactive. Dynamical outer radius of the active disc

corresponds to the radius at which $T_{\rm eff}$ currently equals $T_{\rm p}$, that is, $r_{\rm out} = r(T_{\rm eff} = T_{\rm p})$. In the long-term evolution, $r_{\rm out}$ decreases gradually with slowly decreasing $F_{\rm irr}$. In the earlier work on different neutron star populations, the simulations with $T_{\rm p} \sim 100$ K, and C in the $(1 - 7) \times 10^{-4}$ range reproduced the individual source properties (Benli & Ertan, 2016, 2017, 2018a, 2018b; Çalışkan et al., 2013; Ertan & Çalışkan, 2006; Ertan et al., 2014; Ertan et al., 2007; Gençali & Ertan, 2018; Özcan, Gençali, & Ertan, 2020). The $T_{\rm p}$ values estimated in the model seem to be consistent with the results of the theoretical work indicating that the disc is likely to be active down to very low temperatures (Inutsuka & Sano, 2005). The C values are in the same range as that estimated for the low-mass X-ray binaries (see e.g. Dubus, Lasota, Hameury, & Charles, 1999).

In the WP regime, we calculate the spin-down torque, $\Gamma_{\rm D}$, produced by the disc-field interaction, by integrating the magnetic torques between the co-rotation radius, $r_{\rm co} = (GM/\Omega_*^2)^{1/3}$, and the conventional Alfvén radius, $r_{\rm A} \simeq \left[\mu^4/(GM\dot{M}_{\rm in}^2)\right]^{1/7}$, where μ and Ω_* are the magnetic dipole moment and angular frequency of the neutron star. This allows us to write $\Gamma_{\rm D}$ in terms of $\dot{M}_{\rm in} = \dot{M}_*$ and $r_{\rm A}$ as

$$\Gamma_{\rm D} = \frac{1}{2}\dot{M}_{\rm in}(GMr_{\rm A})^{1/2}[1-(r_{\rm A}/r_{\rm co})^3] \tag{3.1}$$

(Ertan & Erkut, 2008). In this phase, $r_{\rm co} < r_{\rm A} < r_{\rm LC}$, where $r_{\rm LC} = c/\Omega_*$ is the light cylinder radius, and c is the speed of light. The accretion on to the star from $r_{\rm co}$ produces a spin-up torque, $\Gamma_{\rm acc} = \dot{M}_*(GMr_{\rm co})^{1/2}$. The total torque can be written as $\Gamma = \Gamma_{\rm D} + \Gamma_{\rm acc} + \Gamma_{\rm dip}$, where $\Gamma_{\rm dip} = -2\mu^2\Omega_*^3/3c^3$ is the magnetic dipole torque. In this phase, contributions of $\Gamma_{\rm acc}$ and $\Gamma_{\rm dip}$ are usually negligible compared to $\Gamma_{\rm D}$ for the accretion regimes of AXP/SGRs, XDINs, CCOs, and HBRPs except few sources that are very close to rotational equilibrium with relatively high $L_{\rm X}$ (Benli & Ertan, 2016, 2017, 2018a, 2018b; Ertan et al., 2014).

In the strong-propeller (SP) phase, assuming that all the inflowing matter is thrown out of the system from the inner disc, we take $\dot{M}_* = 0$, $\Gamma_{\rm acc} = 0$, and $L_{\rm X} = L_{\rm cool}$. In the absence of a well known critical condition for the transition to the SP phase at low $\dot{M}_{\rm in}$, we assume that this transition takes place when $r_{\rm A} = r_{\rm LC}$, and the system is in the SP phase for lower $\dot{M}_{\rm in}$ that gives $r_{\rm A} > r_{\rm LC}$. Since $r_{\rm A}$ greater than $r_{\rm LC}$ has no physical meaning, we replace $r_{\rm A}$ in the $\Gamma_{\rm D}$ equation with $r_{\rm LC}$ in the SP phase. The $\dot{M}_{\rm in}$ curve enters a sharp decay phase at the end of the WP regime, and the accretion-propeller transition is likely to take place in this sharp decay phase. This means that the exact value of the critical $\dot{M}_{\rm in}$ for this transition does not affect our results significantly. A more realistic model to estimate the WP/SP transition condition was developed by Ertan (2017). In this model, the critical $\dot{M}_{\rm in}$ values for

this transition are close to those obtained from our simplified model. We prefer to use the same simplified model for RRATs as well for a systematic comparison of initial conditions of these sources with those obtained earlier for the other isolated neutron star systems (Benli & Ertan, 2016, 2017, 2018a, 2018b; Çalışkan et al., 2013; Ertan et al., 2014; Gençali & Ertan, 2018). This comparison also requires to use a similar set of main disc parameters, α, $T_{\rm p}$, and C for different populations, since these parameters are expected to be similar for the fallback discs of different neutron star populations. In this way, we are able to compare the evolutionary paths leading to very different source properties resulting only from the changes in the initial conditions, namely the initial period, P_0, the magnetic dipole strength on the pole of the neutron star, B_0, and the initial mass of the disc, $M_{\rm d}$.

Illustrative model curves showing the effects of the initial conditions on the evolutionary curves are plotted in the earlier works (Benli, Çalışkan, & Ertan, 2015; Ertan et al., 2014, 2009b). We can summarize the effects of the initial conditions (P_0, B_0, and $M_{\rm d}$) as follows: For the sources that enter the evolution in the WP phase, the long-term evolution is not sensitive to P_0. For given $M_{\rm d}$ and B_0, there is a minimum critical P_0, such that the sources with P_0 shorter than this critical value cannot enter the WP phase, and always remain in the SP phase. The sources with different P_0 evolve converging to the same period throughout the long-term WP phase (see fig. 3 in Ertan et al., 2009b). During the WP phase, $\dot{P}$ is not sensitive to $\dot{M}_{\rm in}$ evolution which depends on $M_{\rm d}$ (see below). Sources with greater $M_{\rm d}$ evolve with greater luminosities in the WP phase, but the rotational evolution, which is not sensitive to $M_{\rm d}$, is determined mainly by B_0. Large differences in $M_{\rm d}$ values produce only a small scatter in the achieved current properties of the sources after the WP/SP transition. Unlike $M_{\rm d}$, small changes in B_0 produce rather different evolutionary paths in the WP phase leading to a large scatter in the rotational properties after the WP/SP transition. Figs. 1 and 2 in Ertan et al. (2014) compare the effects of B_0 and $M_{\rm d}$ on the long-term evolutions. In this thesis, Figs. 3.1 and 3.2 also show the sensitivity of the long-term evolution to B_0.

In the WP phase when the source is not very close to rotational equilibrium, the dominant torque $\Gamma_{\rm D}$ is proportional to B_0/P^2 and independent of $\dot{M}_{\rm in}$. Since $\Gamma = I\dot{\Omega} \propto \dot{P}/P^2$, where I is the moment of inertia of the neutron star, $\dot{P}$ depends only on B_0 which we take constant during the long-term evolution. Simulations indicate that this phase terminates at an age smaller than $\sim 5 \times 10^5$ yr. The age of a source that has been evolving in the WP phase starting from the initial phase of evolution is equal to $P/\dot{P}$, comparable to characteristic age, $\tau_{\rm c} = P/2\dot{P}$. In the SP phase following an WP phase, $\dot{P}$ is proportional to $\dot{M}_{\rm in}$ which decreases rapidly in this late phase of evolution. Consequently, the maximum $\dot{P}$ achieved in the WP phase

also decreases sharply after termination of this phase. This causes P to remain almost constant after the WP/SP transition. This maximum P achieved at the end of the WP phase depends sensitively on B_0, and does not change significantly with $M_{\rm d}$. That is, we can estimate B_0 from the measured P for the sources currently in the SP phase.

3.1.2 Evolution of RRATs with Fallback Discs

For systems starting the evolution in the WP phase, the transition to the SP phase occurs at an age smaller than about 5×10^5 yr. The age of a source is close to its characteristic age when it is in a long-lasting WP phase. After the transition to the SP phase, $\dot{P}$ decreases rapidly due to sharp decrease in $\dot{M}_{\rm in}$. The increase in P during the WP phase stops after the WP/SP transition, P remains almost constant in the SP phase (see Ertan et al., 2014, for details). It is crucial for our analysis that this maximum P reached at the end of the WP phase depends basically on B_0, and has a weak dependence on $M_{\rm d}$. This allows us to estimate B_0 for the RRATs that have periods sufficiently greater than their P_0 and $\tau_{\rm c} \gtrsim 5 \times 10^5$ yr.

These sources with $\tau_{\rm c} \gtrsim 5 \times 10^5$ yr should be evolving in the SP phase at present. This conclusion is independent of the details of the evolution in the past. The sources with $\tau_{\rm c} < 5 \times 10^5$ yr could be in the SP or WP phase depending on the initial conditions. For a given source, if $\tau_{\rm c} > 5 \times 10^5$ yr, there are two basic possibilities for the history of the source: (1) a long lasting WP phase followed by a SP phase, (2) an evolution permanently in the SP phase. From the earlier applications of the model, we estimate that most of RRATs follow the evolutionary phases described in case (1). In this thesis, we investigate these solutions, and try to estimate the range of B_0 allowed for RRATs. For case (2), a large fraction of the sources evolve towards the properties of normal radio pulsars, while the remaining fraction enters the WP phase at a later time of evolution, and subsequently evolves as in case (1).

To estimate the RRATs evolving in the SP phase, the $\tau_{\rm c} > 5 \times 10^5$ yr condition is reliable only for the sources with P sufficiently greater than P_0. In the first part of our analysis, we select the sources with $P > 0.7$ s (30 out of 34). It is remarkable that $\tau_{\rm c} \gtrsim 5 \times 10^5$ yr for all these sources (except J1819). For the neutron stars starting the evolution in the WP phase, P_0 does not affect the long-term evolution significantly. The periods of the sources with different P_0 values converge to the same level at the end of the WP phase (see e.g. Ertan et al., 2009b, for details). For the model calculations, we set $P_0 = 300$ ms, the estimated average value for the

young pulsars (Faucher-Giguère & Kaspi, 2006).

Since the period achieved at the end of the WP phase depends mainly on B_0 (see Ertan et al., 2014, figs. 1 and 2), for all model calculations, we use the same initial conditions ($M_{\rm d} = 3.16 \times 10^{-6}\ M_{\odot}$ and $P_0 = 300$ ms) and the same set of main disc parameters ($\alpha = 0.045$, $T_{\rm p} = 67$ K, and $C = 7 \times 10^{-4}$), which are similar to those employed in the earlier work (Benli & Ertan, 2016, 2017, 2018a, 2018b; Çalışkan et al., 2013; Ertan & Çalışkan, 2006; Ertan et al., 2014; Ertan et al., 2007; Gençali & Ertan, 2018; Özcan et al., 2020). In this first step of our analysis, we obtain different model curves by changing the initial condition B_0 only. Illustrative model curves tracing the P and $\dot{P}$ ranges of RRATs with $P > 0.7$ s are given in Fig. 3.1. The model curves show how P, $\dot{P}$, and $L_{\rm X}$ evolution change depending on B_0. The solid and dashed parts of the curves correspond to the WP and SP phases respectively. There is a single $L_{\rm X}$ curve (top panel), since we use the same $M_{\rm d}$ for all model sources. In the top panel, the dotted curve is the theoretical cooling curve for the neutron stars with conventional dipole fields. In Fig. 3.1, it is seen that all these sources are evolving in the SP phase as we have initially estimated from their characteristic ages. They are powered by the cooling luminosity at ages $(\sim 2 - 6) \times 10^5$ yr.

In Fig. 3.2, we plot the model curves for long-P RRATs in the P – $\dot{P}$ diagram using the same color code as in Fig. 3.1. For comparison, we kept the constant $\tau_{\rm c}$ and B_0 lines estimated from the dipole torque formula. The horizontal and vertical branches of the curves in Fig. 3.2 correspond to the WP and SP phases respectively. The numbers seen on the model curves show the ages of the sources in the units of 10^5 yr. It is seen in Figs. 3.1 and 3.2 that the sources with stronger fields evolve to longer periods. It is remarkable that the B_0 values between $\sim 2 \times 10^{11}$ G and $\sim 6 \times 10^{11}$ G produce the model curves tracing the entire P and $\dot{P}$ ranges of all RRATs with $P > 0.7$ s. In Fig. 3.2, constant–B_0 lines show the actual B_0 of the sources only at the end points of the model curves where the disc torque becomes negligible compared to the dipole torque. There are $L_{\rm X}$ upper limits estimated for 5 of these RRATs. These upper limits, together with measured P and $\dot{P}$ of the sources are listed in Table 3.1. From the model curves given in Fig. 3.2, the ages of these sources can be estimated. It is seen in Fig. 3.1 that the cooling luminosities corresponding to these ages are in agreement with the estimated $L_{\rm X}$ upper limits.

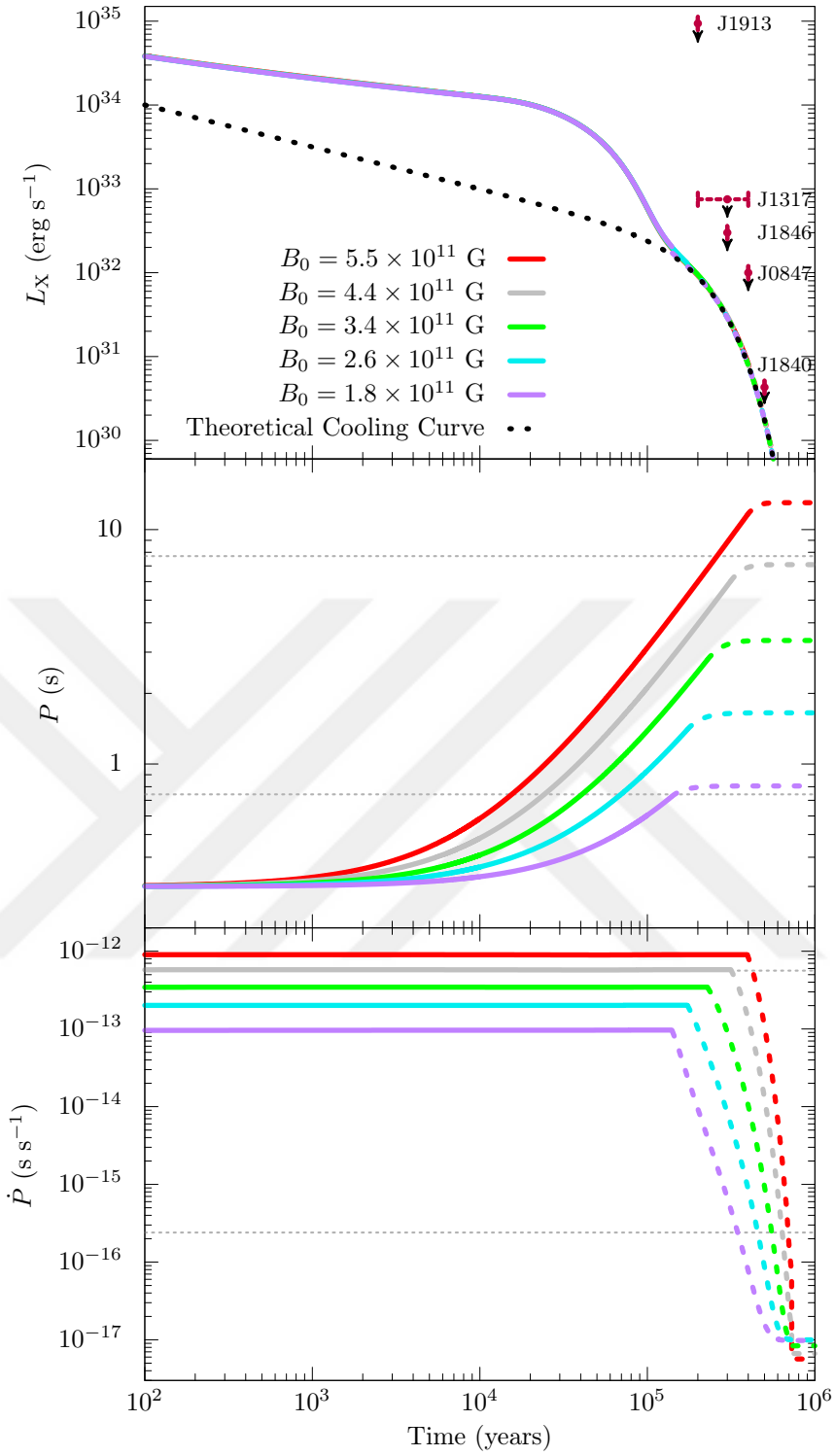

Figure 3.1 The model curves produced by changing B_0 only (given in the top panel) for RRATs with $P > 0.7$ s. For all the curves, $\alpha = 0.045$, $T_p = 67$ K, $C = 7 \times 10^{-4}$, $P_0 = 0.3$ s and $M_d = 3.16 \times 10^{-6}$ $M_\odot$ (see the text for the details). The dotted curve in the top panel shows the theoretical cooling curve (Page, 2009). The WP and SP phases are shown by the solid and dashed curves respectively. The X-ray upper limits of 5 RRATs and their approximate ages (see Table 3.1) obtained from the model are shown with error bars in the top panel. The thin horizontal lines in the middle and the bottom panels show the observed P and $\dot{P}$ ranges for RRATs with $P > 0.7$ s respectively.

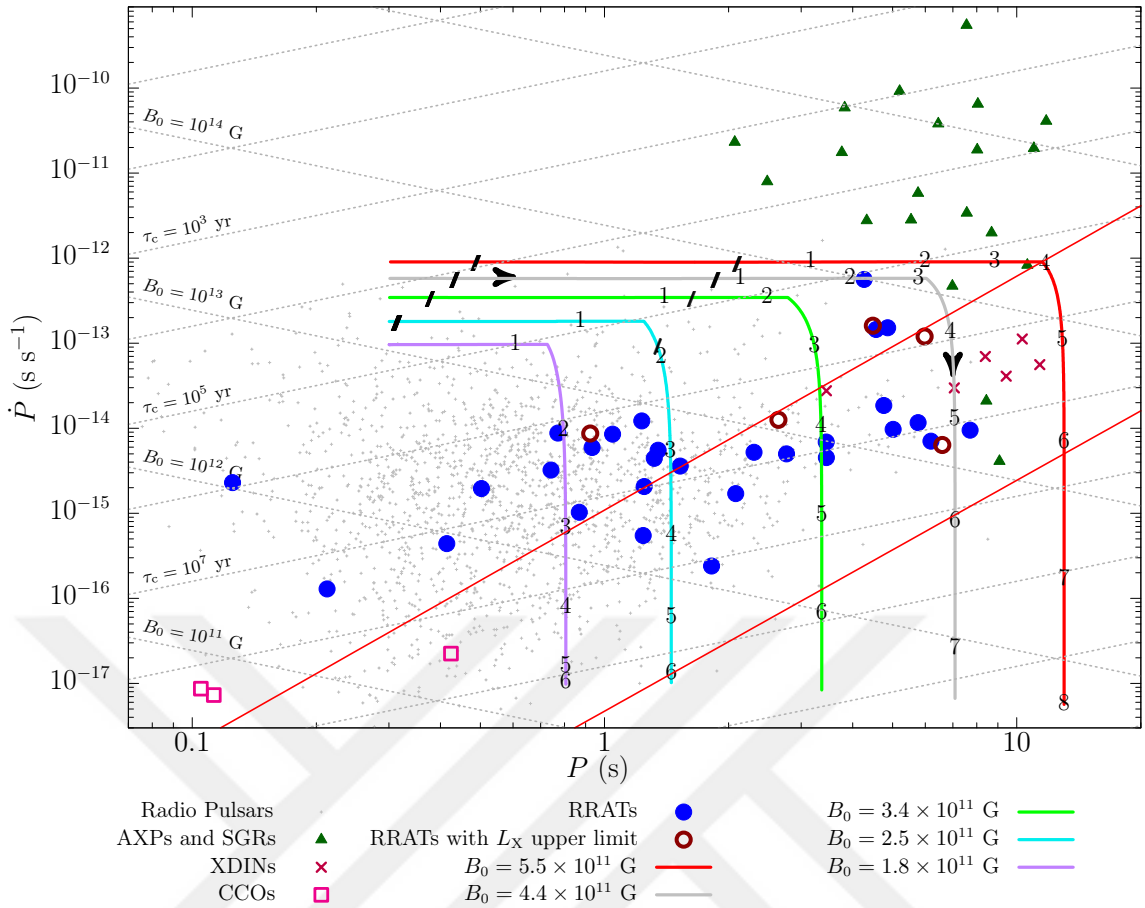

Figure 3.2 Evolutions in the P – $\dot{P}$ diagram for the same model sources given in Fig. 3.1. Filled circles show RRATs. Empty circles indicate the RRATs with L_X upper limits. Red solid lines are the upper and lower boundaries of the death valley (K. Chen & Ruderman, 1993). Constant τ_c and B_0 calculated from the dipole-torque formula are also given for comparison with those estimated in our model (given in the figure). The numbers on the model curves show the ages of the sources in units of 10^5 yr. The ticks on the curves correspond to the periods at which the sources cross the upper and lower borders of the death valley in our model. It is seen that the sources with $B_0 \gtrsim 3 \times 10^{11}$ G find themselves below the pulsar death line at the end of the WP phase (horizontal branches of the curves). The constant–B_0 lines show the actual B_0 of the sources only at the end points of the model curves. Ordinary radio pulsars, AXP/SGRs, XDINs, RRATs, and CCOs are also plotted the data is taken from the ATNF Pulsar Catalogue (version 1.63, Manchester et al., 2005, https://www.atnf.csiro.au/research/pulsar/psrcat/).

Among the RRATs with measured $\dot{P}$, the other sources have periods in the 0.1 – 0.5 s range. For these sources, we cannot estimate the evolutionary phase from the τ_c, since their P could be close to P_0. Nevertheless, for a particular source, we could estimate two different B_0 values for each of the two possible phases of evolution, WP and SP, at present. This analysis is important in that it is likely to give the minimum possible dipole fields for the RRAT population in our model. For these sources, we leave P_0 free in addition to B_0, and do not change M_d and the main disc

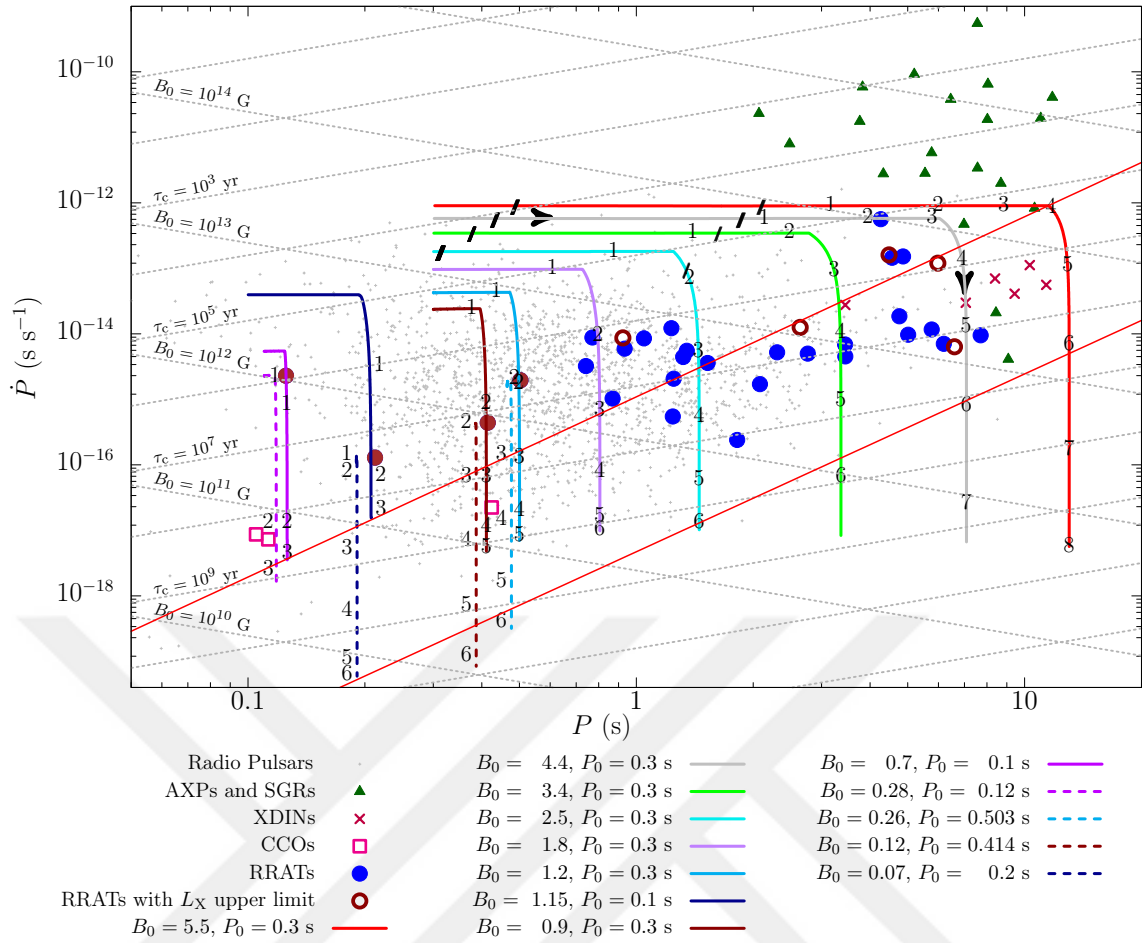

Figure 3.3 The same as Fig. 3.2, but the model curves for the sources with $P < 0.7$ s are also added (brown filled circles). The dashed and solid curves show the evolutionary paths crossing the current source properties in the WP and SP phases respectively. The P_0 and B_0 values in the unit of 10^{11} G are given in the figure.

parameters used for the $P > 0.7$ s sources. In Fig. 3.3, the model curves obtained for all RRATs are seen together. The model fits indicate that the sources with $P < 0.7$ s could have B_0 ranging from $\sim 7 \times 10^9$ G to $\sim 10^{11}$ G. For a given source, the minimum possible B_0 is estimated assuming that the source in the WP phase at present. We estimated these minimum possible B_0 values in our earlier work (see Gençali & Ertan, 2018, fig. 2).

The B_0 values estimated in our model are also given in the $B_0 - P$ diagram in Fig. 3.4. The solid lines show the upper and lower boundary of the pulsar death valley (K. Chen & Ruderman, 1993). The B_0 values inferred from the dipole torque formula are also plotted for comparison (empty triangles). Filled triangles show B_0 values of the sources with $P < 0.7$ s in the case that they are currently in the WP phase. The solutions producing the source properties in the SP phase can be obtained with greater B_0 depending on P_0. For the two sources with smallest P, the upper B_0 values given in Figs. 3.3 and 3.4 correspond to the maximum B_0 leaving

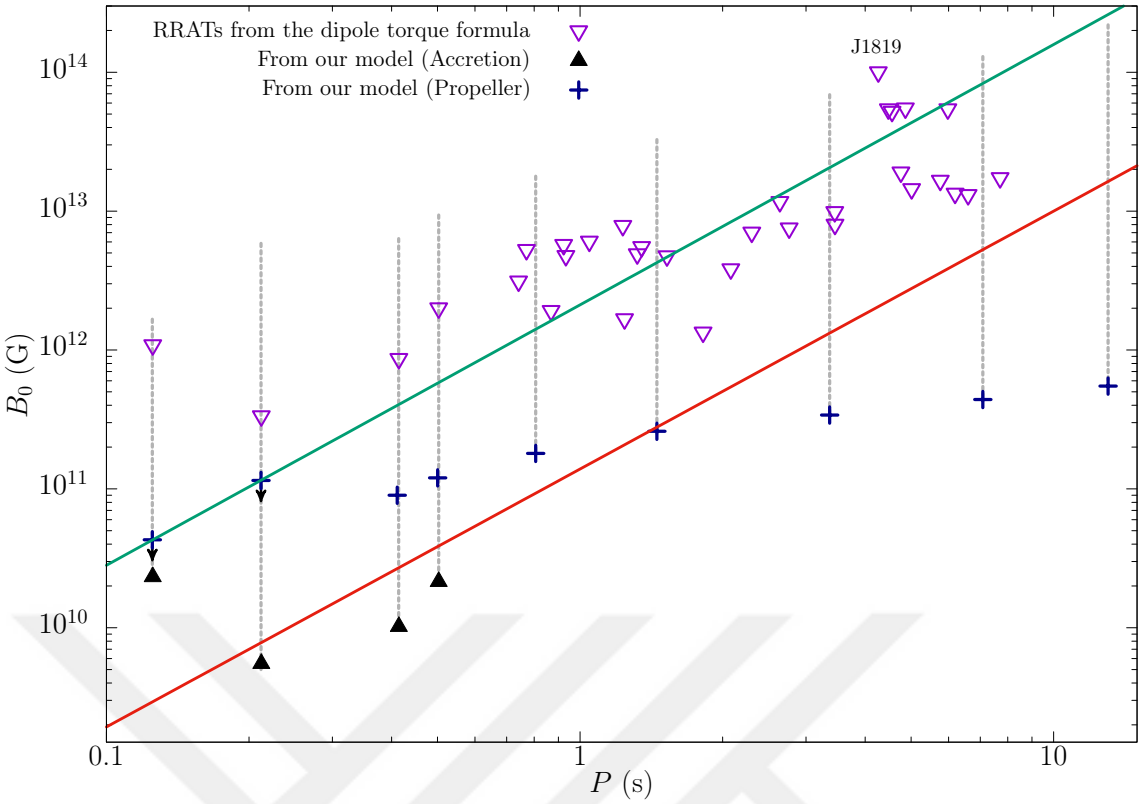

Figure 3.4 RRATs in the B_0 – P diagram. Plus signs and filled triangles show the B_0 values and final periods for the evolutions seen in Fig. 3.3. The solid lines show the upper and lower borders of the death valley (K. Chen & Ruderman, 1993). Empty triangles indicate the B_0 values inferred from the dipole-torque formula using measured P and $\dot{P}$ values (see Table 3.1). Vertical dashed lines show the ranges of B_0 deduced from the dipole torque formula during the long-term evolution. For the four sources with $P < 0.7$ s, plus signs and filled triangles show the B_0 values in the case that the sources are currently in the SP phase and the WP phase respectively. For $P > 0.7$ s, there is only one source (J1819) in the the WP phase, while the others are in the SP phase.

the sources inside the death valley. We estimate that the death point of the RRAT with minimum P is close to the upper border of the death valley (see conclusion). It is seen in Fig. 3.4 that all these sources could be located inside the death valley or below the pulsar death line with the B_0 values estimated in our model.

The estimated ages and $L_{\rm X}$ values in our model together with the observed rotational properties are given in Table 3.1. As seen in Fig. 3.1, most of the RRATs are powered in X-rays by the intrinsic cooling of the neutron star. We should note that the cooling curve depends on some unknown details of the neutron star properties, such as the equation of state and mass (see e.g. Potekhin, Zyuzin, Yakovlev, Beznogov, & Shibanov, 2020, for a recent detailed discussion). In our numerical calculations, we have employed the cooling curve obtained by Page (2009). Any corrections to the cooling curve could change the $L_{\rm X}$ values estimated in our illustrative model,

without a significant change in the B_0 values.

The ages of most RRATs estimated in our model are one to two orders of magnitude smaller than their characteristic ages. This indicates that RRATs could have cooling luminosities in soft X-rays that are much higher than those corresponding to their characteristic ages and comparable to those of XDINs. This puts a significant fraction of RRATs, especially those within 2 kpc, into the list of detectable sources for the 4-year extended Roentgen Survey with an Imaging Telescope Array (eROSITA) all-sky survey (eRASS) which started on December 13, 2019 (Merloni et al., 2012; Pires, Schwope, & Motch, 2017). All known XDINs are within a distance of 500 pc from the Sun, while most of the RRATs are at larger distances (see Table 3.1). Nevertheless, the eRASS sensitivity will be about 25 times greater than the ROSAT all-sky survey sensitivity in the 0.2 – 2.3 keV soft X-ray range (Predehl et al., 2020). Through Monte Carlo simulations, Pires et al. (2017) estimated that, on average, about 90 thermally emitting new isolated neutron stars could be detected by the eRASS.

Discussion & Conclusions:

We have estimated the B_0 range for RRATs with measured $\dot{P}$ in the fallback disc model. Comparing our results with those obtained earlier for the other young neutron star populations, we see that the B_0 range of RRATs ($\sim 7\times10^9$ – $\sim 6\times10^{11}$ G) could fill the gap between the B_0 ranges of CCOs and XDINs ($\sim 4\times10^9$ – $\sim 3\times10^{11}$ G) estimated in the same model (Benli & Ertan, 2018a; Ertan et al., 2014).

In the dipole torque model, almost all RRATs are located above the pulsar death line, and about half of them are even above the upper border of the pulsar death valley in the B_0 – P diagram. With the B_0 values estimated in our model, we find that all these sources could be either inside the death valley or below the death line. Given that RRATs do not show strong continuous radio pulses, we estimate that they are close to or below their individual death points. Then, what could be the reason for their repetitive, short radio bursts? We tentatively propose that these bursts could be ignited through interaction of the inner disc with the dipole field of the star at the inner boundary of the disc. The flux of the open field lines through the magnetic poles could be occasionally enhanced during the continual opening and reconnection of the lines passing through the inner disc boundary (Lovelace, Romanova, & Bisnovatyi-Kogan, 1995, 1999).

The enhancement of the open field line flux was proposed earlier by Parfrey,

Spitkovsky, and Beloborodov (2016) in a different context related to the effect of this enhancement on the torques acting on the millisecond pulsars. For the neutron stars with long P, like RRATs, contribution of the field-line opening to the spin-down torque is negligible compared to the disc torque. Nevertheless, we estimate that this mechanism could transiently build up the condition required for the strong radio emission near the poles. The field lines, that are closed inside the light cylinder radius of a neutron star rotating in vacuum, open up from $r_{\rm LC}$ to $\sim r_{\rm in}$ when there is a disc around the star. Outside the inner boundary the lines are estimated to be decoupled from the disc, while the lines passing through the boundary interact with the disc. This interaction inflates and opens up the closed lines on a short interaction time scale. The reconnections of the lines are also estimated to occur on a similar time-scale (Lovelace et al., 1999; Ustyugova, Koldoba, Romanova, & Lovelace, 2006). As a result of these cycles, the field density and the flux of the open field lines through the poles are likely to show continual variations, which might trigger the observed brief radio bursts of RRATs when the appropriate condition for the burst is built up for short time intervals.

In this picture, the disc torque should be sufficiently strong to ignite radio bursts when the star is actually below its death point. By comparison, XDINs have relatively long periods and are estimated to be in the strong-propeller phase with fields placing them well below the pulsar death line in the fallback disc model (Ertan et al., 2014). This might indicate that their disc torques are not strong enough to produce radio bursts. In other words, we estimate that the RRAT behavior is not likely to be observed beyond a certain period. Below this period, there could be a P range along which both XDINs and RRATs could show radio bursts depending on their locations of the death points. The fact that 5 of XDINs have periods greater than the maximum period (~ 7 s) of RRATs seems to support this idea. For the evolutions that end up inside the death valley, a given source could show normal radio pulses or RRAT behavior depending on the position of its death point inside the valley. For instance, the model source with $B_0 = 1.8 \times 10^{11}$ G and $P_0 = 0.3$ s (Fig. 3.3), is estimated to be inside the valley after the inactivation of the disc (at the end point of the model curve). If its end point of evolution is above the death point, the source could be a radio pulsar during and after the SP phase. If the end point of evolution is below the death point, the source could be observed as an RRAT in the SP phase. In this picture, the effect of the disc is to boost the source transiently above its death point inside the valley. This affect is strongest at the beginning of the SP phase when $r_{\rm in} \simeq r_{\rm co}$, and becomes negligible towards the end points of the evolutionary curves (Fig. 3.3). The radio bursts are likely to terminate when the flux enhancements become insufficient to trigger radio bursts.

This is likely to occur when a given source is apparently either inside the valley or possibly, for low-period sources, below the upper border of the valley. Investigation of the conditions that could trigger radio bursts, which is beyond the scope of this work, could be studied through numerical simulations of the disc-field interaction.

Considering that RRATs have relatively high birth rate among the young neutron star populations (Popov et al., 2006), our results imply that a large fraction of the neutron stars are born with B_0 in the $(1 - 10) \times 10^{11}$ G range. Among these sources, those with relatively high B_0 tend to evolve to longer periods leaving them well below the pulsar death line at the end of the WP phase. These sources are likely to have XDIN properties, and unlikely to show the RRAT behavior. The sources with relatively weak fields, could enter the radio pulsar or RRAT phase depending on the positions of their death points inside the death valley. If the disc-field interaction is indeed required for the RRAT bursts, then the duration of the RRAT phase could be limited by the active lifetime of the disc which we estimate to be less than 10^6 yr. For all RRATs plotted in Fig. 3.3, the ages are in the range of $(\sim 2 - 6) \times 10^5$ yr in our model, while the characteristic ages are mostly greater than 10^6 yr. At ages $\gtrsim 10^6$ yr, RRATs are not likely to be detected in X-rays since the cooling luminosities remain below the X-ray detection limits. With the ages estimated in our model (Fig. 3.3), some of the RRATs could be detected with $L_{\rm X} = L_{\rm cool} \sim (10^{31} - 10^{32})$ erg s^{-1}. For the five RRATs with estimated $L_{\rm X}$ upper limits (Table 3.1), these limits are consistent with the cooling luminosities corresponding to their ages estimated in our model (Figs. 3.1 and 3.2).

For the evolutionary curves seen in Fig. 3.2, all RRATs with $P > 0.7$ s are expected to be in the SP phase with one exception, namely J1819. This is the only source with known $L_{\rm X}$, and we estimated that the source is in the WP phase, and close to the WP/SP transition at present (Gençali & Ertan, 2018). Continuous radio pulsations are estimated to be switched off by mass-flow on to the neutron star. Nevertheless, it is not clear whether very short radio bursts could be emitted in the accretion phase. For the accreting sources close to the WP/SP transition, the short radio bursts might be emitted when the accretion is occasionally hindered. We are not sure about the current phases of the RRATs with smallest periods. Except these one or two sources that are close to the WP/SP transition, we do not find any RRAT in the WP phase. Finally, we note that the 3 CCOs given in Figs. 3.2 and 3.3 are estimated to be in the accretion phase at present with $B_0 \sim (1 - 5) \times 10^9$ G in the fallback disc model (Benli & Ertan, 2018a). The simulations show that their periods will not change significantly until the WP/SP transition. This means that these sources are likely to evolve into the RRAT phase after or close to the termination of the WP phase.

Table 3.1 RRATs with the quantities estimated in the model (Age and $L_{\rm X}$) together with the observed properties (P, $\dot{P}$, d, $L_{\rm X,upper}$, $\dot{E}$ and $\tau_{\rm c}$) (ATNF Pulsar Catalogue, version 1.63, Bates et al., 2012; Keane et al., 2011; Manchester et al., 2005). $B_{\rm db}$ shows the dipole field strengths at the pole of the star inferred with dipole braking assumption (see Fig. 3.3 for B_0 values estimated in our model). $L_{\rm X,upper}$ shows the X-ray upper limits in the $0.3 - 5$ keV energy band for J1913+1330 and J1317–5759 (Rea & McLaughlin, 2008), and in the $0.3 - 8$ keV energy band for J1846–0257 and J0847–4316 (Kaplan, Esposito, et al., 2009). $L_{\rm X,upper}$ for J1840–1419 is calculated from blackbody temperature upper limit (Keane et al., 2013). Unlike other long-P RRATs, J1819 is estimated to be in the WP phase and its $L_{\rm X}$ value is obtained from detailed model fits in earlier work (for details see Gençali & Ertan, 2018).

Source Name	P (s)	$\dot{P}$ (10^{-15} s s^{-1})	d (kpc)	$L_{\rm X,upper}$ (10^{32} erg s^{-1})	$\dot{E}$ (10^{32} erg s^{-1})	$\tau_{\rm c}$ (10^{5} yr)	$B_{\rm db}$ (10^{12} G)	Age (10^{5} yr)	$L_{\rm X}$ (10^{30} erg s^{-1})
J1554–5209	0.13	2.29	3.08	–	460	8.65	0.54	1	240
J1647–3607	0.21	0.13	15.94	–	5.30	261	0.17	2	90
J1848–1243	0.41	0.44	3.15	–	2.40	149	0.43	2	90
J1623–0841	0.50	1.96	4.64	–	6.10	40.8	1	2	90
J1909+0641	0.74	3.22	1.33	–	3.10	36.5	1.56	$2-3$	$30-90$
J1826–1419	0.77	8.78	3.24	–	7.60	13.9	2.63	2	90
J2325–0530	0.87	1.03	1.49	–	0.62	134	0.96	3	30
J1913+1330	0.92	8.68	6.18	< 940	4.40	16.9	2.86	2	90
J1839–0141	0.93	5.94	6.07	–	2.90	24.9	2.38	$2-3$	$30-90$
J1513–5946	1.05	8.53	3.76	–	2.90	19.4	3.02	$2-3$	$30-90$
J1048–5838	1.23	12.2	1.01	–	2.60	16	3.92	$2-3$	$30-90$
J0628+0909	1.24	0.55	1.77	–	0.11	359	0.84	4	8
J0139+3336	1.25	2.06	1.47	–	0.42	95.8	1.62	3	30
J1754–3014	1.32	4.43	2.52	–	0.76	47.2	2.45	$3-4$	$8-30$
J0201+7005	1.35	5.51	1.17	–	0.89	38.8	2.76	3	30
J0912–3851	1.53	3.59	0.52	–	0.40	67.4	2.37	3	30
J1739–2521	1.82	0.24	4.41	–	0.02	1200	0.67	$4-5$	$2-8$
J1919+1745	2.08	1.71	4.09	–	0.08	193	1.91	4	8

Table 3.1 (Continued)

Source Name	P (s)	$\dot{P}$ (10^{-15} s s^{-1})	d (kpc)	$L_{\rm X,upper}$ (10^{32} erg s^{-1})	$\dot{E}$ (10^{32} erg s^{-1})	$\tau_{\rm c}$ (10^5 yr)	$B_{\rm db}$ (10^{12} G)	Age (10^5 yr)	$L_{\rm X}$ (10^{30} erg s^{-1})
J2105+6223	2.31	5.22	2.72	–	0.17	70	3.51	$3-4$	$8-30$
J1317–5759	2.64	12.6	3.77	< 7.5	0.27	33.3	5.83	$3-4$	$8-30$
J1807–2557	2.76	4.99	18.56	–	0.09	87.7	3.76	4	8
J1538+2345	3.45	6.89	1.31	–	0.07	79.3	4.93	4	8
J1854–1557	3.45	4.52	10.90	–	0.04	121	4	$4-5$	$2-8$
J1819–1458	4.26	563	3.30	–	2.90	1.2	49.6	2	4000
J1846–0257	4.48	161	4.00	< 3	0.71	4.42	27.1	3	30
J1854+0306	4.56	145	4.50	–	0.61	4.98	26	3	30
J1444–6026	4.76	18.5	5.82	–	0.07	40.7	9.51	4	8
J0736–6304	4.86	152	0.90	–	0.52	5.07	27.5	$3-4$	$8-30$
J2033+0042	5.01	9.70	2.93	–	0.03	81.9	7.06	$4-5$	$2-8$
J1707–4417	5.76	11.7	14.05	–	0.02	78.4	8.29	5	2
J0847–4316	5.98	120	6.55	< 1	0.22	7.9	27.1	4	8
J1226–3223	6.19	7.05	2.17	–	0.01	139	6.69	5	2
J1840–1419	6.60	6.35	0.72	< 0.043	0.009	165	6.55	5	2
J1652–4406	7.70	9.50	5.11	–	0.008	129	8.66	5	2

Summary of the Results:

We have shown that the evolutionary avenues of the model sources depend mainly on the dipole field strength, B_0, which we have estimated to have a continuous distribution from a few 10^9 G to about 10^{13} G. As seen in Fig. 3.3, the sources with lowest B_0 values are born as either CCOs accreting matter from the disc or RRATs in the SP phase. After termination of the WP phase, CCOs could become radio pulsar or RRAT depending on its B_0, current P and the position of death point inside the death valley. We estimate that a large fraction of the sources have B_0 in the rage of ($\sim 10^{11}$ – 10^{12}) G. These sources evolve to longer periods in the WP phase, during which some of them could be identified as AXPs due to their apparently high B_0 inferred from the dipole torque formula (see Fig. 3.2). When the accretion is switched off, a large fraction of these neutron stars could enter the SP phase as RRATs. Among these systems, those with relatively short periods ($\lesssim 1$ s) could become either radio pulsar or RRAT depending on the positions of their death points inside the death valley. The stronger dipole fields lead the systems to longer periods during the WP phase. Sources reaching the WP/SP transition with periods longer than a critical level are likely to become XDIN immediately after the transition to the SP phase. It is seen in Fig. 3.2 that the periods of RRATs and XDINs overlap in roughly in the ~ 3 – 8 s range. It is possible that the XDINs in this range could actually be RRATs with unseen radio bursts due to narrow beaming and viewing geometry, or alternatively their RRAT phases terminated at an earlier time, and now they are evolving in the XDIN phase emitting no radio bursts.

In the same model, it is found that a large fraction of HBRPs and persistent AXP/SGRs have B_0 in the (10^{12} – 10^{13}) G range (Benli et al., 2015; Benli & Ertan, 2016, 2017, 2018b), greater than the B_0 values estimated for CCOs, RRATs, and XDINs (Benli & Ertan, 2018a; Ertan et al., 2014). Most of these HBRPs with relatively strong fields evolve from the SP phase to the WP phase achieving the AXP/SGR properties. There are also HBRPs evolving always in the SP phase apparently converging to the properties of normal radio pulsars (Benli & Ertan, 2017, 2018b). A fraction of these neutron stars could reach their death points while the disc torques are still efficient. They become RRATs during their late phase of evolution. The remaining fraction of these HBRPs always evolve as radio pulsars slowing down initially with the disc torques in the SP phase, and eventually with dipole torques until they reach their critical periods switching off the radio pulses. Note that, there is no evolution from the RRAT to the radio pulsar phase. At the end of the RRAT phase, sources find themselves below their death points in the B_0 – P diagram.

We estimate that most of the AXP/SGRs are currently evolving in the WP phase. In this population, sources with $B_0 > 10^{12}$ G could achieve periods longer than XDIN periods at the end of their WP phases due to their relatively strong dipole fields (Benli & Ertan, 2016). These sources are not likely to show radio pulses or bursts after the WP phase due to their long periods placing them well below the pulsar death line. On the other hand, most of the transient AXPs, which seem to have a birth rate greater than that of persistent AXP/SGRs (Keane & Kramer, 2008), could have relatively weak fields ($B_0 \lesssim 10^{12}$ G), and evolve first into the RRAT phase and later become XDIN, or possibly evolve directly into the XDIN phase if they reach sufficiently long periods at the end of the WP phase.

To sum up, in our model, RRATs seem to have evolutionary connections with all the other isolated neutron star populations. Different systems show RRAT behavior along a certain late phase of their observable long-term evolution. These connections, complicating the total birth-rate estimation of isolated neutron stars, imply that the total birth rate could be a small fraction of the sum of the birth rates estimated for each population.

3.1.3 Application to LPP GLEAM-X

The model curves in Fig. 3.5 show illustrative evolutionary paths that reach the observed period of GLEAM-X J162759.5–523504.3 at a time when $L_{\rm X}$ and $\dot{P}$ satisfy the observational upper limits (horizontal dotted lines). The model curves are obtained with disc parameters similar to those employed for other neutron star systems ($\alpha = 0.045$, $C = 7 \times 10^{-4}$, $T_{\rm p} = 100$ K), and with the initial conditions $P_0 = 0.3$ s, $M_{\rm d} = 1.6 \times 10^{-5}\ M_\odot$, except B_0. The solid and dashed lines are for B_0 values of 4×10^{12} G and 7×10^{12} G respectively. The results are not sensitive to P_0 and $M_{\rm d}$.

Viable models are obtained with $B_0 \simeq (4-8) \times 10^{12}$ G. For fields stronger than this range, the source attains the observed period at an earlier time when $L_{\rm X}$ is above the observational upper limit, while for fields below this range the disc becomes inactive before the observed period is reached. The model curves in Fig. 3.5 are for $B_0 = 4 \times 10^{12}$ G (solid curves) and $B_0 = 7 \times 10^{12}$ G (dashed curves). The source is in the WP phase at an age of $\gtrsim 3 \times 10^5$ yr in both cases.The sharp drop in the $\dot{P}$ curves takes place when the disc becomes completely inactive at time $\sim 7 \times 10^5$ yr when $P \sim 10^3$ s for this source. Subsequently, the source evolves with the magnetic dipole torque alone, with $\dot{P} \simeq 4 \times 10^{-18}$ s s^{-1} for $B_0 = 7 \times 10^{12}$ G. For $B_0 \simeq 4 \times 10^{12}$ G, the source arrives at the 1091 s period shortly before the inactivation of the disc and

the period levels off at this value as the subsequent spin-down is negligible. This weaker field option is also a possibility for the current state of the source considering the large uncertainty in the $\dot{P}$ measurement (Hurley-Walker et al., 2022). Further observations of the source during future radio burst epochs could better constrain the $\dot{P}$ and the current state of the source.

Long-term evolution of GLEAM-X J162759.5–523504.3 seems likely to be very similar to those of some of AXP/SGRs with relatively strong dipole moments. In earlier work using the same model, it was estimated that those AXP/SGRs could reach 10^3 s periods (see Benli & Ertan, 2016, fig. 2 and 3). Indeed, it is seen in Fig. 3.5 that the long-P pulsar would have been identified as an AXP/SGR if it were observed at earlier phases of evolution. The reason for the non-detection of such sources is likely to be their very faint X-ray luminosity and their lack of continuous, normal pulsed radio emission. Even in the case that the disc is active, it is not likely to be detected in the infrared (IR) bands because of the weak X-ray irradiation and large $r_{\rm in}$ ($\sim 2\times10^{10}$ cm). An evolutionary model for young neutron star families can be tested by observations of the progenitors of the long-period systems as proposed by that particular model. In our model, the AXP/SGRs are the progenitors expected to evolve to the long periods as exhibited by GLEAM-X J162759.5–523504.3. AXP/SGRs do have the high X-ray luminosities providing strong X-ray irradiation sufficient to irradiate and excite their discs to produce emission in the IR bands that should be detectable with the James Webb Space Telescope.

This long-P pulsar was discovered by means of its radio burst events (Hurley-Walker et al., 2022). The observed pulsed radio emission obviously cannot be powered by magnetic dipole radiation alone, since the upper limit of $\dot{E}$ is smaller than the pulsed radio luminosity, while in normal pulsars the radio luminosity is orders of magnitude smaller than the rotational power. At its present period, the inferred magnetic moment $\mu\sim10^{30}$ G places GLEAM-X J162759.5–523504.3 below the radio pulsar death valley by four orders of magnitude. The physical mechanism producing the radio bursts is beyond the scope of the present work. Recently, Ronchi, Rea, Graber, and Hurley-Walker (2022) proposed that a neutron star with a fallback disc and a magnetar dipole field can achieve the properties of this source at a young age($\sim 10^4-10^5$ yr). This model is completely different from the model we employ here. In their calculations, it is not clear why the disc is assumed to be inactive immediately after the source period is reached, while the current $\dot{M}_{\rm in}$ is still high ($\sim 10^{15}$ g s^{-1}). Furthermore, at these young ages $L_{\rm cool}$ alone is estimated to be well above the $L_{\rm X}$ upper limit, which is another source of heating for the disc that should be taken into account in the disc evolution models.

As a final remark, we would like to stress an important point about the comparison of the X-ray variability and the torque noise behavior of AXPs with the accreting neutron stars in binaries. For this comparison two important criteria should be satisfied: (1) the neutron star should have a field strength and accretion rate comparable to those estimated in the fallback disc model, and more importantly, (2) the dipole field of the neutron star in the binary should be interacting with a geometrically thin, optically thick disc, since AXPs in the fallback disc model have no companions. If the companion is a high-mass star, or a low-mass giant star, then their winds significantly affect both the X-ray variability and the torques acting on the neutron star. Analyses that do not take these criteria into account (see e.g. Doroshenko, Santangelo, Suleimanov, & Tsygankov, 2020) produce misleading results.

Conclusions:

We have shown that the properties of GLEAM-X J162759.5–523504.3 can be accounted for as a product of long-term evolution in the fallback disc model. The long period of the source is obtained with a dipole moment of a few 10^{30} G cm^3 with the present state satisfying the upper bounds on $L_{\rm X}$ and $\dot{P}$. Our results are not very sensitive to $M_{\rm d}$ and P_0. There are two different evolutionary avenues compatible with the present source properties: (1) The disc is still active and the source is in the WP phase at an age of $\sim 3\times10^5$ yr at present. For these solutions P will continue to increase to a few 10^3 s with $\dot{P}\sim10^{-10}$ s s^{-1} until the disc becomes inactive at an age of $\sim 7\times10^5$ yr. (2) With a weaker field in the allowed range, the disc becomes inactive when the source achieves the observed period, and P levels off at the present value because the dipole torque wields negligible spin-down after disc torques turn off: The source should be evolving with $\dot{P}\sim4\times10^{-18}$ s s^{-1} at the present age greater than $\sim 7\times10^5$ yr. A tighter constraint on $\dot{P}$ with future observations of the source could provide a test for these model predictions.

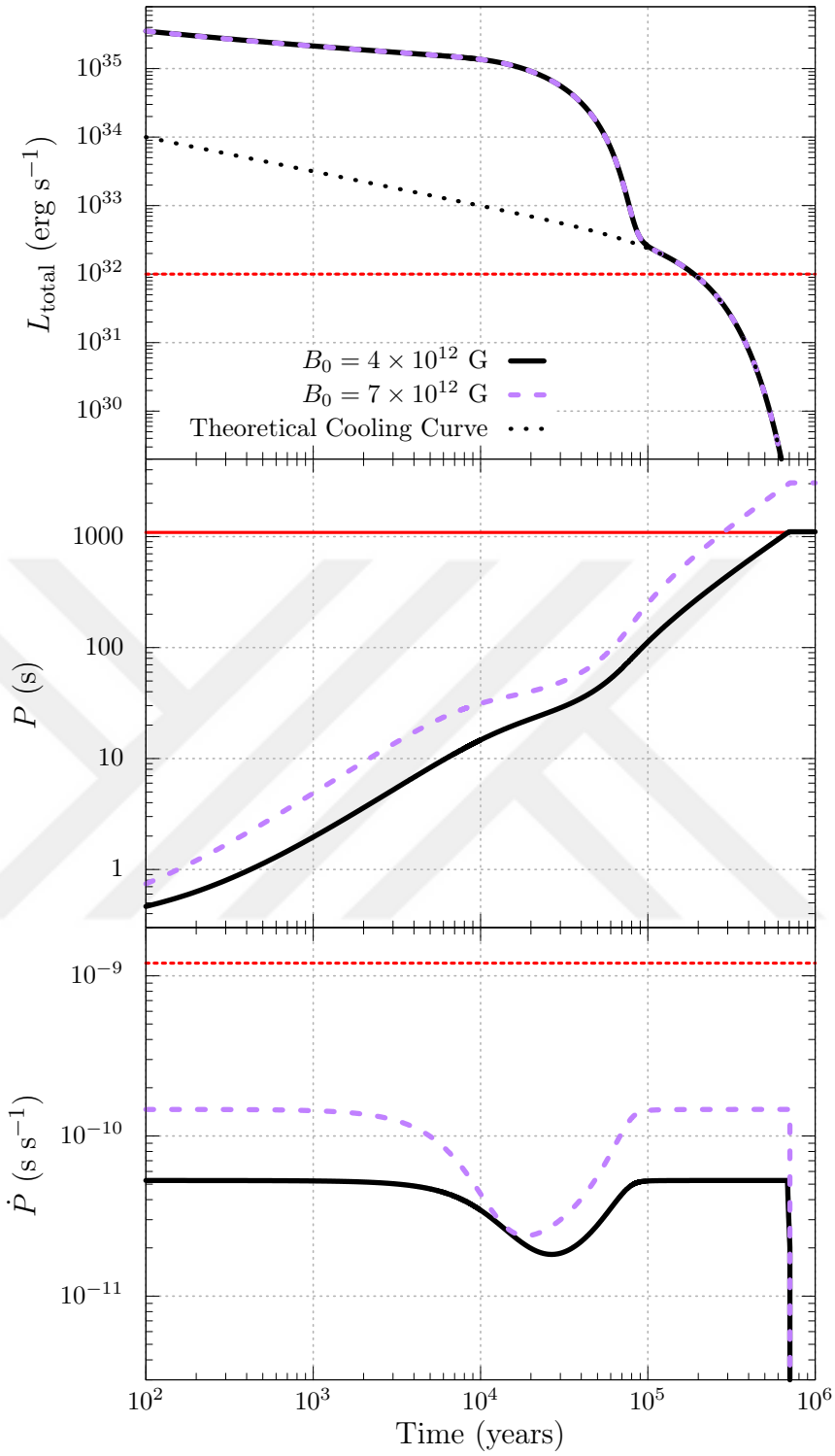

Figure 3.5 Illustrative model curves for the long-term evolution of GLEAM-X J162759.5–523504.3. B_0 values are given in the top panel. For both models, the other parameters are the same ($\alpha = 0.045$, $T_{\rm p} = 100$ K, $C = 7 \times 10^{-4}$, $P_0 = 0.3$ s, and $M_{\rm d} = 1.6 \times 10^{-5}$ $M_\odot$). The horizontal dotted lines show the upper limits, $\dot{P} < 1.2 \times 10^{-9}$ s s^{-1} and $L_{\rm X} < 10^{32}$ erg s^{-1}. In the top panel, the dotted curve shows the evolution of the cooling luminosity (Page, 2009; Page et al., 2006). The solid horizontal line in the middle panel shows the period of the source (1091 s).

3.1.4 Application to LPP PSR J0901-4046

Illustrative model curves seen in Fig. 3.6 show that the model can reproduce the P and $\dot{P}$ of J0901 simultaneously with a range of $L_{\rm X}$ values above a minimum $L_{\rm X} \sim 10^{28}$ erg s^{-1} and consistent with the estimated $L_{\rm X}$ upper limits ($\sim 10^{30}$ erg s^{-1}). The current properties are reached at an age $t \sim (6-8) \times 10^5$ yr, while the source is in the SP phase, slowing down with the $\Gamma_{\rm D}$. These model curves are obtained with disc parameters α, C and $T_{\rm p}$ similar to those employed for GLEAM-X and other sources from different neutron star families evolving under fallback disc torques. Our results are not sensitive to the P_0. For the model curves in Fig. 3.6, $M_{\rm d} = 1.6 \times 10^{-5}$ $M_\odot$ and $M_{\rm d} = 7.6 \times 10^{-6}$ $M_\odot$ for the solid and the dashed curves respectively, while $P_0 = 0.3$ s for both model curves. We obtain reasonable model curves for J0901 with $B_0 \sim 10^{12}$ G. This dipole field strength together with the 76 s period place the source below the pulsar death line (K. Chen & Ruderman, 1993), as was the case for the current evolutionary phase of GLEAM-X in the same model (Gençali et al., 2022).

Transient radio epochs and variable pulse profiles of J0901 and GLEAM-X are similar to the pulsed radio behaviour observed from a few AXP/SGRs. This might imply that a common radio emission mechanism is operating in these systems (Hurley-Walker et al., 2022), possibly similar to the origin of the brief radio bursts of RRATs, for which the occasional enhancement of the magnetic field flux in open field lines by means of disc-field interaction could be responsible (Gençali & Ertan, 2021; Parfrey et al., 2016; Parfrey, Spitkovsky, & Beloborodov, 2017). Even if a source is below the relevant pulsar death line, inward propagation of the inner disc radius and subsequent opening of the closed field lines could provide the power required for the radio emission. The same effect could produce different radio behaviour in different accretion and rotation regimes, and might power the transient radio pulses of the LPPs as well (for discussion see Gençali & Ertan, 2021; Parfrey et al., 2016, 2017; Tong, 2022). Details of the physical processes responsible for the observed radio emission of these sources are beyond the scope of the present work.

Ronchi et al. (2022) recently proposed that a neutron star evolving with a fallback disc and a *magnetar* dipole field can achieve the rotational properties of GLEAM-X and J0901 at young ages ($\sim 10^3 - 10^5$ yr). Their model is quite different from the model employed in this work. They use a simplified analytical model for the $\dot{M}_{\rm in}$ evolution (Ertan et al., 2009a; Menou, Perna, & Hernquist, 2001b) without including the heating by the X-ray irradiation of the disc produced by accretion luminosity and the cooling of the neutron star; and assumed that the disc becomes inactive (at

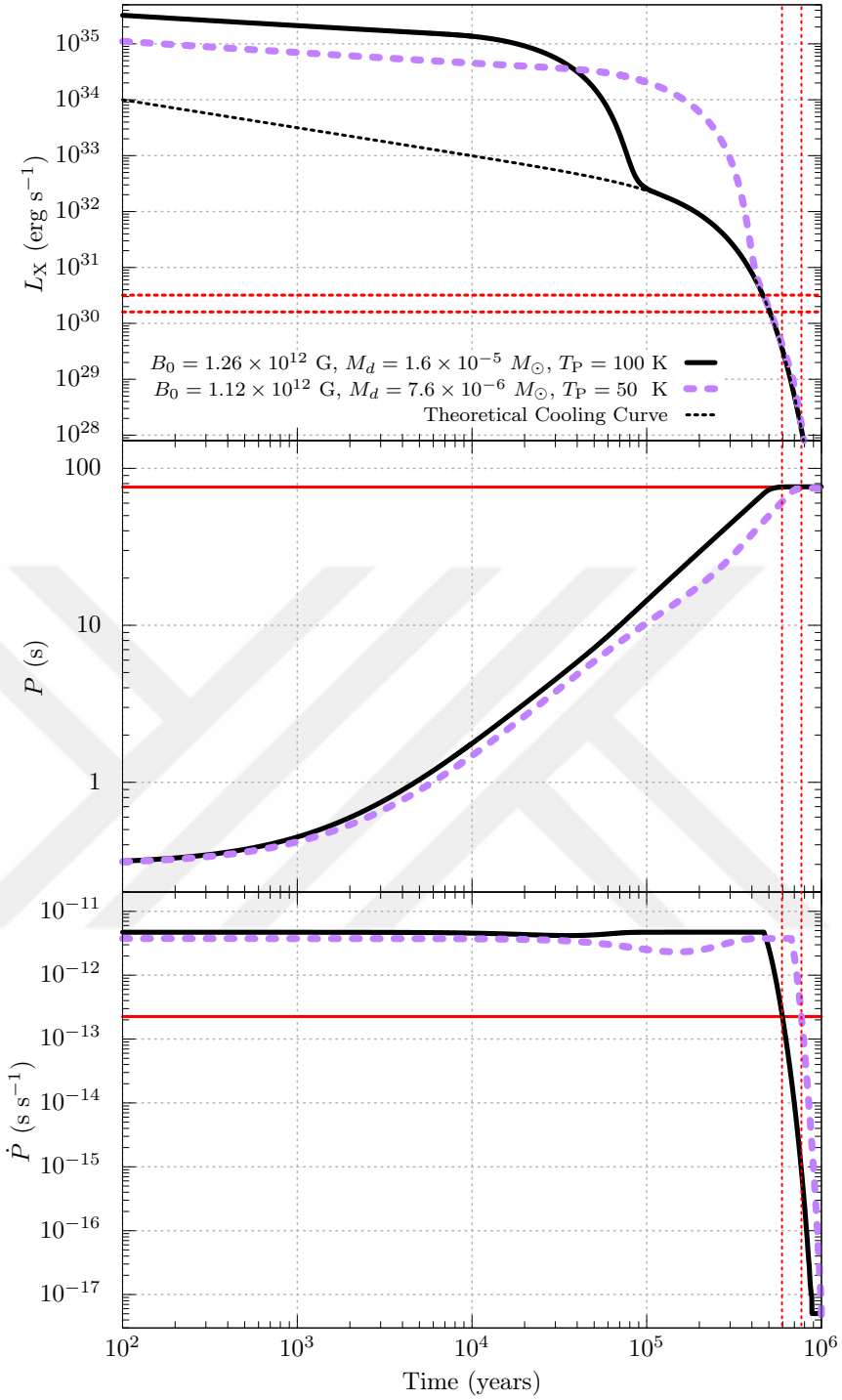

Figure 3.6 Illustrative model curves for the long-term evolution of J0901. These curves are obtained with the initial conditions B_0 and M_d values given in the top panel, while $P_0 = 0.3$ s for both model curves. For both models, we take $\alpha = 0.045$, and $C = 7 \times 10^{-4}$. The T_p values are given in the figure. In the top panel, the horizontal dashed lines show the estimated the upper limits. The dotted curve shows the evolution of the cooling luminosity L_cool of the star (Page et al., 2006, 2009). The solid horizontal lines in the middle and bottom panels show the measured P and $\dot{P}$ of the source respectively. These illustrative models achieve the current rotational properties of the source at the ages shown by the vertical dotted lines.

different $\dot{M}_{\rm in}$ values) when the model sources reach their presently observed periods. Furthermore, at the ages of the LPPs predicted in model ($< 10^5$ yr), the $L_{\rm X}$ values estimated from the theoretical cooling curves (Page et al., 2006, 2009; Potekhin & Chabrier, 2018; Potekhin et al., 2020) remain above a few 10^{32} erg s^{-1} even without contribution of the magnetar field decay (see Viganò et al., 2013). This $L_{\rm X}$ level is two orders of magnitude greater than $\sim 10^{30}$ erg s^{-1}, the $L_{\rm X}$ upper limit estimated for J0901. For a crustal field stronger than 10^{13} G, $L_{\rm X}$ is estimated to decrease below the upper limit at an age > 1 Myr. Thus, Ronchi et al. (2022) model with simplifying assumptions reproduces the rotational properties of these LPPs at the expense of inconsistency with the $L_{\rm X}$ upper limits (Rea et al., 2022).

Is there any evolutionary link between the LPPs and other neutron star populations? In our model, evolutionary paths of the two LPPs pass through the ranges of $L_{\rm X}$ and rotational properties of AXP/SGRs at ages of a few 10^4 yrs, similar to the ages estimated for present day AXP/SGRs (see Fig. 3.6). From the model curves, we estimate that AXP/SGRs with relatively strong dipole fields ($B_0 \sim 10^{13}$ G) evolve to the GLEAM-X properties (Gençali et al., 2022), while an average AXP/SGR ($B_0 \sim$ a few 10^{12} G) is likely to become a source similar to J0901 at $t \sim (6-8) \times 10^5$ yrs, in a state close to the final inactivation of the entire disc. These evolutionary paths leading AXP/SGRs to long periods were already predicted in our earlier work (Benli & Ertan, 2016, see fig. 2 and 3). In this model, AXP/SGRs are not likely to exhibit normal radio pulsar behaviour. Since most of these systems are estimated to be in the WP phase at present, accretion on to the star prevents their normal pulsed radio emission. On the other hand, after the transition to the SP phase, the radio emission would not be hindered by accretion, but their rotational power is not sufficient at their current long periods. In this late phase of evolution with very low $L_{\rm X}$, detections in X-rays are not likely. Emission of the disc in the IR bands is also weak because of the currently weak X-ray irradiation. In other words, if the LPPs were not able to show their unusual transient radio emission, we probably would not be aware of their existence. Long period neutron stars as endpoints of evolution with fallback discs without transient activity must constitute an abundant population, as is also the case for descendants of isolated radio pulsars which have spun down below the pulsar death valley.

These results imply that the persistent AXP/SGRs are likely to be progenitors of the LPP population. The birth rate of AXP/SGRs is estimated to be ~ 3 kyr^{-1} (Keane & Kramer, 2008). Less than half of the known AXP/SGRs are persistent (11 sources; Olausen & Kaspi, 2014, see Magnetar Catalogue)[1] and can achieve long

[1] http://www.physics.mcgill.ca/~pulsar/magnetar/main.html

periods. From the simulations, we estimate that the periods of LPPs could range from a few 10 s to a few 10^3 s for the B_0 range estimated for AXP/SGRs with the same model. We have estimated the ages of the two LPPs around 5×10^5 yr, while the AXP/SGR ages vary from $\sim 10^3$ yr to a few 10^4 yr. We therefore estimate that the number of LPP candidates could be an order of magnitude greater than that of AXP/SGRs.

Our results imply that the X-ray luminosities of LPPs sharply decrease to below $\sim 10^{31}$ erg s^{-1} after ages of a few 10^5 yr. This means that older LPPs are not likely to be detected in X-rays with present generation observatories, except for nearby sources, and that they are not likely to show normal radio pulsar behaviour either. Considering the differences in the observed P and estimated B_0 of the two LPPs, we estimate that a significant fraction of LPP candidates could show detectable pulsed radio-burst epochs. However, the physical mechanism activating pulsed-radio emission and the recurrence times of the radio epochs are not known yet, one is not able to make statistical predictions about radio detections.

Conclusions:

We have shown that a neutron star evolving with a fallback disc and a conventional dipole field ($B_0 \sim 10^{12}$ G) can acquire the rotational properties of J0901 at an age of $\sim (6-8) \times 10^5$ yr. Our results are not sensitive to the P_0. The expected $L_{\rm X}$ is below the estimated $L_{\rm X}$ upper limit of the source. Our model results indicate that, like GLEAM-X, J0901 was also an AXP/SGR in the early phase of its evolution: The LPPs are evolutionary descendants of AXP/SGRs. The model can reproduce the properties of these sources with the same disc parameters ($\alpha = 0.045$, $C = (1-7) \times 10^{-4}$, and $T_{\rm p} = 50-150$ K) as those employed for the other young neutron star populations in earlier work. All isolated neutron star populations including AXP/SGRs, XDINs, HBRPs, CCOs, RRATs and the newly discovered LPPs can be explained in the fallback disc model with similar parameters of disc physics. The differences between the evolutionary paths arise from different initial conditions, namely the initial disc mass, magnetic dipole moment, and the initial period. We will continue to investigate the evolutionary links between all these populations in more detail in future work.

3.2 Model II with an Application to the Torque Reversals of 4U 1626–67

In this section, we will describe the critical conditions for the transition between the rotational phases, the $r_{\rm in}$ and torque calculations in the recently developed analytical model (Model II; Ertan, 2017, 2018, 2021) together with its application to the torque reversals of 4U 1626–67. This model will also be used to analyse the details of the long-term evolutionary links among the NS families in Chapter 4.

Sections 3.2.1, 3.2.2, and 3.2.3 were published in Astronomy & Astrophysics, February 2022, Volume A13. A. A. Gençali, N. Niang, O. Toyran, Ü. Ertan, A. Ulubay, S. Şaşmaz, E. Devlen, A. Vahdat, Ş. Özcan and M. A. Alpar

3.2.1 Introduction

Neutron stars in low-mass X-ray binaries (LMXBs) receive matter from their companion through the Roche-lobe overflow. The interaction between the magnetosphere and the accretion disk as well as the mass accretion onto the neutron star govern the X-ray luminosity and the rotational behavior of the star (for a review of disk accretion onto magnetic stars, see Lai, 2014). Comparing observations of these systems with the theoretical models, it is estimated that there are mainly three rotational phases of neutron stars in LMXBs; namely, the strong-propeller (SP), the weak-propeller (WP), and the spin-up (SU) phases. In the SP phase, all the inflowing mass is expelled from the inner boundary of the disk by the magnetic torques and the star spins down. In the WP phase, most of the matter from the inner disk is accreted onto the star, while the star slows down. In the SU phase, all the matter arriving at the inner disk flows onto the star along the closed magnetic field lines and the star spins up (Bildsten et al., 1997; Papitto & de Martino, 2020).

Accretion onto the star takes place when the inner disk radius, $r_{\rm in}$, is equal to or smaller than the co-rotation radius, $r_{\rm co}$, at which the angular frequency of the neutron star, Ω_*, equals the Keplerian angular speed, $\Omega_{\rm K}$, of the disk matter. In the models, for a given disk mass-flow rate, $\dot{M}_{\rm in}$, and magnetic dipole moment, μ, almost all the rotational and accompanying radiative properties of the star depend on the location of $r_{\rm in}$. The inner disc radius, $r_{\rm in}$, was conventionally estimated to be close to the Alfvén radius, $r_{\rm A} \simeq \left[\mu^4/(GM\ \dot{M}_{\rm in}^2)\right]^{1/7}$, determined by equating the magnetic and viscous stresses. Here G is the gravitational constant and M is the mass of the star (Davidson & Ostriker, 1973; Lamb, Pethick, & Pines, 1973). With $r_{\rm in} = r_\xi = \xi r_{\rm A}$ and $0.5 \leq \xi \leq 1$ (Arons, 1993; Ghosh & Lamb, 1979a; Illarionov & Siuniaev, 1975; Ostriker & Shu, 1995), these models encounter the following difficulties in explaining the characteristic X-ray luminosity, $L_{\rm X}$, and the rotational behavior of neutron stars in LMXBs (Archibald et al., 2009; Bassa et al., 2014; Bildsten et al., 1997; Jaodand et al., 2016; Papitto & de Martino, 2020; Papitto et al., 2013): (1) There is ongoing accretion with rates that are much smaller than the rate corresponding to the $r_{\rm A} = r_{\rm co}$ condition; (2) for a broad range of accretion rates $\dot{M}_{\rm in}$ (up to two orders of magnitude depending on the ξ, η, μ, and P parameters described in Sect. 3.2.2), spin-down continues while there is mass accretion onto the star; (3) the transition to the SP phase takes place at very low $\dot{M}_{\rm in}$ when $r_{\rm A} \gg r_{\rm co}$ (Archibald et al., 2015; Bassa et al., 2014; Papitto & de Martino, 2020; Papitto et al., 2015); (4) transitions occur between the spin-up and spin-down regimes with similar torque magnitudes without a significant change in $L_{\rm X}$ (Bildsten et al., 1997; Camero-Arranz, Finger, Ikhsanov, Wilson-Hodge, & Beklen, 2010; Chakrabarty, Bildsten, Finger, et al., 1997;

Chakrabarty, Bildsten, Grunsfeld, et al., 1997; Deeter, Boynton, Lamb, & Zylstra, 1989; İnam, Şahiner, & Baykal, 2009; Takagi et al., 2016).

In the early detailed models of disk-field interaction, accretion disks were assumed to be threaded by the closed magnetic field lines of the star (Ghosh & Lamb, 1979a, 1979b). Later, Y. M. Wang (1987) showed that this picture is not self-consistent because the winding of the toroidal field lines resulting from the disk-field interaction would destroy most of the disk. Magnetically threaded disk models also encounter difficulties in attempting to explain the abrupt torque reversals corresponding to small changes in the accretion rate. A series of works showed that the field lines interacting with the inner disk tend to inflate and open up when the toroidal field strength becomes comparable to that of the poloidal field (Aly & Kuijpers, 1990; Lovelace et al., 1995; Lynden-Bell & Boily, 1994; Uzdensky, 2002; van Ballegooijen, 1994). In the model proposed by Lovelace et al. (1995), this result was found to be applicable to the propeller phase as well (Lovelace et al., 1999; Ustyugova et al., 2006). In this model, the field lines and the inner disk interact in a narrow boundary region with ongoing opening and reconnection cycles of the magnetic field lines on dynamical timescales, while the field lines are decoupled from the disk outside the boundary region (see Sect. 3.2.2). This model was supported by the results of the numerical simulations (Goodson, Winglee, & Böhm, 1997; Hayashi, Shibata, & Matsumoto, 1996; Miller & Stone, 1997).

Adopting the basic principles of the model proposed by Lovelace et al. (1995, see Sect. 3.2.2), it was shown through analytic calculations within a new torque model that a steady SP phase can be established with a value of $r_{\rm in}$ that is much smaller than $r_{\rm A}$ (Ertan, 2017, 2018). Applying this model to the transitional millisecond pulsars (tMSPs), the critical $\dot{M}_{\rm in}$ level for the SP-WP transition was found to be consistent with the estimated accretion rates and the torque variations corresponding to transitions between the radio pulsar and X-ray pulsar states (Archibald et al., 2009; Bassa et al., 2014; Jaodand et al., 2016; Papitto & de Martino, 2020; Papitto et al., 2013). The extended version of this model, including the SU phase as well, can also account for the general torque-reversal characteristics summarized above (Ertan, 2021). The model estimates of $r_{\rm in}$ are seen to be much smaller than the conventional $r_{\rm A}$ in the SU phase as well. It is only for a narrow range of $\dot{M}_{\rm in}$, around the torque-reversal that $r_{\rm in}$ is found to trace r_{ξ} (for details, see Ertan, 2021).

In this subsection, we investigate the detailed torque-reversal behavior of 4U 1626–67 in the model proposed by Ertan (2021). Overall, 4U 1626–67 seems to be the best source for testing the thin disk torque-reversal models (for a detailed discussion, see Camero-Arranz et al., 2010), as the source shows torque reversals

purely by disk torques due to the lack of wind accretion from the companion. In addition, there are many period derivative and X-ray luminosity measurements available on either side of the torque reversal (Camero-Arranz et al., 2010; Takagi et al., 2016). 4U 1626–67 was first discovered with Uhuru in 1972 (Giacconi et al., 1972) in a 42 min ultracompact binary system, accreting matter from a companion with mass $M \sim 0.04\ M_{\odot}$, with some uncertainties depending on the inclination angle of the LMXB (Chakrabarty, 1998; Chakrabarty, Bildsten, Grunsfeld, et al., 1997; Levine et al., 1988; Middleditch, Mason, Nelson, & White, 1981). With a spin period of $P = 7.66$ s (Rappaport et al., 1977), the source shows torque reversals without a significant change in its X-ray luminosity ($L_{\rm X} \sim 10^{36} - 10^{37}$ erg s^{-1}; Camero-Arranz et al., 2010; Chakrabarty, Bildsten, Grunsfeld, et al., 1997). The distance is estimated to be in the $5 - 13$ kpc range (Chakrabarty, 1998; Takagi et al., 2016). Magnitudes of the measured period derivatives are in the range of $1.8 \times 10^{-12} < |\dot{P}| < 1.3 \times 10^{-10}$ s s^{-1} (Takagi et al., 2016, and references therein).

The detection of double-peaked emission lines in the X-ray band indicates the presence of an accretion disk (Schulz et al., 2001). A cyclotron line detected at ~ 37 keV corresponds to a surface magnetic field strength of $B \sim 3 \times 10^{12}$ G (Coburn et al., 2002; D'Aì, Cusumano, Del Santo, La Parola, & Segreto, 2017; Orlandini et al., 1998). While the X-ray flux increased by a factor of ~ 3 from 2006 to 2010, no concurrent changes in the magnetic field strength, as inferred from cyclotron line energies, accompanied the flux changes and associated torque reversals (Camero-Arranz et al., 2012). The range of inner disk radii recently estimated for 4U 1626–67 from the double-peaked emission lines observed with Chandra/LETGS (Hemphill, Schulz, Marshall, & Chakrabarty, 2021) indicates that $r_{\rm in} \simeq r_{\rm co}$ for plausible neutron star masses within the uncertainty in the disk inclination angle. During the torque reversals, the shape of the pulse profile changes, which could be a sign of a change in the emission geometry of the accretion column (Beri, Jain, Paul, & Raichur, 2014; Koliopanos & Gilfanov, 2016).

We summarize the model (Ertan, 2021) in Sect. 3.2.2 and discuss our results together with a summary of other torque-reversal models in Sect. 3.2.3. Our conclusions are summarized in Sect. 3.2.3.

3.2.2 The Model II

For the inner disk radius, $r_{\rm in}$, and the torque calculations, we used the model that was previously developed for neutron stars accreting from geometrically thin accre-

tion disks (for details, see Ertan, 2017, 2018, 2021). We describe the model in brief as follows. The inner disk interacts with the magnetic field lines in a boundary layer between $r_{\rm in}$ and $r_{\rm in}+\Delta r$. In this region, the closed field lines cannot slip through the disk since the interaction time-scale, $\tau_{\rm int} \simeq |\Omega_* - \Omega_{\rm K}|^{-1}$, is orders of magnitude shorter than the diffusion time-scale of the magnetic field lines (Fromang & Stone, 2009). In this boundary region, field lines inflate and open up within $\tau_{\rm int}$. In the SP phase, matter can be expelled from the inner disk along the open field lines. The open field lines reconnect on a dynamical timescale comparable to $\tau_{\rm int}$, completing the cycle. The field lines are decoupled from the disk at radii greater than $r_{\rm in}+\Delta r$ (Lovelace et al., 1999; Ustyugova et al., 2006).

A strong-propeller mechanism can be sustained at $r_{\rm in} > r_{\rm co} = (GM/\Omega_*^2)^{1/3}$, provided that the field lines can throw out all the matter flowing into the boundary region. This requires that the field lines are able to force the matter into co-rotation in the interaction boundary. The maximum inner disk radius, $r_{\rm in,max}$, at which this strong-propeller mechanism is satisfied is determined by the implicit condition (Ertan, 2017):

$$R_{\rm in,max}^{25/8}\,|1-R_{\rm in,max}^{-3/2}| \;\simeq\; 1.26\;\alpha_{-1}^{2/5}\;M_{1.4}^{-7/6}\;\dot{M}_{\rm in,16}^{-7/20}\;\mu_{30}\;P^{-13/12}, \tag{3.2}$$

where $R_{\rm in,max} = r_{\rm in,max}/r_{\rm co}$, and $\alpha_{-1} = (\alpha/0.1)$ is the kinematic viscosity parameter, $M_{1.4} = (M/1.4M_\odot)$, $\dot{M}_{\rm in,16} = \dot{M}_{\rm in}/(10^{16}\ {\rm g\ s^{-1}})$, $\mu_{30} = \mu/(10^{30}\ {\rm G\ cm^3})$, and P is the rotational period of the star. We define $r_\eta \equiv \eta\ r_{\rm in,max}$, where $\eta \leq 1$ is likely to be close to unity because of the sharp variation of magnetic torques with radial distance. In the SP phase, $r_{\rm in} = r_\eta$ is always found to be much smaller than $r_\xi = \xi r_{\rm A}$. For a given dipole field strength, the dependence of $r_{\rm in}$ on $\dot{M}_{\rm in}$ is much weaker than that of $r_{\rm A} \propto \dot{M}^{-2/7}$ in the SP phase.

The speed of the closed field lines rotating with the star is greater than the escape speed, $v_{\rm esc}$, outside the radius $r_1 = 1.26\ r_{\rm co}$, while it is smaller than the value of $v_{\rm esc}$ between $r_{\rm co}$ and r_1. A steady-state SP phase is possible only with $r_{\rm in} > r_1$. In the case that $r_{\rm in}$ is instantaneously between $r_{\rm co}$ and r_1, the field lines can effectively throw the matter from the inner disk, while the matter returns back to the disk at larger radii. Due to the growing pile-up of this matter, the inner disk moves inwards down to $r_{\rm in} = r_{\rm co}$, eventually switching to accretion mode, and then the system enters the WP phase. The SP-WP transition takes place when $r_{\rm in} = r_\eta = r_1$, and r_ξ is much greater than r_η and $r_{\rm co}$. In the WP phase, the inner disk cannot penetrate inside $r_{\rm co}$, while matter flows to the star from $r_{\rm co}$. For the inner disk to protrude inside $r_{\rm co}$, the viscous stresses should dominate the magnetic stresses at this radius. With increasing $\dot{M}_{\rm in}$, r_ξ approaches $r_{\rm co}$ in the WP phase. The inner disk

starts to propagate inwards of $r_{\rm co}$ when $\dot{M}_{\rm in}$ exceeds the critical rate corresponding to $r_\xi = r_{\rm co}$ (for details, see Ertan, 2021). The torque reversal takes place at a certain $\dot{M}_{\rm in}$, when $r_{\rm in} = r_{\rm co}$, and r_ξ is close to $r_{\rm co}$ depending on the actual value of ξ.

In the SU phase, a steady $r_{\rm in}$ cannot be established at r_ξ beyond a certain $\dot{M}_{\rm in}$ level. The inner disk extends inwards opening the field lines until $r_{\rm in} = r_\eta$, which is the stable inner disk radius corresponding to the same accretion rate $\dot{M}_*$. For higher accretion rates, $r_{\rm in}$ tracks r_η, which could be several times smaller than r_ξ depending on the magnetic dipole moment and the period of the source. Considering that the field lines are decoupled from the disk for $r > r_{\rm in} + \Delta r$, we estimate that the spin-down torque, $\Gamma_{\rm D}$, switches off when $r_{\rm in}$ enters inside $r_{\rm co}$ by a small radial extent comparable to Δr (for a detailed description, see Ertan, 2021).

The total torque acting on the star can be expressed as:

$$\Gamma = -\frac{\mu^2}{r_{\rm in}^3}\left(\frac{\Delta r}{r_{\rm in}}\right) + \sqrt{GMr_{\rm in}}\,\dot{M}_* + \Gamma_{\rm dip}, \tag{3.3}$$

where the first term is the spin-down torque, $\Gamma_{\rm D}$, produced by the interaction between the inner disk and the magnetic field of the star in the narrow boundary region with radial width $\Delta r < r$. The second term is the spin-up torque, $\Gamma_{\rm acc}$, associated with the mass accretion from the inner disk onto the star (Pringle & Rees, 1972). We note that $\dot{M}_*$ is the accretion rate onto the star, while $\dot{M}_{\rm in}$ denotes mass inflow-rate of the disk. The magnetic dipole torque, $\Gamma_{\rm dip} \simeq -2\mu^2\Omega_*^3/3c^3$, where c is the speed of light, also contributes to the spin-down torque, and this is, in most cases, negligible in comparison with $\Gamma_{\rm D}$. In the SP phase ($r_{\rm in} = r_\eta > r_1$), there is no mass accretion onto the star and thus $\Gamma_{\rm acc} = 0$. In the WP phase, both spin-up and spin-down torques are active with $r_{\rm in} = r_{\rm co}$. In this phase, with an increasing accretion rate, $|\Gamma_{\rm acc}|$ increases, while $|\Gamma_{\rm D}|$ remains constant, since $r_{\rm in} = r_{\rm co}$ persists for a large $\dot{M}_*$ range in the WP phase. Eventually, at a certain $\dot{M}_*$, the spin-up and spin-down torques are balanced, and the system makes a transition to the SU phase (torque reversal). We note that the torque reversal does not necessarily take place when r_ξ is exactly equal to $r_{\rm co}$. Nevertheless, our results indicate that these two radii are close to each other during the torque reversals. With increasing $\dot{M}_{\rm in}$, $r_{\rm in}$ enters inside $r_{\rm co}$ tracking r_ξ for a narrow range of $\dot{M}_*$. Outside this $\dot{M}_{\rm in}$ range, $r_{\rm in}$ is significantly smaller than r_ξ, depending on B, P, and $\dot{M}_{\rm in}$ (for a detailed description, see Ertan, 2021).

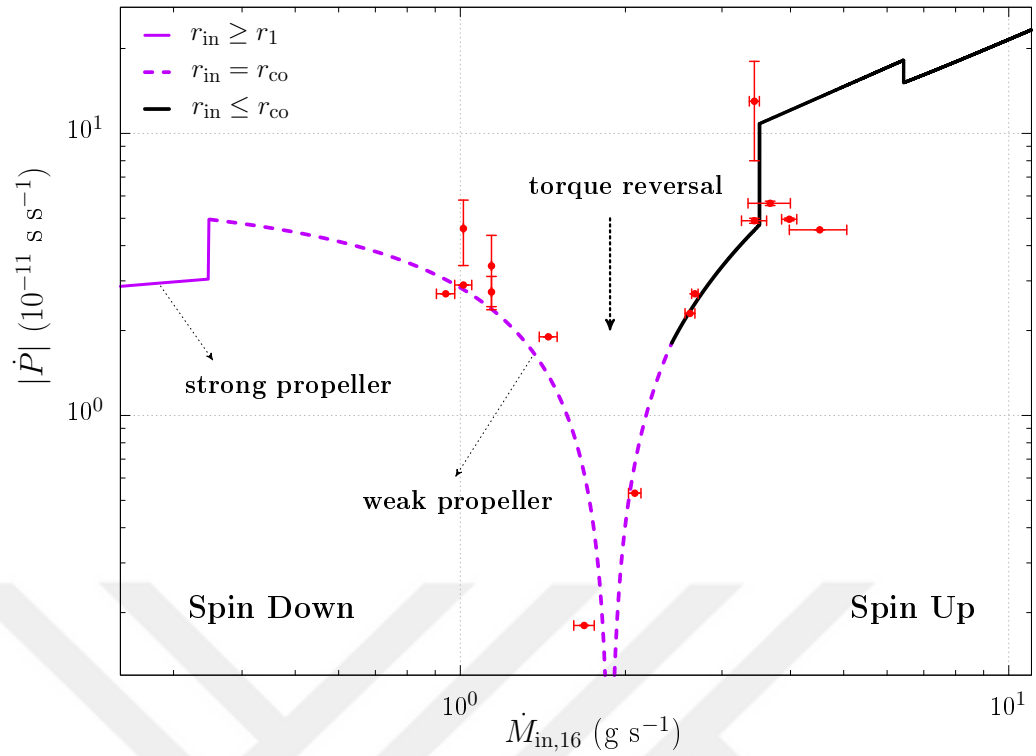

(a) $\xi = 0.68$

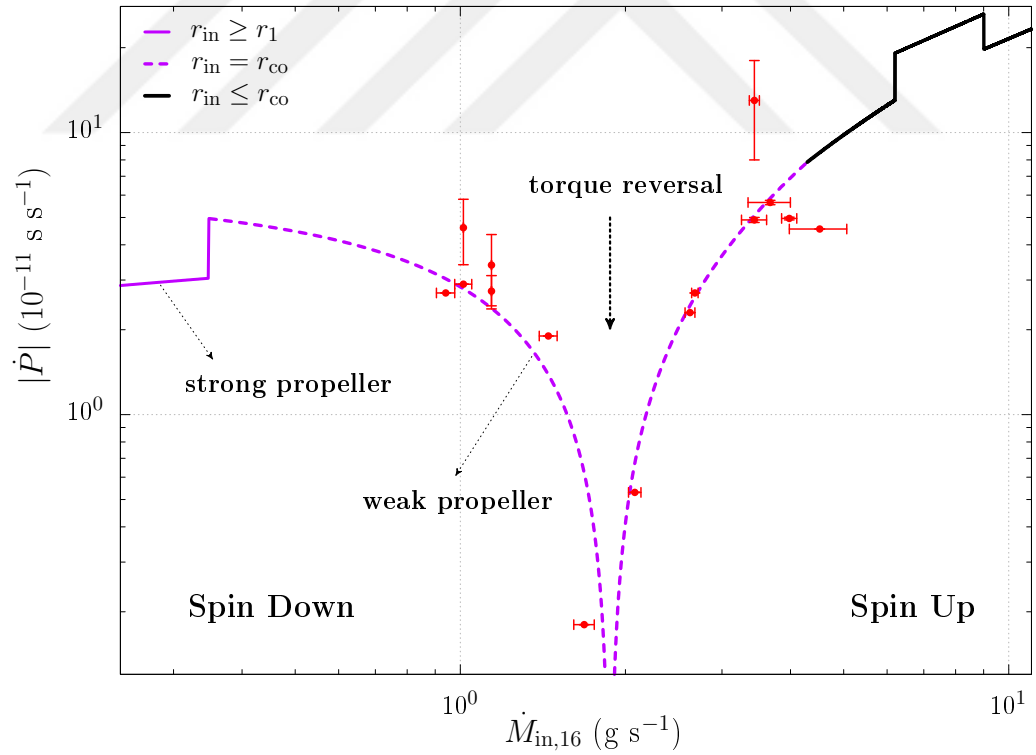

(b) $\xi = 0.80$

Figure 3.7 Torque reversal of 4U 1626–67 for different ξ values. The model parameters are $B = 3 \times 10^{12}$ G, $\Delta r/r = 0.2$, $\eta = 1$, $d = 5.3$ kpc. We obtained the data from Takagi et al. (2016, and references therein). For both models, the spin-down torque is inactivated when $r_{\rm in} = r_{\rm co} - \Delta r/2$ (see the text for details).

3.2.3 Application to the Torque Reversals of 4U 1626–67

We take the measured $\dot{P}$ and bolometric X-ray flux, $F_{\rm x,bol}$, values of the source from Takagi et al. (2016, and references therein). The distance, d, has an estimated range from 5 to 13 kpc (Chakrabarty, 1998; Takagi et al., 2016). Our model calculations are sensitive to $\dot{M}_*$ (and thus to the distance). The $F_{\rm x,bol}$ values are converted to bolometric X-ray luminosity and $\dot{M}_*$ using $L_{\rm X} = 4\ \pi\ d^2\ F_{\rm x,bol} = GM\dot{M}_*/R_*$ neglecting beaming effects. The beaming correction was estimated to be at most 50% for Her X-1 (Basko & Sunyaev, 1975). Due to similarity of the two sources, Takagi et al. (2016) estimated a similar correction for 4U 1626–67. In this case, we obtain reasonable model fits with somewhat larger distances. For instance, if the actual beaming correction is 50%, the same model fit given in Fig. 3.7 is obtained with a $\sim 40\%$ larger distance (~ 7.5 kpc), while still remaining within the estimated distance range. In our model, the relation between the torques and the accretion rates is obtained for steady-state disks. Torque reversals are short-term events and during these transitions, there could be fluctuations in the local mass inflow rate, X-ray luminosity, and structure of the inner disk that could deviate from the steady-state disk properties. Since these time-dependent fluctuations are not addressed in our model, we looked for the seemingly best fits to the observed data without performing a χ^2 test. We obtained the model curves in Fig. 3.7, tracing the critical $\dot{M}_*$ values for the torque reversal and the corresponding B values for the period of 4U 1626–67. It is seen in Fig. 3.7 that the model produces the observed torque reversal of 4U 1626–67 quite well. Reasonable model curves are obtained with $B \simeq 3 \times 10^{12}$ G, and the torque-reversal takes place at $\dot{M}_* \simeq 1.9 \times 10^{16}$ g s^{-1} , which corresponds to $d \simeq 5.3$ kpc. For larger distances, d, which require greater B and higher $\dot{M}_*$ values during the torque reversal, the model cannot reproduce the observed $\dot{M}_{\rm in} - \dot{P}$ relation (see Fig. 3.8).

The critical $\dot{M}_{\rm in}$ for the torque reversal is sensitive to the ξ parameter. For $0.63 < \xi < 1$, the torque reversal takes place when $r_{\rm in} = r_{\rm co}$ and $r_\xi \gtrsim r_{\rm co}$ with reasonable model fits. For instance, for the models seen in Fig. 3.7, the WP-SU transitions take place when, $r_\xi \simeq 1.07\ r_{\rm co}$ for $\xi = 0.68$ and $r_\xi \simeq 1.27\ r_{\rm co}$ for $\xi = 0.80$. For this range of ξ, the rotational equilibrium is obtained at the same $\dot{M}_{\rm in}$. For $0.50 < \xi < 0.63$, r_ξ penetrates within $r_{\rm co}$ while the spin-down torque is still dominant. In this case, the spin-down torque is switched off and the torque changes sign at a relatively low value of $\dot{M}_{\rm in}$. This type of torque reversal gives reasonable model curves only for a very narrow range of ξ ($0.60 - 0.63$), favoring $r_{\rm in} = r_\xi$ and $r_\xi \lesssim r_{\rm co}$ during the torque reversal.

In Fig. 3.7, the sharp increase in $\dot{P}$ in the spin-up regime is due to the inactivation of the spin-down torque, $\Gamma_{\rm D}$, while the subsequent sharp decrease is produced by the rapid inward propagation of $r_{\rm in}$ from r_ξ to r_η, as described in Sect. 3.2.2. Figure 3.7 illustrates how these features depend on the ξ parameter. The abrupt rise in $\dot{P}$ during the SP-WP transition corresponds to the inward motion of $r_{\rm in}$ from r_1 to $r_{\rm co}$, which results from the growing pile-up at the inner disk when $r_{\rm in}$ gets into the range between $r_1 = 1.26\ r_{\rm co}$ and $r_{\rm co}$ (See Sect. 3.2.2). The η parameter affects the critical $\dot{M}_{\rm in}$ for the SP-WP transition, while it does not change the critical $\dot{M}_{\rm in}$ or the morphology of the torque reversal. With smaller η values, the SP-WP transition takes place at lower $\dot{M}_{\rm in}$ levels.

Illustrative model curves showing the dependence of torque-reversal characteristics on the model parameters were given by Ertan (2021). These model curves indicate that the morphologies of the torque reversals are likely to be similar for sources with very different dipole moments, periods, and accretion rates during the torque reversals, assuming that all these systems have similar ξ and η values and that they are not affected by the winds of their companions. This is a testable prediction of the model in addition to the abrupt torque variations without significant changes in $L_{\rm X}$ in the SU phase (see Fig. 3.7).

Recently, Benli (2020) showed that the torque-reversal behavior of 4U 1626–67 can be accounted for based on the assumption that $r_{\rm in}$ remains equal to $r_{\rm co}$ before and after the torque reversal without addressing the physical reason for this behavior and the condition for $r_{\rm in}$ to penetrate inside $r_{\rm co}$. Investigating the functional behavior of the torque reversal of the same source, Türkoğlu, Özsükan, Erkut, and Ekşi (2017) found that the torque variation as a function of $\dot{M}_*$ contradicts the estimates of the conventional models that assume the torque reversal occurs when $r_\xi = \xi r_{\rm A} = r_{\rm co}$.

There have been different proposals and models proposed to explain the physical mechanism of the torque reversal. The transition of a warped disk into a retrograde regime was suggested as the reason for the spin-up-spin-down transition (Beri, Paul, & Dewangan, 2015; Chakrabarty, Bildsten, Grunsfeld, et al., 1997; Makishima et al., 1988; Nelson et al., 1997; van Kerkwijk, Chakrabarty, Pringle, & Wijers, 1998; Wijers & Pringle, 1999). The difficulty related to this model is that there is evidence for the presence of a prograde disk in the spin-down phase from the quasi-periodic oscillation analysis (van Kerkwijk et al., 1998). Another idea is related to the variation of $r_{\rm in}$ due to transitions of the inner disk between the optically thin and thick regimes (H. L. Dai & Li, 2006; Vaughan & Kitamoto, 1997; Yi & Vishniac, 1999; Yi, Wheeler, & Vishniac, 1997). In this model, the inner disk is Keplerian in the optically thick state, while the mass inflow is spherical-like and sub-Keplerian in the

optically thin state. For 4U 1626–67, with a high accretion rate ($\dot{M}_{\rm in} > 10^{16}$ g s^{-1}) and large radius ($r_{\rm in} \sim 7 \times 10^8$ cm) during the transition, the inner disk is likely to be optically thick. For comparison, tMSPs are estimated to have optically thick disks in their sub-luminous ($L_{\rm X} \sim 10^{33}$ erg s^{-1}) LMXB states with $r_{\rm in} \sim 20$ km (Papitto & de Martino, 2020). Lovelace et al. (1999) proposed that the spin-down torque is produced by a strong propeller mechanism throwing most of the inflowing matter out of the system when $r_{\rm in} > r_{\rm co}$. The propeller mechanism is switched off, accretion onto the star is allowed, and the star spins up when $r_{\rm in} < r_{\rm co}$. The transitions between the two phases, which are stochastic in nature, could take place at different accretion rates, with small variations in the disk mass-flow rate or in the magnetic field configuration. This model can reproduce the transitions with comparable torque magnitudes, but has trouble when it comes to the observed torque reversals with small variation in $L_{\rm X}$.

In the model proposed by Perna, Bozzo, and Stella (2006), the disk-magnetosphere interaction for an oblique rotator leads to a cyclic variation in the accretion-rate, $\dot{M}_{\rm acc}$, while the mass-flow rate from the outer disk is constant. In this model, in the propeller phase, a fraction of the inflowing matter that is ejected from the inner disk returns to the disk at larger radii, which is the reason for the $\dot{M}_{\rm acc}$ variation. Neglecting the magnetic torques, Perna et al. (2006) proposed that the changes in the material torques arising from the accretion-propeller transition that is due to the changes in $\dot{M}_{\rm acc}$ could be responsible for the observed torque reversal. As discussed by these authors, during the torque-reversal, a significant $L_{\rm X}$ variation is estimated in the model, which is not in agreement with the observed torque reversal of 4U 1626–67. We do not encounter this luminosity problem in our model because there is mass accretion onto the star on either side of the torque reversal.

Conclusions:

In this subsection, we show that the torque reversal behavior of 4U 1626–67, the only source known thus far with Roche-lobe overflow and a likely thin disk, and observed through torque reversals, can be reproduced in the comprehensive model developed by Ertan (2021) that expands upon earlier works on the SP/WP transition (Ertan, 2017, 2018) to include the torque reversal and the SU phase as well. The model calculates the inner disk radius, torque, and X-ray luminosity as functions of the mass-flow rate for neutron stars accreting from steady, geometrically thin accretion disks. In the model, the observed torque reversals are produced naturally when the system makes transitions between the WP and SU phases with an accretion disk that remains geometrically thin (optically thick) across the torque reversal. We

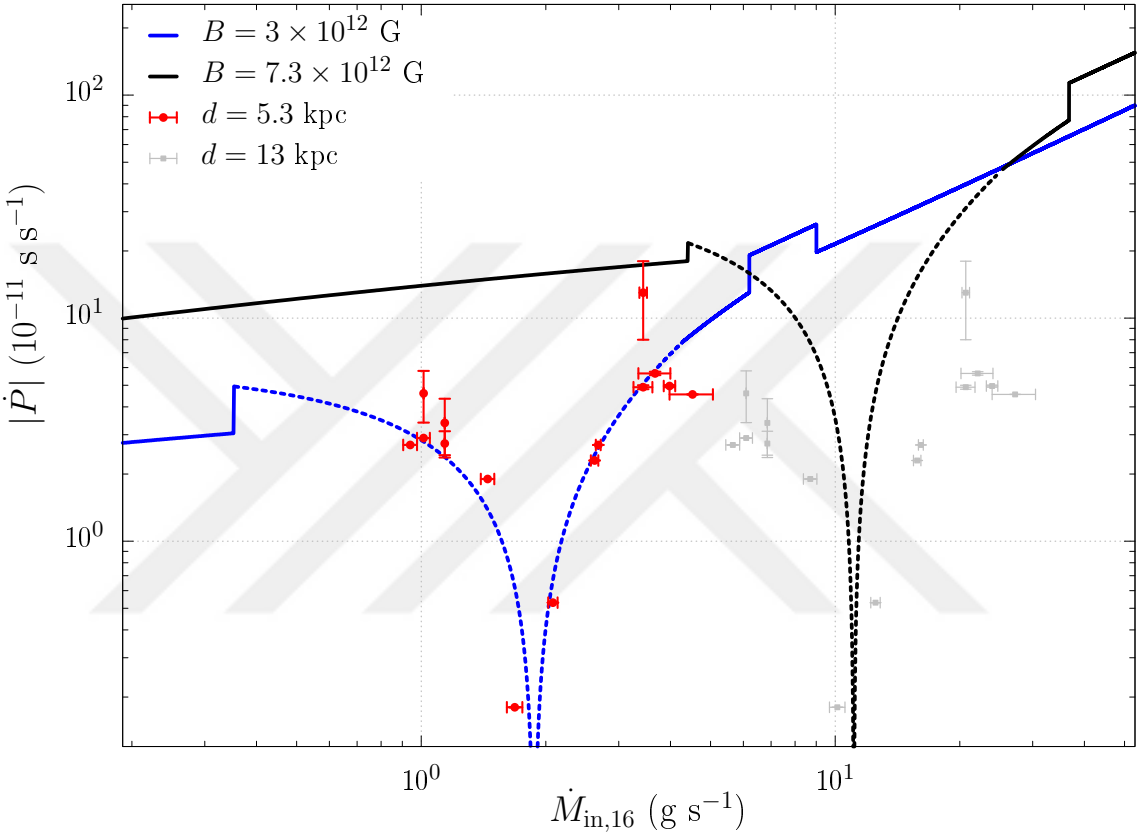

Figure 3.8 Illustrative model curves with torque-reversals corresponding to $\dot{M}_{\rm in}$ values. The blue model curve is the same as given in Fig. 3.7b ($\Delta r/r = 0.2$, $\eta = 1$ and $\xi = 0.8$). The black curve is also obtained with the same disk parameters, but for a larger distance that requires a stronger B and a higher $\dot{M}_{\rm in}$ during the torque reversal. The magnetic field B and distance d values used in the models are given in the figure. It is clearly seen that the model with the larger d cannot reproduce the data (grey data points).

have obtained reasonable model curves with $B \simeq 3 \times 10^{12}$ G and $d \simeq 5.3$ kpc, which produce the torque reversal at an accretion rate of $\dot{M}_* \simeq 1.9 \times 10^{16}$ g s^{-1} (Fig. 3.7). This field strength is in agreement with the B values estimated from the observed cyclotron lines in the $(2.4 - 6.3) \times 10^{12}$ G range (Chakrabarty, 1998; Coburn et al., 2002; D'Aì et al., 2017; Orlandini et al., 1998) and the distance is close to the lower edge of the estimated distance range of $5 - 13$ kpc (Chakrabarty, 1998; Takagi et al., 2016).

We find that $r_{\rm in} = r_{\rm co}$, and r_ξ is close to, but not necessarily equal to $r_{\rm co}$ during the torque reversal. A strong indication in support of our model results is that both spin-down and spin-up torques are operating on either side of the torque reversal. The spin-down torque produced by the disk-field interaction remains roughly constant during the WP phase and across the torque reversal. With increasing $\dot{M}_*$ in the WP phase, the accretion torque gradually dominates the spin-down torque, decreasing the magnitude of the net spin-down torque, and eventually the neutron star makes a transition to the SU phase. The magnitudes of the net spin-down and spin-up torques on either side of the transition are found to be naturally commensurate in this model.

3.3 Long-term Evolution with Model II

3.3.1 A Comparison with Model I

Details of Model I and Model II are described in Sections 3.1.1 and 3.2.2 respectively. Here we summarise the differences between these two models in the torque and $L_{\rm X}$ calculations in the SU, WP, and SP phases, as well as in the critical conditions for the transition between these phases.

Spin-Up (SU) Phase:

During the long-term evolution, isolated NS populations almost never enter this phase. In Model I, $r_{\rm in} = r_{\rm co}$ when accretion is allowed in both spin-up and spin-down regimes. In Model II, there is a well-defined condition for $r_{\rm in}$ to penetrate into

$r_{\rm co}$ (see Section 3.2.2), which also approximately corresponds to WP/SU transition (torque reversal) in this model. With increasing $\dot{M}_{\rm in}$ above this critical level, $r_{\rm in}$ approaches the star as described in Section 3.2.2.

Weak-Propeller (WP) Phase:

In this phase, $r_{\rm in} = r_{\rm co}$ and all the inflowing mass is accreted on to the star from this radius in both models. When, Model I was developed there was no well-known theoretical condition for WP/SP transition that is consistent with observations. The $\dot{M}_{\rm in}$ level corresponding to $r_{\rm A} = r_{\rm co}$ was assumed to be the critical condition for the WP/SU transition, and system remains in the WP phase when $r_{\rm co} < r_{\rm A} < r_{\rm LC}$. In Model II, the WP/SP transition condition is $r_{\rm in} = r_1$, and $r_{\rm in} = r_\eta$ is calculated from Equation 3.2 in the SP phase. Depending on the B_0 and current P values, the source could remain in the WP phase for a large range of $\dot{M}_{\rm in}$ while $r_{\rm in} = r_{\rm co}$, and for given $\dot{M}_{\rm in}$ and B_0, the net torque acting on the star as well as $L_{\rm X}$ are found to be similar in the two models.

Strong-Propeller (SP) Phase:

For both models, $L_{\rm X} = L_{\rm cool}$ in this phase. In Model I, $\Gamma_{\rm D}$ is calculated replacing $r_{\rm A}$ with $r_{\rm LC}$ in Eq. 3.1 while $r_{\rm in} \simeq r_{\rm co}$ in the SP phase. This is equivalent to the case that $r_{\rm in} \propto \dot{M}_{\rm in}^{-1/3}$ while $\Gamma_{\rm D}$ equals the magnetic torque integrated between the current $r_{\rm in}$ and $r_{\rm LC}$. In Model II, $r_{\rm in} = r_\eta$ (Eq. 3.2), and $\Gamma_{\rm D}$ is found by integrating the magnetic torques within a narrow interaction boundary with radial width $\Delta r < r_{\rm in}$ in the SP phase. Due to the sharp $r_{\rm in}$ dependence of the magnetic torques, $\Gamma_{\rm D}$ is found to be similar in the two models for given $r_{\rm in}$, $\dot{M}_{\rm in}$, and B_0 values. Nevertheless, $\dot{M}_{\rm in}$ dependence of $r_{\rm in}$ in the SP phase is different in the two models. From Eq. 3.3, it can be shown that $r_{\rm in} \propto \dot{M}_{\rm in}^{-14/125}$ in Model II. This leads to a disparity in rotational evolutionary routes in the two models. From the demonstrative model curves given in Fig. 3.9, it is seen that the $\dot{P}$ decay with decreasing $\dot{M}_{\rm in}$ is faster in Model I. This discrepancy gives rise to additional evolutionary links in Model II (see Section 4.2).

Both models can produce the properties of a given source with small differences in the initial conditions. For instance, rotational properties of a particular source can be reproduced with a somewhat higher B_0 (within a factor of ~ 2) in Model II than in Model I. To reproduce different source properties in a self-consistent way, the minimal cooling curve works better in Model I, while better results are obtained with maximal cooling curve in Model II (Page et al., 2006, 2009). In addition,

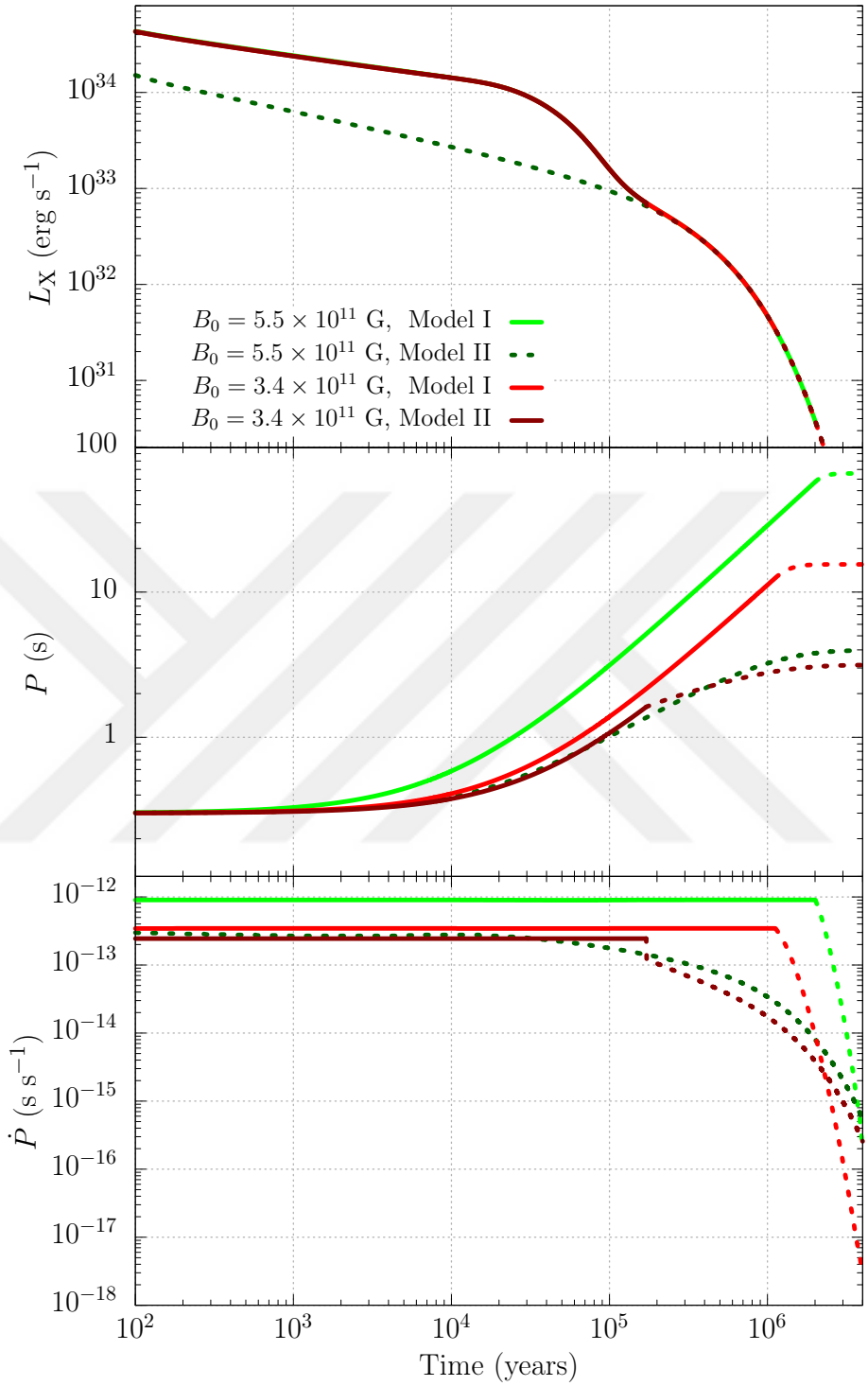

Figure 3.9 Illustrative model curves for Model I and Model II. For all the curves, $\alpha = 0.045$, $C = 7 \times 10^{-4}$, $T_p = 67$ K, $P_0 = 0.3$ s, and $M_d = 3.2 \times 10^{-6}\ M_\odot$. For Model II we take, $\Delta r/r = 0.25$, $\eta = 0.7$, and $\xi = 0.7$. The B_0 values are given in the upper panel. Solid and dashed segments of the curves correspond to the WP and SP phases respectively.

during the initial phases of evolution, the SP/WP transition requires greater P_0 and/or higher $M_{\rm d}$ for a given B_0 in Model II. In both models, it is the value of B_0 that yields characteristic distinctions in the long-term evolutionary avenues, which are discussed in the following section.

3.3.2 Effects of the Initial Conditions on the Long-term Evolution

The disc parameters α, C, and $T_{\rm p}$ are discussed in Section 3.1.1. These parameters are estimated to be similar for the fallback discs of different NS populations. In our earlier work, we obtained reasonable results with $\alpha = 0.045$, $C = (1-7)\times10^{-4}$, and $T_{\rm p} = 50-150$ K for all NS populations (Benli & Ertan, 2016, 2017, 2018a, 2018b; Ertan et al., 2014; Gençali & Ertan, 2018, 2021; Gençali et al., 2022, 2023; Özcan et al., 2020). A detailed parameter study with illustrative model curves can be found in e.g. Ertan et al. (2009a), Ertan et al. (2014), and Benli and Ertan (2016).

In this section, we will show how the initial conditions, namely B_0, $M_{\rm d}$, and P_0, alter the long-term evolutionary paths. In this study, we take $\alpha = 0.045$, $C = 1\times10^{-4}$, and $T_{\rm p} = 50$ K for all illustrative model sources.

Initial period, P_0:

We obtained the model curves in Fig. 3.10 by changing P_0 only. The dashed and solid curves show the SP and WP phases respectively. For given B_0 and $M_{\rm d}$, there is a critical P_0, such that the sources with P_0 longer than this critical value starts its evolution in the WP phase, while the sources with smaller P_0 are in the SP phase during the initial phase of evolution. This critical P_0 is around 200 ms for the sources ($B_0 = 6\times10^{11}$ G, $M_{\rm d} = 9.6\times10^{-6}$ $M_\odot$) seen in Fig. 3.10.

For the systems that enter the WP phase at an early time of the evolution, the rotational properties achieved in the late phases of evolution, with $P \gtrsim$ several seconds, are not sensitive to P_0. For instance, in Fig. 3.10, the sources with P_0 values of 0.3 and 0.7 s are seen to evolve converging to the same P and $\dot{P}$ levels. These sources make a transition from the WP phase to the SP phase at an age $\sim 2\times10^5$ yr. Afterwords, their X-rays are produced by $L_{\rm cool}$. In Fig. 3.10, the sources with P_0 values of 0.03 and 0.1 s are evolving in the SP phase over their entire lifetime. These sources also show similar rotational and $L_{\rm X}$ evolution.

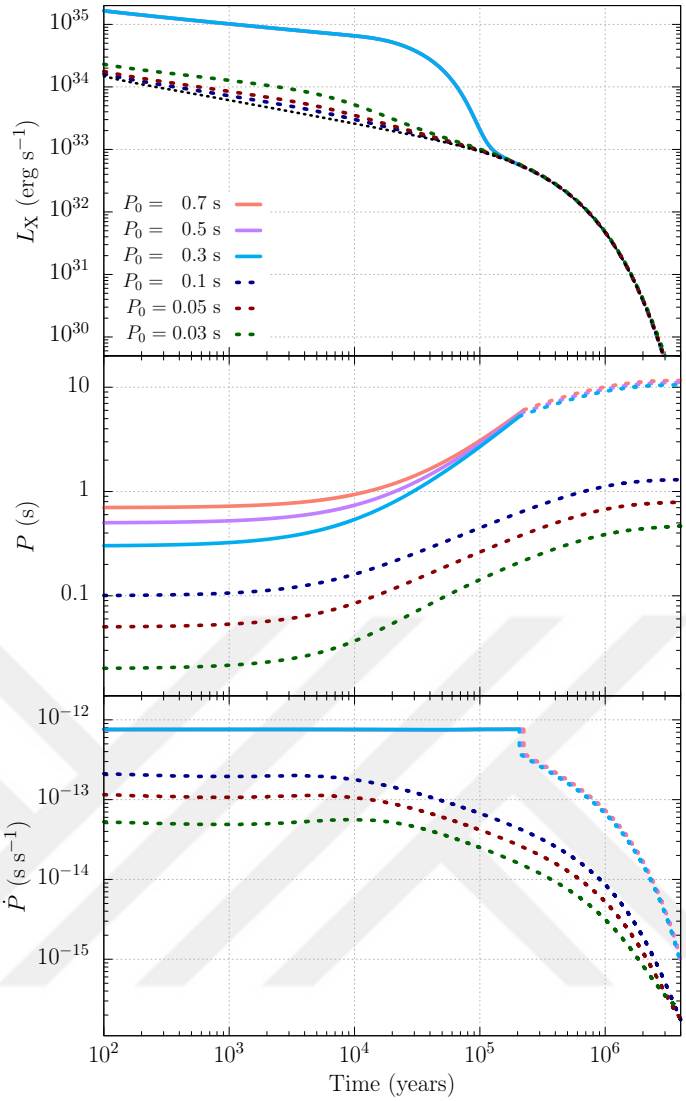

Figure 3.10 Illustrative model curves for different P_0 values (given in the upper panel). For all the curves, $\Delta r/r = 0.25$, $\eta = 0.7$, $\xi = 0.7$, $\alpha = 0.045$, $T_{\rm p} = 50$ K, $C = 1 \times 10^{-4}$, $B_0 = 6 \times 10^{11}$ G, and $M_{\rm d} = 9.6 \times 10^{-6}$ $M_\odot$. The dotted black curve in the top panel shows the theoretical maximal cooling curve (Page et al., 2006, 2009).

Disc mass, $M_{\rm d}$:

For numerical calculations, we initially set $r_{\rm out} = 5 \times 10^{14}$ cm. After the first time step, the dynamical outer radius of the disc, $r_{\rm out}$, tracks the radius at which currently $T_{\rm eff} = T_{\rm p}$. The initial disc mass is calculated by integrating the disc surface density profile, $\Sigma(r) = \Sigma_0 (r/r_{\rm in})^{-3/4}$, from $r_{\rm in}$ to $r_{\rm out} = 5 \times 10^{14}$ cm. That is, the $M_{\rm d}$ value for a particular source may not reflect the actual initial mass of the disc. For a sufficiently large initial $r_{\rm out}$, it is the value of Σ_0 that determines the $\dot{M}_{\rm in}$, and thus $L_{\rm X}$ evolution of that source. A relatively high value of $M_{\rm d}$ yields $\dot{M}_{\rm in}$ and $L_{\rm X}$ evolutions at higher levels.

We obtained the model curves in Fig.3.11 for different $M_{\rm d}$ values, using the same

B_0 and P_0 values. For the sources starting the evolution in the WP phase, there is a critical minimum $M_{\rm d}$. For smaller $M_{\rm d}$ the sources initially evolves in the SP phase. For instance, for the model parameters given in Fig. 3.11, this critical $M_{\rm d}$ is $\sim 10^{-5}\ M_\odot$. It is seen that the evolutionary paths passing through the WP phase reach relatively long periods. For these sources, the rotational properties acquired in the late phases of evolution are not sensitive to $M_{\rm d}$. It is seen in Fig. 3.11, that about an order of magnitude difference in $M_{\rm d}$ does not change the rotational evolution significantly. Similarly, P and $\dot{P}$ evolutions of the sources in the SP phase are not sensitive to $L_{\rm X}$ history either.

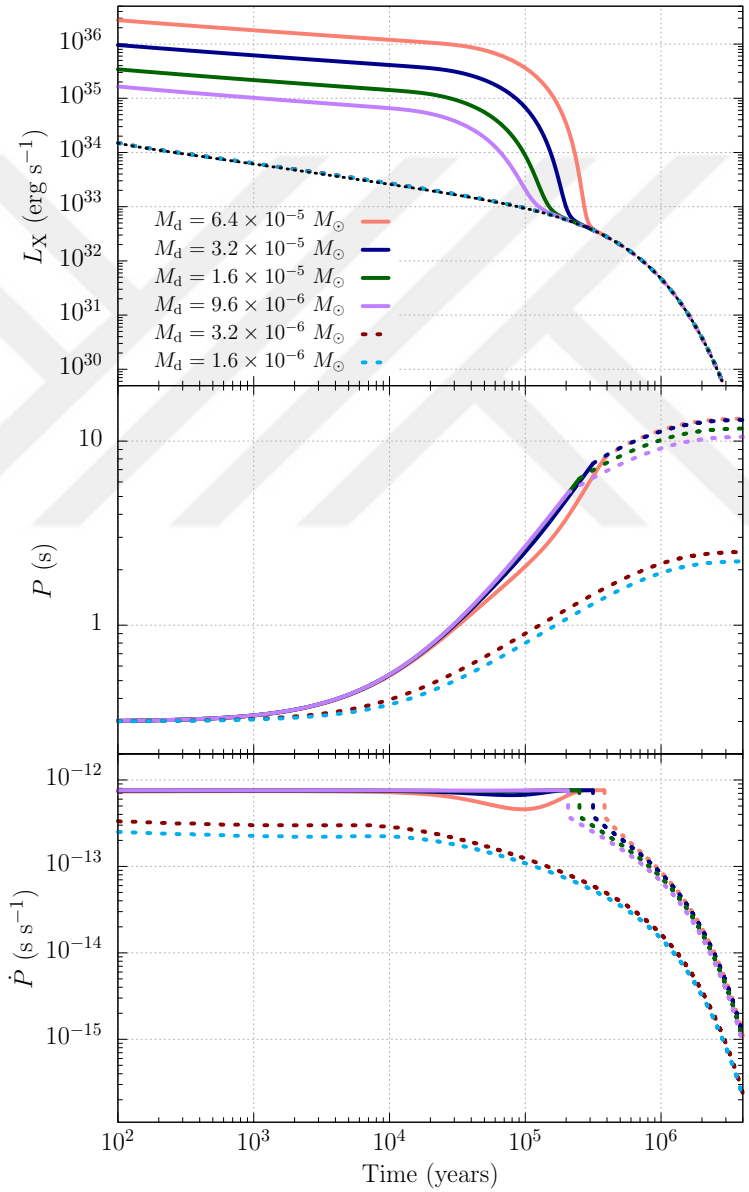

Figure 3.11 Illustrative model curves for different $M_{\rm d}$ values. For all the curves, $\Delta r/r = 0.25$, $\eta = 0.7$, $\xi = 0.7$, $\alpha = 0.045$, $T_{\rm p} = 50$ K, $C = 1 \times 10^{-4}$, $P_0 = 0.3$ s, and $B_0 = 6 \times 10^{11}$ G. The M_d values are given in the upper panel. Dotted black curve in the top panel shows the theoretical maximal cooling curve (Page et al., 2006, 2009).

Magnetic dipole field strength, B_0:

In Fig. 3.12, the models are generated with different B_0 values without changing $M_{\rm d}$ and P_0. As seen in the figure, small differences in B_0 yield significant variation in the rotational evolutionary curves. The value of B_0 seems to be the most important factor that determines the fate of the sources basically through the interaction between the inner disc and the magnetosphere of the source. Because $\Gamma_{\rm D}$, the dominant torque in both SP and WP phases, is very sensitive to B_0.

For given P_0 and $M_{\rm d}$ values, there are three different typical evolutionary avenues depending on the dipole field strength B_0: (i) SP+WP+SP with high B_0 values. Initialy, high B_0 prevents the penetration of the inner disc into r_1, and these sources begin their evolution in the SP phase. Strong spin-down torque $\Gamma_{\rm D}$ associated with high B_0, rapidly slows down the sources. The inner disc approaches and eventually penetrate into r_1 taking the system from the SP to the WP phase. After a long-term evolution in the WP phase, the star returns to the SP phase below a certain $\dot{M}_{\rm in}$. (ii) Permanent SP phase with intermediate B_0 values. For these systems, the dipole field is strong enough to keep the inner disc outside r_1, while it is not sufficiently strong for $r_{\rm in}$ to catch r_1 during the entire evolution. These sources always remain in the SP phase. (iii) WP+SP with low B_0 values. The dipole field is sufficiently weak, such that, initially $r_{\rm in} < r_1$ and the evolution starts in the WP phase. Like in case (i), the star enters the SP phase below a critical $\dot{M}_{\rm in}$ level. For very low B_0 values ($\lesssim 10^{10}$ G), the evolution could start in the SU phase as well. With decreasing $\dot{M}_{\rm in}$, the system reaches the rotational equilibrium, and subsequently makes a transition to the WP phase. Finally, when $\dot{M}_{\rm in}$ decrease below a critical level the source enter the SP phase.

These evolutionary paths described above can be seen from Fig. 3.12. Sources with $B_0 \gtrsim 3 \times 10^{12}$ follow the evolutionary path (i). Evolutionary curves with $B_0 \sim 6 \times 10^{11} - 2 \times 10^{12}$ G show the evolution described in case (ii). The sources with $B_0 \lesssim 5 \times 10^{11}$ G evolve as described in case (iii). It is important to note that these ranges of B_0 values depend on the other initial conditions.

In Fig. 3.12, it is also seen that the periods of the sources with extremely strong B_0 ($\gtrsim 10^{13}$ G) increases sharply, which is not consistent with the rotational behaviour of AXP/SGRs and other NS populations. This is the main reason for the fallback disc model to explain the source properties of these systems only with conventional dipole field strengths.

Some sources could approach the rotational equilibrium in the WP phase depending on the values of $M_{\rm d}$ and B_0. This happens when $\Gamma_{\rm acc}$ becomes comparable to the

$\Gamma_{\rm D}$. This leads to a transient decrease in the magnitude of the net spin-down torque. The minimum in the upper $\dot{P}$ curve ($B_0 = 1 \times 10^{13}$ G) in Fig. 3.12 is produced by this effect.

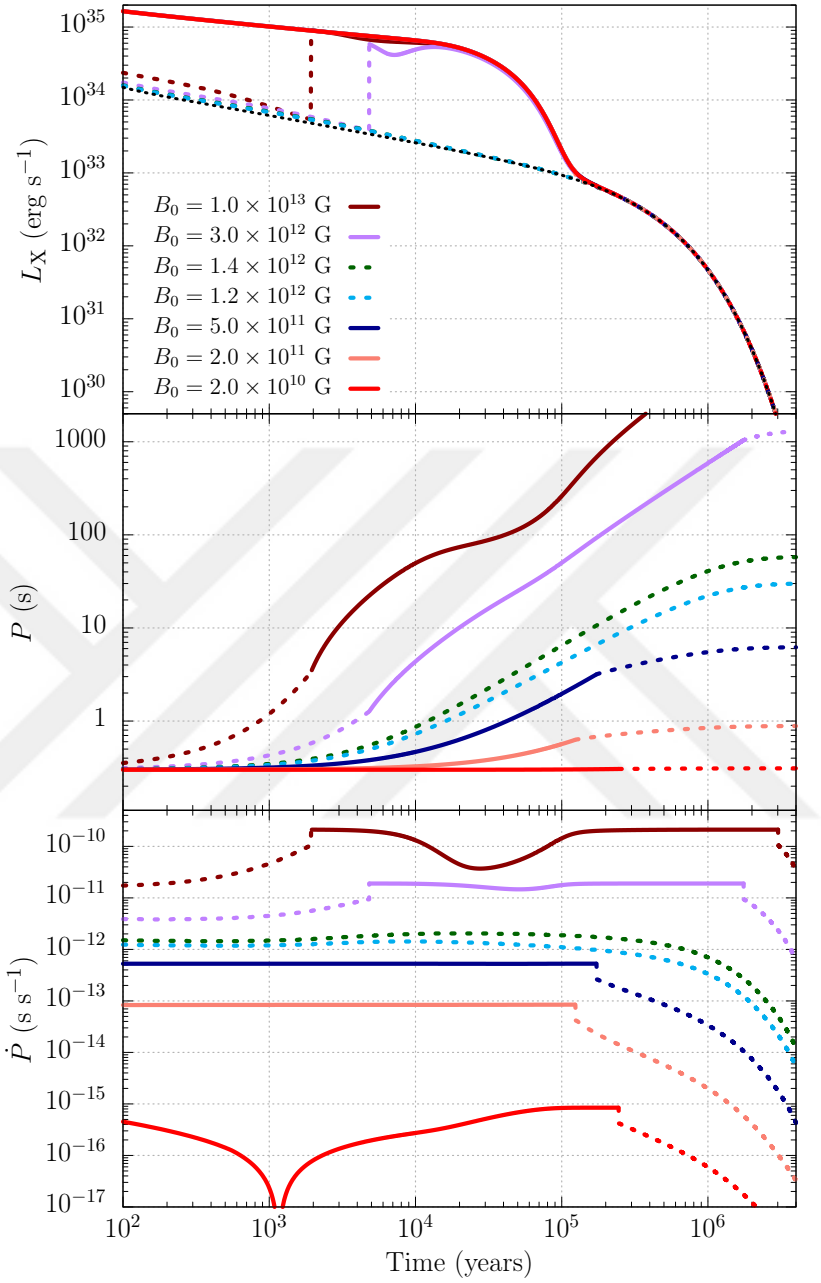

Figure 3.12 Illustrative model curves for different B_0 values (given in the upper panel). For all the curves, $\Delta r/r = 0.25$, $\eta = 0.7$, $\xi = 0.7$, $\alpha = 0.045$, $T_{\rm p} = 50$ K, $C = 1 \times 10^{-4}$, $P_0 = 0.3$ s, and $M_{\rm d} = 9.6 \times 10^{-6}$ $M_{\odot}$. The dotted black curve in the top panel shows the theoretical maximal cooling curve (Page et al., 2006, 2009).

In the following chapter, evolutionary links between the isolated NS populations will be discussed on the $P - \dot{P}$ diagram with the curves obtained with both models.

4. LONG-TERM EVOLUTIONARY LINKS BETWEEN THE ISOLATED NEUTRON STAR POPULATIONS

This chapter will be submitted to a scientific journal with some modifications.

4.1 The Birth Rates of the Isolated NS Populations

NSs are formed by core collapse supernovae (CCSN). In our galaxy, the rate of CCSN is estimated to be $\beta_{\rm CCSN} \sim 1.9 \pm 1.1$ century^{-1} (Diehl et al., 2006; Rozwadowska et al., 2021). It is assumed that approximately 80% of this rate corresponds to the formation of the isolated NSs. Sources are classified into different populations based on their unique observed properties. Statistical calculations and Monte Carlo simulations have been performed to estimate the birth rates of different NS populations (Beniamini et al., 2019; Faucher-Giguère & Kaspi, 2006; Gullón et al., 2014; Jawor & Tauris, 2022; Lorimer et al., 2006; Vranesevic et al., 2004).

In most studies, the birth rate of radio pulsars, $\beta_{\rm PSR}$, is estimated under the assumption that they evolve in a vacuum with dipole torques. Simulation results are interpreted on the $P - \dot{P}$ diagram. It is assumed that synthetic sources evolving on the $P - \dot{P}$ diagram could not be detected when they lose their ability to emit radio pulsations as they approach the pulsar death line and/or become too faint in the radio band. To maintain a steady-state condition consistent with the observed radio pulsars and age of the Galaxy, the flow of radio pulsars across the $P - \dot{P}$ diagram can be considered as a "current" obeying a continuity equation (Phinney & Blandford, 1981; Vivekanand & Narayan, 1981). This current equals the rate of the sources formed as radio pulsars minus the rate of sources that lose their radio abilities. From this assumption, the maximum value of this current is estimated to be the $\beta_{\rm PSR}$, which varies depending on the models and assumptions taken into account (e.g. Galactic electron density distribution and the beaming fraction). The

estimated birth rates for radio pulsars are in the range of $1-3$ century^{-1} (Faucher-Giguère & Kaspi, 2006; Keane & Kramer, 2008; Lorimer et al., 2006; Popov et al., 2006; Vranesevic et al., 2004).

Total numbers of the RRATs are assumed to be a factor of those of radio pulsars ($N_{\rm PSR} \sim (1-3)\ N_{\rm RRAT}$) (Keane & Kramer, 2008; McLaughlin et al., 2006; Popov et al., 2006; Vranesevic et al., 2004). The birth rate can be written as $\beta \approx N/\tau$, where τ and N are average active lifetimes and the total number of sources in a given population respectively. For RRATs, $\tau_{\rm RRAT}$ is estimated to be $\sim 5 \times 10^6$ yr (Popov et al., 2006). From the formula, $\beta_{\rm RRAT}$ is estimated to be $1-6$ century^{-1} (Keane & Kramer, 2008; Popov et al., 2006). Additionally, it appears that the radio pulsar region serves as a transit route for most sources, and sources may spend less time in the radio pulsar region than in the RRAT or XDIN regions (Popov, 2023).

Up to now, there are only 7 sources that have been identified as XDINs. All these objects located within a distance of 500 pc. Their active life times are estimated to be ≈ 1 Myr from their current $L_{\rm X}$ levels assuming they evolve with $L_{\rm cool}$. Due to low $L_{\rm X}$ levels, it is hard to detect XDINs. Statistical calculations and population synthesis have been conducted considering their distributions in the galaxy to estimate their total number and birth rate. Results indicated that $\beta_{\rm XDINs} \sim 2.1 \pm 1$century^{-1} (Gill & Heyl, 2007; Keane & Kramer, 2008; Popov et al., 2006). Similar work have been performed for AXP/SGRs as well. Birth rate of AXP/SGRs is estimated to be about an order of magnitude lower than those of RRATs (Ferrario & Wickramasinghe, 2008; Gill & Heyl, 2007; Keane & Kramer, 2008; Kouveliotou et al., 1998; Muno, Gaensler, Nechita, Miller, & Slane, 2008).

From these earlier studies, it is seen that the estimated total birth rate of the isolated NS populations exceeds the $\beta_{\rm CCSN}$ (Faucher-Giguère & Kaspi, 2006; Keane & Kramer, 2008; Popov et al., 2006). To overcome this problem, it has been proposed that there should be evolutionary connections, particularly between radio pulsars, RRATs, and XDINs (Faucher-Giguère & Kaspi, 2006; Keane & Kramer, 2008; Popov et al., 2006). Below, we investigate this problem in the frame of the fallback disc model.

4.2 Long-term Evolutionary Links Between the Isolated Neutron Star Populations

The long-term evolutionary paths generated by Model I and Model II (see Chapter 3) are presented in Fig. 4.1 and Fig. 4.2, respectively. In Model I, the curves are obtained using the minimal theoretical $L_{\rm cool}$ curve (Page et al., 2006, 2009), with the disc parameters $\alpha = 0.045$, $C = 7 \times 10^{-4}$, and $T_{\rm p} = 67$ K. While, in Model II, we employ the maximal theoretical $L_{\rm cool}$ curve (Page et al., 2006, 2009) with the disc parameters $\alpha = 0.045$, $C = 1 \times 10^{-4}$, and $T_{\rm p} = 50$ K. With these sets of disc parameters, we obtain reasonable model curves that can reproduce the individual source properties ($L_{\rm X}$, P, $\dot{P}$, and n) simultaneously with both models. For all model curves, the solid and dashed lines correspond to the WP phase (accretion is allowed) and the SP phase (no accretion) respectively. Model II produces almost all the evolutionary paths produced by Model I (Fig. 4.1). In most cases, Model II yields evolutionary curves similar to those obtained with Model I. There are also some additional different evolutionary routes estimated with Model II. Here, we will discuss the evolutionary links between the NS families indicated by the results obtained with Model II (see Fig. 4.2).

In Fig. 4.2, with some exceptions, the model sources evolving with relatively high $\dot{P}$ values have stronger dipole fields, and reach longer periods. From Fig. 4.2, it is seen that the sources with $B_0 \gtrsim 1 \times 10^{12}$ G pass through the persistent AXP/SGR region. The properties of these sources are reproduced during the WP phase (curves 1, 2, 3, 4, and 7). In this phase, ordinary radio pulses are estimated to be quenched by mass accretion on to the star. Indeed, none of these sources show normal radio pulsar behaviour. Few of them exhibit transient and unusual radio epochs (see the related discussion in Sec. 3.1.4).

In the early phases of evolution, the model sources with relatively high B_0 values ($\gtrsim 1.5 \times 10^{12}$ G) start their evolution in the SP phase and pass through the region that contains HBRPs with $\dot{P} \gtrsim 10^{-12}$ s s^{-1} (curves $1-5$). Some of these sources evolve with increasing $\dot{P}$ in the SP phase and subsequently make a transition to the WP phase (curves $1-4$). In the late phases of evolution, they undergo a WP/SP transition when $\dot{M}_{\rm in}$ decrease below a critical level. Note that these sources (curves $1-4$) evolve passing through persistent AXP/SGR region and have no evolutionary links with known CCOs, RRATs, and XDINs. Nevertheless, they can evolve to long periods achieving the properties of LPPs like GLEAM-X and GPM J1839–10. After the transition to the SP phase, they remain below the pulsar death line, and cannot

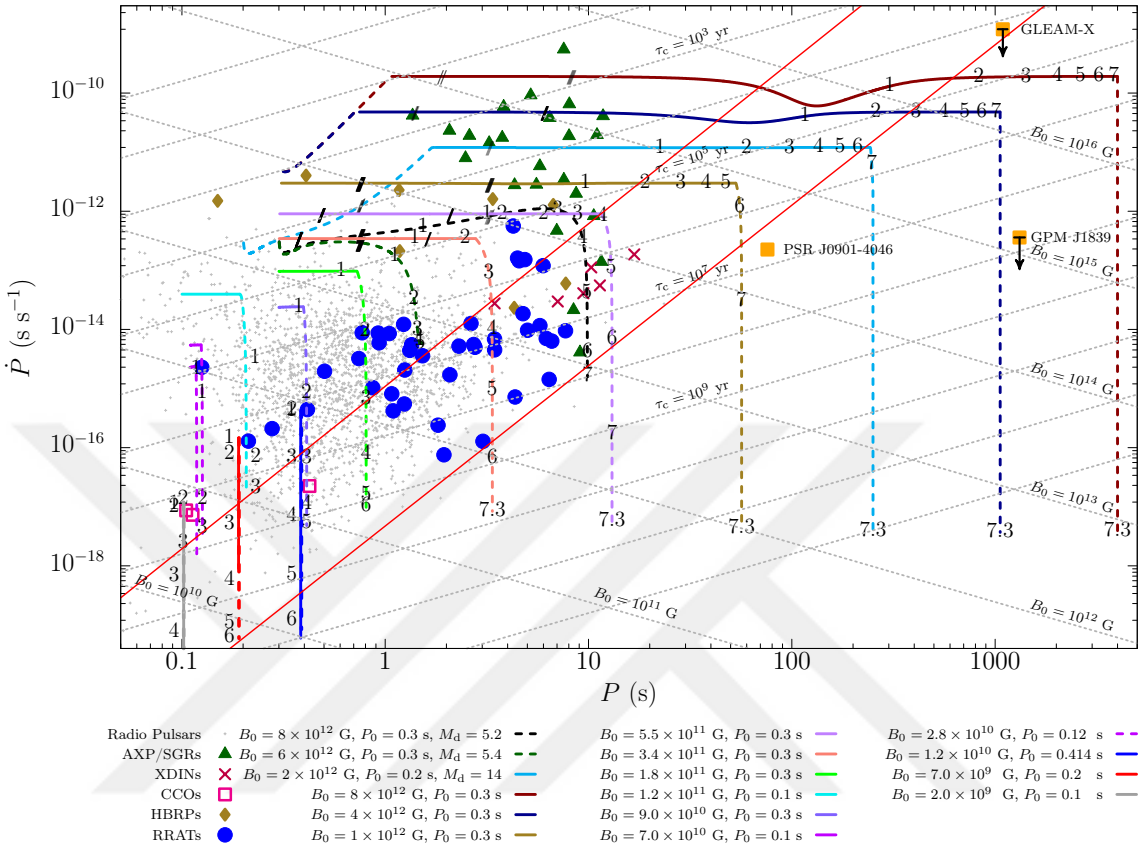

Figure 4.1 Evolutionary paths in the $P - \dot{P}$ diagram for Model I. For all models, $\alpha = 0.045$, $C = 7 \times 10^{-4}$, and $T_p = 67$ K. All these curves are obtained with $M_d = 3.2 \times 10^{-6}$ $M_\odot$ (except three curves, M_d values in the unit of 10^{-6} $M_\odot$ are given in the figure), while values of B_0 and P_0 are given in the figure. Solid and dashed curves represent the WP and SP phases respectively. The upper and lower boundaries of the death valley are represented by red solid lines (K. Chen & Ruderman, 1993). For comparison, constant τ_c and B_0 lines, calculated from the dipole-torque formula, are also given. The numbers on the model curves show the ages of the sources in units of 10^5 yr. The markings on the curves indicate the periods at which the sources cross the upper and lower boundaries of the death valley in our model. At the end of the evolution, the constant-B_0 lines indicate the actual B_0 values of the sources. The data for radio pulsars, AXP/SGRs, XDINs, RRATs, HBRPs and CCOs are obtained from the ATNF Pulsar Catalogue (version 1.70, Manchester et al., 2005). Recently discovered LPPs, GLEAM-X, J0901, and GPM J1839, are shown by filled squares. The arrows on the GLEAM-X and GPM J1839 data points show the $\dot{P}$ upper limits of the sources.

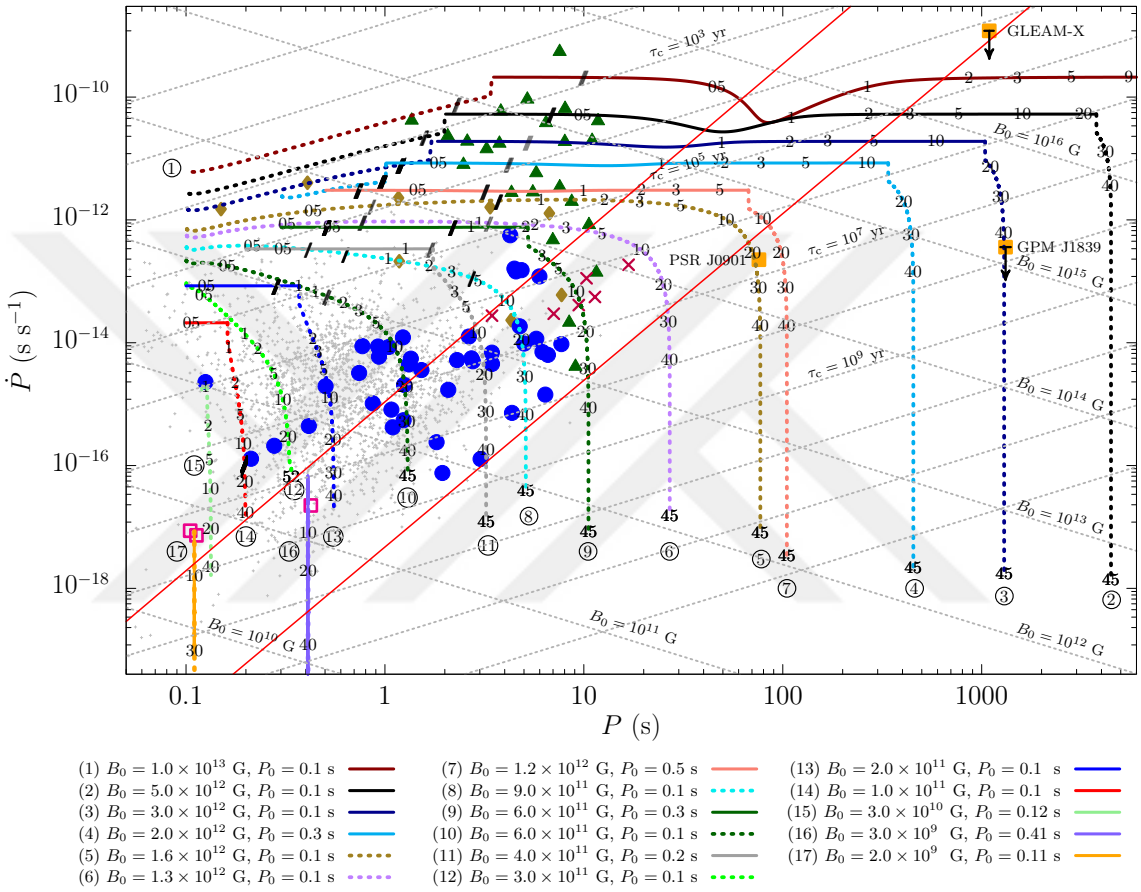

Figure 4.2 Same as Figure 4.1. All the curves are obtained with Model II. For all curves, $\alpha = 0.045$, $C = 1 \times 10^{-4}$, $T_{\rm p} = 50$ K, $\Delta r/r = 0.25$, $\eta = 0.7$, and $\xi = 0.7$. All these curves are generated with $M_{\rm d} \simeq 1 \times 10^{-5}\ M_\odot$ (except for the curves 16 and 17, $M_{\rm d} \sim 1.6 \times 10^{-6}\ M_\odot$). The values of B_0 and P_0 are given below the figure. The numbers in circles are identified the curves for the discussion in the text.

show ordinary pulsed radio emission. It is seen that the model curves sweeping the AXP/SGR region crosses some HBRPs in the early phases of evolution.

The model curves $6-15$ are produced with B_0 values in the $\sim 3\times10^{10}-1.3\times10^{12}$ G range. It is seen that these curves trace most of the RRAT population. These curves connect only a small fraction of RRATs to the entire known XDIN population (curves 6, 8, 9, 11). Like the high$-B_0$ case, these model curves also traces some HBRPs before they reach the RRAT region (curve 8). The sources with relatively high B_0 in this group can acquire the properties of LPPs similar to J0901 in the late phases of evolutions (see curves 6). Depending mainly on P_0 and B_0 values, these sources could start the evolution in either the SP phase or the WP phase. Along the evolutionary paths 6, 8, 10, and 12, the sources always remain in the SP phase. These routes indicate a significant connection between the normal radio pulsars and RRATs, since there is no accretion on to the NS, and the pulsed radio emission is allowed in the SP phase. The radio pulsar-RRAT-XDIN connection seen in these simulations provides a natural solution to the birth-rate problem. These populations have the highest estimated birth rates. It is interesting that the NSs that can achieve the XDIN properties could be initially identified as radio pulsars, HBRPs and possibly transient AXP/SGRs (with relatively low $\dot{P}$ values). Note that, in the model, a system can be HBRP or radio pulsar only in the SP phase (see curves shown by dashed curves in Fig. 4.1 and 4.2).

The model curves with lowest B_0 values ($\sim 10^9$ G) pass through the CCO region. CCOs are probably the youngest sources among the populations considering their SNR associations. In our models, the sources with smallest B_0 values could reproduce the rotational properties of CCOs (see curves 16 and 17 in Fig. 4.2, and Benli & Ertan, 2018a). Depending on B_0 and $M_{\rm d}$ values, the evolution of these sources could start in the SU or WP phase. Currently known CCOs are slowing down. Nevertheless, some CCOs could be discovered in the SU phase in the early phase of evolution. Due to very small $\dot{P}$ values, the periods of known CCOs are not likely to change significantly over a long timescale ($\gtrsim 10^6$ yr). After the WP/SP transition, CCOs could become normal radio pulsars or RRATs depending on their death points inside the pulsar death valley. Note that, there are many RRATs within the P range of CCOs with unknown $\dot{P}$. There are also CCO candidates without P and $\dot{P}$ measurements (see CCO catalogue[1]). Further observations are required to understand the potential evolutionary links between RRATs and CCOs.

It is seen in Fig. 4.2 that the model curves with a continuous B_0 distribution in the a few 10^9-10^{13} G range sweeps out the regions of all the NS families. Among

[1] http://www.iasf-milano.inaf.it/~deluca/cco/main.htm

these sources, the highest birth-rate is estimated for RRATs. Fig. 4.2 shows that the model curves evolving through the entire RRAT region also pass through the properties of the other populations except for persistent AXP/SGRs (with relatively high $\dot{P}$ values). Since AXP/SGRs are estimated to have a relatively low birth rate (see Section 4.1), their likely evolutionary links do not bring a solution to the birth-rate problem. The evolutionary links especially with RRATs which have the highest estimated birth-rate seem to be important in the estimation of the total birth-rate.

The birth-rate estimated for XDINs is smaller than, but close to that of RRATs. It was proposed earlier that a fraction of RRATs could be progenitors of XDINs (see Sec. 3.1.2). In Fig. 4.2, it is seen that the known XDINs could indeed be progenitors of a small fraction of RRATs. Following the results obtained by Parfrey et al. (2016, 2017), it was proposed that the radio bursts of RRATs could be produced by the penetration of the accretion disc into the light cylinder, which enhances the flux of the open field lines through the magnetic poles of the star, and produce radio burst occasionally (Gençali & Ertan, 2021). After the disc torques decrease below the level to induce these short radio bursts, these RRATs are likely to become XDINs which are hard to detect in the X-ray band due to their low $L_{\rm X}$ levels at these ages ($\gtrsim 10^6$ yr). Their currently long periods do not allow pulsed radio emission either. Indeed, no pulsed radio emissions have been observed from XDINs (Haberl, 2007; Turolla, 2009). In this picture, note that only a small fraction of RRATs are evolving into the region of known XDINs properties (Fig. 4.2), and XDIN phase is the final phase of these systems which can be observed only if they are located at close distances. In other words, XDINs are not expected to evolve to show radio pulsar or RRAT properties. It is worth mentioning that RRATs with periods smaller than XDIN periods could also gain XDIN properties with lower P values. Nevertheless, most of these sources find themselves below the pulsar death line once the RRAT activity terminates, making it challenging to detect them due to their low X-ray luminosity levels at these ages. This means that there could be undetected XDINs with short periods, evolved from RRATs. Further observations are needed to clarify these possibilities.

Each radio pulsar has its own death point inside the death valley depending on its dipole field geometry (K. Chen & Ruderman, 1993). A given source above this point shows normal radio pulsar behaviour, while the pulses are switched off below the death point. We estimate that the disc-magnetosphere interaction enhancing the flux of the open field lines through the poles occasionally boost the sources above their death points. If there were no disc effect, these NSs would find themselves either inside or below the death valley (Gençali & Ertan, 2021). In our model, this means that all radio sources evolving with fallback discs close to and below their

death points are estimated to exhibit RRAT behaviour. Eventually, with increasing $r_{\rm in}$, RRAT bursts are also likely to be switched off, and the sources enter the XDIN phase. Note that, for some sources the lifetime of the fallback disc could terminate when the sources above their death points. In this case, these radio pulsars continue to emit radio pulses until they reach their death points by means of magnetic dipole torques.

The possibility of evolutionary connection between the radio pulsars and RRATs raises the question of whether these evolutionary curves are consistent with the measured braking indices of radio pulsars and HBRPs. It was shown earlier that P, $\dot{P}$, $L_{\rm X}$, and n can be reproduced simultaneously for all HBRPs with measured braking indices varying in the range of $0.7-2.9$ (Benli & Ertan, 2017).

For the radio sources evolving in vacuum the braking index, $n=2-P\ddot{P}/\dot{P}^2$, is estimated to be close to 3. Long-term braking indices have been measured for a limited number of the youngest pulsars (see Lyne, Graham-Smith, & Stappers, 2022, Table 5.1). Measuring the true braking indices of older pulsars is challenging due to the small expected values of $\ddot{P}$ and the presence of glitches or timing noise, which often obscure the long-term effects. The recoveries from glitches can lead to considerable changes in $\ddot{P}$ values between glitches, resulting in braking indices as large as many tens, which do not accurately represent the long-term rotational evolution of pulsars. Recent observations indicate that n could be significantly larger than 3 (Parthasarathy et al., 2020, 2019). For the model curves connecting radio pulsars and RRATs in Fig. 4.2 (curves 8, $10-14$) the braking indices traces a large range from ~ 1.5 to ~ 500. During the late phase of evolution, n could become as large as ~ 500 due to the sharply decreasing $\dot{P}$ in this phase.

The evolutionary connections discussed above could be summarised as follows. With a continuous B_0 distribution in the range of a few 10^9-10^{13} G all the single NS populations can be reproduced in the fallback disc model with various evolutionary links between these systems. Considering the birth-rate problem, it seems that most important links are those that connect RRATs to the other systems, especially XDINs and radio pulsars. Our results indicate that RRATs have evolutionary links with almost all other populations except persistent AXP/SGRs which are relatively low birth-rate. Most of RRATs could be radio pulsars, a small fraction could be HBRP as well in their early phases of evolution, while a small fraction of RRATs could evolve to the properties of currently known XDINs.

5. RESULTS & CONCLUSIONS

We have investigated the long-term evolutions and evolutionary links between the isolated NS populations. Our results and conclusions can be summarised as follows:

Among the populations of isolated NSs, RRATs are estimated to have the highest birth-rate. Therefore, it is crucial to investigate the long-term evolution of RRATs to understand the possible evolutionary connections between the populations. We investigated the long-term evolution of RRATs, which have no $L_{\rm X}$ information (except J1819), using Model I by tracing the initial conditions. The model yields the rotational properties of all the RRATs with B_0 values in the $\sim 7\times10^{9}-\sim 5.5\times10^{11}$ G range. This B_0 range fills the gap between the B_0 ranges estimated for CCOs and XDINs in the same model. Even though many RRATs are located above the pulsar death valley with the fields inferred from the dipole-torque formula, none of them exhibit normal radio pulses. The estimated B_0 values in the model place all the RRATs either in the death valley or below the pulsar death line. We estimate that RRATs are the sources located below their individual death points. We tentatively proposed that the disc-field interaction enhancing the flux of open field lines through the magnetic pole occasionally triggers observed short radio bursts (Gençali & Ertan, 2021). Our results indicate the possibility of evolutionary links between RRATs, XDINs, and some of AXP/SGRs, as well as the connections between RRATs and CCOs. From the simulations, we estimated that there is no evolutionary link between AXP/SGRs and CCOs.

Recently, the discovery of two LPPs, J0901 ($P\simeq 76$ s) and GLEAM-X ($P\simeq 1091$ s), exhibiting radio emissions distinct from normal radio pulsars enabled their detection in radio band. The evolutions of AXP/SGRs with relatively high B_0 to such long periods had already been predicted before their discovery (Benli & Ertan, 2016). LPPs exhibit transient pulsed-radio epochs with unusual and variable pulse shapes, reminiscent of the radio behaviour observed in a small number of radio-emitting AXP/SGRs. Similar to RRATs, the disc-field interactions could be responsible for these observed radio pulsar epoch of LPPs. We have analysed the long-term evolution of these LPPs using Model I and demonstrated that their rotation and

$L_{\rm X}$ properties could be simultaneously reproduced with $B_0 \sim 10^{12}$ G (for details see Gençali et al., 2022, 2023).

Since GLEAM-X has an upper limit to the $\dot{P}$, the properties of GLEAM-X can be accounted for by our model in both the SP and the WP phases. J0901, on the other hand, has a measured $\dot{P}$, providing a better constraint on the evolutionary model. The observed features of J0901 can only be achieved in the SP phase in the model. Our results with Model I indicate that LPPs pass through the AXP/SGR epoch in their early stages of evolution at ages around a few 10^4 yrs. We estimated their current ages in the range of $\sim (6-8) \times 10^5$ yr, depending on the chosen $L_{\rm cool}$ curve.

In our earlier work, we investigated the torque-reversals behaviour of 4U 1626–67 using the Model II. The model successfully reproduces the observed torque reversals consistently with the accompanying $L_{\rm X}$ variations. Our results indicate that: (i) torque reversals occur when the system approaches the rotational equilibrium when $r_{\rm in} = r_{\rm co}$, while $r_{\rm A} \gtrsim r_{\rm co}$; (ii) on either side of the torque reversal, both $\Gamma_{\rm D}$ and $\Gamma_{\rm acc}$ are active; (iii) with increasing $\dot{M}_{\rm in}$, $\Gamma_{\rm acc}$ become dominant. The occurrence of torque reversals is a natural outcome of transitions between the WP and SU phases of a system with a stable, geometrically thin accretion disc.

In the last part of our study, we have extended our evolutionary analysis to cover all the isolated NS populations using both Model I and Model II. Our results indicate that both models can successfully reproduce the rotational properties of these NS families with a continuous B_0 distribution in the range of a few $10^9 - 10^{13}$ G, while yielding various evolutionary connections between these populations. In comparison with Model I, some additional evolutionary paths are produced in Model II. These new avenues, favour the SP phase for the initial phase of evolution and generate additional evolutionary links, particularly between radio pulsars, HBRPs, RRATs, and XDINs.

Considering the estimated birth rates of the populations, it seems more important to show evolutionary connections between RRATs, XDINs and radio pulsars. We have found that, except for the persistent AXP/SGRs which have relatively low birth rates, RRATs have evolutionary connections with almost all other populations. In the early stages of their evolution, a large majority of RRATs could be observed as radio pulsars and/or HBRPs, while XDINs could be decedents of a fraction of RRATs. Our detailed model results support earlier predictions to account for the long-lasting birth-rate problem.

Finally, our analyses in this thesis together with the earlier work show that the properties of isolated NS populations can be reproduced with the fallback disc model

as a natural outcome of differences in the initial conditions P_0, B_0, and $M_{\rm d}$ in a single picture. We obtain reasonable results with conventional dipole field strengths for all these NS systems, while the presence of small-scale magnetar fields in higher multipoles, required to explain soft-gamma bursts, is compatible with the fallback disc model.

BIBLIOGRAPHY

Abdo, A. A., Ajello, M., Allafort, A., Baldini, L., Ballet, J., Barbiellini, G., ... et al. (2013). The Second Fermi Large Area Telescope Catalog of Gamma-Ray Pulsars. *ApJS*, *208*, 17. doi: 10.1088/0067-0049/208/2/17

Alpar, M. A. (2001). On Young Neutron Stars as Propellers and Accretors with Conventional Magnetic Fields. *Astrophysical Journal*, *554*, 1245-1254. doi: 10.1086/321393

Alpar, M. A. (2007). Dim isolated neutron stars, cooling and energy dissipation. *Astrophysics and Space Science*, *308*(1-4), 133-136. doi: 10.1007/s10509-007-9376-0

Alpar, M. A., Ankay, A., & Yazgan, E. (2001). Pulsar Spin-down by a Fallback Disk and the P-P Diagram. *Astrophysical Journal, Letters*, *557*(1), L61-L65. doi: 10.1086/323140

Aly, J. J., & Kuijpers, J. (1990). Flaring interactions between accretion disk and neutron star magnetosphere. *Astronomy and Astrophysics*, *227*, 473-482.

Antonopoulou, D., Weltevrede, P., Espinoza, C. M., Watts, A. L., Johnston, S., Shannon, R. M., & Kerr, M. (2015). The unusual glitch recoveries of the high-magnetic-field pulsar J1119-6127. *Monthly Notices of the Royal Astronomical Society*, *447*(4), 3924-3935. doi: 10.1093/mnras/stu2710

Archibald, A. M., Bogdanov, S., Patruno, A., Hessels, J. W. T., Deller, A. T., Bassa, C., ... Wijnands, R. (2015). ACCRETION-POWERED PULSATIONS IN AN APPARENTLY QUIESCENT NEUTRON STAR BINARY. *Astrophysical Journal*, *807*(1), 62. Retrieved from `https://doi.org/10.1088/0004-637x/807/1/62` doi: 10.1088/0004-637x/807/1/62

Archibald, A. M., Stairs, I. H., Ransom, S. M., Kaspi, V. M., Kondratiev, V. I., Lorimer, D. R., ... Remillard, R. A. (2009). A radio pulsar/x-ray binary link. *Science*, *324*(5933), 1411–1414. Retrieved from `https://science.sciencemag.org/content/324/5933/1411` doi: 10.1126/science.1172740

Archibald, R. F., Burgay, M., Lyutikov, M., Kaspi, V. M., Esposito, P., Israel, G., ... Tendulkar, S. P. (2017). Magnetar-like X-Ray Bursts Suppress Pulsar Radio Emission. *Astrophysical Journal, Letters*, *849*(2), L20. doi: 10.3847/2041-8213/aa9371

Archibald, R. F., Kaspi, V. M., Tendulkar, S. P., & Scholz, P. (2016). A Magnetar-like Outburst from a High-B Radio Pulsar. *Astrophysical Journal, Letters*, *829*(1), L21. doi: 10.3847/2041-8205/829/1/L21

Arons, J. (1993). Magnetic Field Topology in Pulsars. *Astrophysical Journal*, *408*, 160. doi: 10.1086/172576

Baring, M. G., & Harding, A. K. (1998). Radio-Quiet Pulsars with Ultrastrong Magnetic Fields. *Astrophysical Journal, Letters*, *507*(1), L55-L58. doi: 10.1086/311679

Baring, M. G., & Harding, A. K. (2001). Photon Splitting and Pair Creation in Highly Magnetized Pulsars. *Astrophysical Journal*, *547*(2), 929-948. doi: 10.1086/318390

Basko, M. M., & Sunyaev, R. A. (1975). Radiative transfer in a strong magnetic field and accreting X-ray pulsars. *Astronomy and Astrophysics*, *42*(3), 311-321.

Bassa, C. G., Patruno, A., Hessels, J. W. T., Keane, E. F., Monard, B., Mahony, E. K., ... Tendulkar, S. (2014). A state change in the low-mass X-ray binary XSS J12270-4859. *Monthly Notices of the Royal Astronomical Society*, *441*(2), 1825-1830. Retrieved from https://doi.org/10.1093/mnras/stu708 doi: 10.1093/mnras/stu708

Bates, S. D., Bailes, M., Barsdell, B. R., Bhat, N. D. R., Burgay, M., Burke-Spolaor, S., ... van Straten, W. (2012). The High Time Resolution Universe Pulsar Survey — VI. An artificial neural network and timing of 75 pulsars. *Monthly Notices of the Royal Astronomical Society*, *427*(2), 1052-1065. doi: 10.1111/j.1365-2966.2012.22042.x

Beniamini, P., Hotokezaka, K., van der Horst, A., & Kouveliotou, C. (2019). Formation rates and evolution histories of magnetars. *Monthly Notices of the Royal Astronomical Society*, *487*(1), 1426-1438. doi: 10.1093/mnras/stz1391

Benli, O. (2020). On the peculiar torque reversals and the X-ray luminosity history of the accretion-powered X-ray pulsar 4U 1626–67. *Monthly Notices of the Royal Astronomical Society*, *495*(4), 3531-3537. Retrieved from https://doi.org/10.1093/mnras/staa998 doi: 10.1093/mnras/staa998

Benli, O., Çalışkan, Ş., & Ertan, Ü. (2015). Long-term evolution, X-ray outburst and optical/infrared emission of SGR 0501+4516. *Monthly Notices of the Royal Astronomical Society*, *447*(3), 2282-2286. doi: 10.1093/mnras/stu2569

Benli, O., & Ertan, Ü. (2016). Long-term evolution of anomalous X-ray pulsars and soft gamma repeaters. *Monthly Notices of the Royal Astronomical Society*, *457*, 4114-4122. doi: 10.1093/mnras/stw235

Benli, O., & Ertan, Ü. (2017). On the evolution of high-B radio pulsars with measured braking indices. *Monthly Notices of the Royal Astronomical Society*, *471*, 2553-2557. doi: 10.1093/mnras/stx1735

Benli, O., & Ertan, Ü. (2018a). Central Compact Objects: some of them could be spinning up? *Monthly Notices of the Royal Astronomical Society*, *478*(4), 4890-4893. Retrieved from https://doi.org/10.1093/mnras/sty1399 doi: 10.1093/mnras/sty1399

Benli, O., & Ertan, Ü. (2018b). Rotational and X-ray luminosity evolution of high-B radio pulsars. *New Astronomy*, *61*, 78-83. doi: 10.1016/j.newast.2017.12.005

Beri, A., Jain, C., Paul, B., & Raichur, H. (2014). Torque reversals and pulse profile of the pulsar 4U 1626-67. *Monthly Notices of the Royal Astronomical Society*, *439*(2), 1940-1947. doi: 10.1093/mnras/stu087

Beri, A., Paul, B., & Dewangan, G. C. (2015). Pulse-phase dependence of emission lines in the X-ray pulsar 4U 1626-67. *Monthly Notices of the Royal Astronomical Society*, *451*(1), 508-516. doi: 10.1093/mnras/stv922

Bhattacharya, D., & van den Heuvel, E. P. J. (1991). Formation and evolution of binary and millisecond radio pulsars. *Phys. Rep.*, *203*(1-2), 1-124. doi: 10.1016/0370-1573(91)90064-S

Bhattacharya, D., Wijers, R. A. M. J., Hartman, J. W., & Verbunt, F. (1992). On the decay of the magnetic fields of single radio pulsars. *Astronomy and Astrophysics*, *254*, 198-212.

Bildsten, L., Chakrabarty, D., Chiu, J., Finger, M. H., Koh, D. T., Nelson, R. W., ... Wilson, R. B. (1997). Observations of accreting pulsars. *Astrophysical Journal, Supplement*, *113*(2), 367–408. Retrieved from https://doi.org/10.1086/313060 doi: 10.1086/313060

Blackman, E. G., & Perna, R. (2004). Pulsars with Jets May Harbor Dynamically Important Disks. *Astrophysical Journal, Letters*, *601*(1), L71-L74. doi: 10.1086/381802

Burwitz, V., Haberl, F., Neuhäuser, R., Predehl, P., Trümper, J., & Zavlin, V. E. (2003). The thermal radiation of the isolated neutron star RX J1856.5-3754 observed with Chandra and XMM-Newton. *Astronomy and Astrophysics*, *399*, 1109-1114. doi: 10.1051/0004-6361:20021747

Caleb, M., Heywood, I., Rajwade, K., Malenta, M., Stappers, B. W., Barr, E., ... Fender, R. (2022). Discovery of a radio-emitting neutron star with an ultra-long spin period of 76 s. *Nature Astronomy*, *6*(7), 828-836. doi: 10.1038/s41550-022-01688-x

Çalışkan, Ş., Ertan, Ü., Alpar, M. A., Trümper, J. E., & Kylafis, N. D. (2013). On the evolution of the radio pulsar PSR J1734-3333. *Monthly Notices of the Royal Astronomical Society*, *431*, 1136-1142. doi: 10.1093/mnras/stt234

Camero-Arranz, A., Finger, M. H., Ikhsanov, N. R., Wilson-Hodge, C. A., & Beklen, E. (2010). New Torque Reversal and Spin-up of 4U 1626-67 Observed by Fermi/Gamma-ray Burst Monitor and Swift/Burst Alert Telescope. *Astrophysical Journal*, *708*(2), 1500-1506. doi: 10.1088/0004-637X/708/2/1500

Camero-Arranz, A., Pottschmidt, K., Finger, M. H., Ikhsanov, N. R., Wilson-Hodge, C. A., & Marcu, D. M. (2012). 4U 1626-67 as seen by Suzaku before and after the 2008 torque reversal. *Astronomy and Astrophysics*, *546*, A40. doi: 10.1051/0004-6361/201219656

Camilo, F., Kaspi, V. M., Lyne, A. G., Manchester, R. N., Bell, J. F., D'Amico, N., ... Crawford, F. (2000). Discovery of Two High Magnetic Field Radio Pulsars. *Astrophysical Journal*, *541*(1), 367-373. doi: 10.1086/309435

Camilo, F., Ransom, S. M., Halpern, J. P., & Reynolds, J. (2007). 1E 1547.0-5408: A Radio-emitting Magnetar with a Rotation Period of 2 Seconds. *Astrophysical Journal, Letters*, *666*(2), L93-L96. doi: 10.1086/521826

Camilo, F., Ransom, S. M., Halpern, J. P., Reynolds, J., Helfand, D. J., Zimmerman, N., & Sarkissian, J. (2006). Transient pulsed radio emission from a magnetar. *Nature*, *442*(7105), 892-895. doi: 10.1038/nature04986

Camilo, F., Ransom, S. M., Peñalver, J., Karastergiou, A., van Kerkwijk, M. H., Durant, M., ... Cognard, I. (2007). The Variable Radio-to-X-Ray Spectrum of the Magnetar XTE J1810-197. *Astrophysical Journal*, *669*(1), 561-569. doi: 10.1086/521548

Chakrabarty, D. (1998). High-Speed Optical Photometry of the Ultracompact X-Ray Binary 4U 1626-67. *Astrophysical Journal*, *492*(1), 342-351. doi: 10.1086/305035

Chakrabarty, D., Bildsten, L., Finger, M. H., Grunsfeld, J. M., Koh, D. T., Nelson, R. W., ... Wilson, R. B. (1997). On the correlation of torque and luminosity in GX 1+4. *Astrophysical Journal*, *481*(2), L101–L105. Retrieved from `https://doi.org/10.1086/310666` doi: 10.1086/310666

Chakrabarty, D., Bildsten, L., Grunsfeld, J. M., Koh, D. T., Prince, T. A., Vaughan, B. A., ... Wilson, R. B. (1997). Torque reversal and spin-down of the accretion-powered pulsar 4u 1626-67. *Astrophysical Journal*, *474*(1), 414–425. Retrieved from `https://doi.org/10.1086/303445` doi: 10.1086/303445

Chatterjee, P., Hernquist, L., & Narayan, R. (2000). An Accretion Model for Anomalous X-Ray Pulsars. *Astrophysical Journal*, *534*, 373-379. doi: 10.1086/

308748

Chen, K., & Ruderman, M. (1993). Pulsar Death Lines and Death Valley. *Astrophysical Journal*, *402*, 264. doi: 10.1086/172129

Chen, W. C., & Li, X. D. (2006). Why the braking indices of young pulsars are less than 3? *Astronomy and Astrophysics*, *450*(1), L1-L4. doi: 10.1051/0004-6361:200600019

Chevalier, R. A. (1989). Neutron Star Accretion in a Supernova. *Astrophysical Journal*, *346*, 847. doi: 10.1086/168066

Cline, T. L., Desai, U. D., Pizzichini, G., Teegarden, B. J., Evans, W. D., Klebesadel, R. W., ... Vedrenne, G. (1980). Detection of a fast, intense and unusual gamma-ray transient. *Astrophysical Journal, Letters*, *237*, L1-L5. doi: 10.1086/183221

Coburn, W., Heindl, W. A., Rothschild, R. E., Gruber, D. E., Kreykenbohm, I., Wilms, J., ... Staubert, R. (2002). Magnetic Fields of Accreting X-Ray Pulsars with the Rossi X-Ray Timing Explorer. *Astrophysical Journal*, *580*(1), 394-412. doi: 10.1086/343033

Colgate, S. A. (1971). Neutron-Star Formation, Thermonuclear Supernovae, and Heavy-Element Reimplosion. *Astrophysical Journal*, *163*, 221. doi: 10.1086/150760

Cordes, J. M., & Shannon, R. M. (2008). Rocking the Lighthouse: Circumpulsar Asteroids and Radio Intermittency. *Astrophysical Journal*, *682*(2), 1152-1165. doi: 10.1086/589425

D'Aì, A., Cusumano, G., Del Santo, M., La Parola, V., & Segreto, A. (2017). A broad-band self-consistent modelling of the X-ray spectrum of 4U 1626-67. *Monthly Notices of the Royal Astronomical Society*, *470*(2), 2457-2468. doi: 10.1093/mnras/stx1146

Dai, H. L., & Li, X. D. (2006). Accretion torque on magnetized neutron stars. *Astronomy and Astrophysics*, *451*(2), 581-585. doi: 10.1051/0004-6361:20053907

Dai, S., Johnston, S., Weltevrede, P., Kerr, M., Burgay, M., Esposito, P., ... Sarkissian, J. (2018). Peculiar spin frequency and radio profile evolution of PSR J1119-6127 following magnetar-like X-ray bursts. *Monthly Notices of the Royal Astronomical Society*, *480*(3), 3584-3594. doi: 10.1093/mnras/sty2063

Davidson, K., & Ostriker, J. P. (1973). Neutron-Star Accretion in a Stellar Wind: Model for a Pulsed X-Ray Source. *Astrophysical Journal*, *179*, 585-598. doi: 10.1086/151897

De Luca, A. (2017). Central compact objects in supernova remnants. In *Journal of physics conference series* (Vol. 932, p. 012006). doi: 10.1088/1742-6596/932/1/012006

Deeter, J. E., Boynton, P. E., Lamb, F. K., & Zylstra, G. (1989). VELA X-1 Pulse Timing. II. Variations in Pulse Frequency. *Astrophysical Journal*, *336*, 376. doi: 10.1086/167017

Diehl, R., Halloin, H., Kretschmer, K., Lichti, G. G., Schönfelder, V., Strong, A. W., ... Wunderer, C. (2006). Radioactive ^{26}Al from massive stars in the Galaxy. *Nature*, *439*(7072), 45-47. doi: 10.1038/nature04364

Doroshenko, V., Santangelo, A., Suleimanov, V. F., & Tsygankov, S. S. (2020). An observational argument against accretion in magnetars. *Astronomy and Astrophysics*, *643*, A173. doi: 10.1051/0004-6361/202038948

Dubus, G., Lasota, J.-P., Hameury, J.-M., & Charles, P. (1999). X-ray irradiation in

low-mass binary systems. *Monthly Notices of the Royal Astronomical Society*, *303*, 139-147. doi: 10.1046/j.1365-8711.1999.02212.x

Ekşi, K. Y., & Alpar, M. A. (2003). Can Thin Disks Produce Anomalous X-Ray Pulsars? *Astrophysical Journal*, *599*(1), 450-456. doi: 10.1086/379193

Enoto, T., Kisaka, S., & Shibata, S. (2019). Observational diversity of magnetized neutron stars. *Rep. Prog. Phys.*, *82*(10), 106901. doi: 10.1088/1361-6633/ab3def

Ertan, Ü. (2017). The inner disc radius in the propeller phase and accretion-propeller transition of neutron stars. *Monthly Notices of the Royal Astronomical Society*, *466*, 175-180. doi: 10.1093/mnras/stw3131

Ertan, Ü. (2018). Accretion and propeller torque in the spin-down phase of neutron stars: The case of transitional millisecond pulsar PSR J1023+0038. *Monthly Notices of the Royal Astronomical Society*, *479*, L12-L16. doi: 10.1093/mnrasl/sly089

Ertan, Ü. (2021). On the torque reversals of accreting neutron stars. *Monthly Notices of the Royal Astronomical Society*, *500*(3), 2928-2936. Retrieved from `https://doi.org/10.1093/mnras/staa3378` doi: 10.1093/mnras/staa3378

Ertan, Ü., & Alpar, M. A. (2003). On the Enhanced X-Ray Emission from SGR 1900+14 after the August 27 Giant Flare. *Astrophysical Journal, Letters*, *593*(2), L93-L96. doi: 10.1086/378257

Ertan, Ü., & Çalışkan, Ş. (2006). Optical and Infrared Emission from the Anomalous X-Ray Pulsars and Soft Gamma-Ray Repeaters. *ApJ*, *649*, L87-L90. doi: 10.1086/508347

Ertan, Ü., Çalışkan, Ş., Benli, O., & Alpar, M. A. (2014). Long-term evolution of dim isolated neutron stars. *Monthly Notices of the Royal Astronomical Society*, *444*, 1559-1565. doi: 10.1093/mnras/stu1523

Ertan, Ü., Çalışkan, Ş., & Alpar, M. A. (2017). Optical excess of dim isolated neutron stars. *Monthly Notices of the Royal Astronomical Society*, *470*(1), 1253-1258. doi: 10.1093/mnras/stx1310

Ertan, Ü., Ekşi, K. Y., Erkut, M. H., & Alpar, M. A. (2009a). On the Evolution of Anomalous X-ray Pulsars and Soft Gamma-ray Repeaters with Fall Back Disks. *Astrophysical Journal*, *702*, 1309-1320. doi: 10.1088/0004-637X/702/2/1309

Ertan, Ü., Ekşi, K. Y., Erkut, M. H., & Alpar, M. A. (2009b). On the Evolution of Anomalous X-ray Pulsars and Soft Gamma-ray Repeaters with Fall Back Disks. *Astrophysical Journal*, *702*, 1309-1320. doi: 10.1088/0004-637X/702/2/1309

Ertan, Ü., & Erkut, M. H. (2008). On the X-Ray Light Curve, Pulsed-Radio Emission, and Spin Frequency Evolution of the Transient Anomalous X-Ray Pulsar XTE J1810-197 during Its X-Ray Outburst. *Astrophysical Journal*, *673*, 1062-1066. doi: 10.1086/524679

Ertan, Ü., Erkut, M. H., Ekşi, K. Y., & Alpar, M. A. (2007). The Anomalous X-Ray Pulsar 4U 0142+61: A Neutron Star with a Gaseous Fallback Disk. *Astrophysical Journal*, *657*(1), 441–447. Retrieved from `https://doi.org/10.1086/510303` doi: 10.1086/510303

Ertan, Ü., Göğüş, E., & Alpar, M. A. (2006). X-Ray and Infrared Enhancement of Anomalous X-Ray Pulsar 1E 2259+586. *Astrophysical Journal*, *640*(1), 435-440. doi: 10.1086/500097

Espinoza, C. M., Lyne, A. G., Kramer, M., Manchester, R. N., & Kaspi, V. M. (2011). The Braking Index of PSR J1734-3333 and the Magnetar Population. *Astrophysical Journal, Letters*, *741*(1), L13. doi: 10.1088/2041-8205/741/1/L13

Esposito, P., Rea, N., Borghese, A., Coti Zelati, F., Viganò, D., Israel, G. L., ... Zane, S. (2020). A Very Young Radio-loud Magnetar. *Astrophysical Journal, Letters*, *896*(2), L30. doi: 10.3847/2041-8213/ab9742

Faucher-Giguère, C.-A., & Kaspi, V. M. (2006). Birth and Evolution of Isolated Radio Pulsars. *Astrophysical Journal*, *643*, 332-355. doi: 10.1086/501516

Ferrario, L., & Wickramasinghe, D. (2008). Origin and evolution of magnetars. *Monthly Notices of the Royal Astronomical Society*, *389*(1), L66-L70. doi: 10.1111/j.1745-3933.2008.00527.x

Frank, J., King, A., & Raine, D. J. (2002). *Accretion Power in Astrophysics: Third Edition*. Cambridge University Press.

Fromang, S., & Stone, J. M. (2009). Turbulent resistivity driven by the magnetorotational instability. *Astronomy and Astrophysics*, *507*(1), 19-28. doi: 10.1051/0004-6361/200912752

Fu, L., & Li, X.-D. (2013). Population Synthesis of Young Isolated Neutron Stars: The Effect of Fallback Disk Accretion and Magnetic Field Evolution. *Astrophysical Journal*, *775*(2), 124. doi: 10.1088/0004-637X/775/2/124

Fukue, J. (1992). Self-irradiated accretion disks. *Publications of the ASJ*, *44*, 663-667.

Gavriil, F. P., Gonzalez, M. E., Gotthelf, E. V., Kaspi, V. M., Livingstone, M. A., & Woods, P. M. (2008). Magnetar-Like Emission from the Young Pulsar in Kes 75. *Science*, *319*(5871), 1802. doi: 10.1126/science.1153465

Gençali, A. A., & Ertan, Ü. (2018). Long-term evolution of RRAT J1819-1458. *Monthly Notices of the Royal Astronomical Society*, *481*(1), 244-249. doi: 10.1093/mnras/sty2287

Gençali, A. A., & Ertan, Ü. (2021). On the long-term evolution of rotating radio transients. *Monthly Notices of the Royal Astronomical Society*, *500*(3), 3281-3289. doi: 10.1093/mnras/staa3371

Gençali, A. A., Ertan, Ü., & Alpar, M. A. (2022). Evolution of the long-period pulsar GLEAM-X J162759.5-523504.3. *Monthly Notices of the Royal Astronomical Society*, *513*(1), L68-L71. doi: 10.1093/mnrasl/slac034

Gençali, A. A., Ertan, Ü., & Alpar, M. A. (2023). Evolution of the long-period pulsar PSR J0901-4046. *Monthly Notices of the Royal Astronomical Society*, *520*(1), L11-L15. doi: 10.1093/mnrasl/slac164

Ghosh, P. (2007). *Rotation and accretion powered pulsars*. Hackensack, NJ: World Scientific.

Ghosh, P., & Lamb, F. K. (1979a). Accretion by rotating magnetic neutron stars. III. Accretion torques and period changes in pulsating X-ray sources. *Astrophysical Journal*, *234*, 296-316. doi: 10.1086/157498

Ghosh, P., & Lamb, F. K. (1979b). Accretion by rotating magnetic neutron stars. II. Radial and vertical structure of the transition zone in disk accretion. *Astrophysical Journal*, *232*, 259-276. doi: 10.1086/157285

Giacconi, R., Murray, S., Gursky, H., Kellogg, E., Schreier, E., & Tananbaum, H. (1972). The Uhuru catalog of X-ray sources. *Astrophysical Journal*, *178*, 281-308. doi: 10.1086/151790

Gill, R., & Heyl, J. (2007). The birthrate of magnetars. *Monthly Notices of the Royal Astronomical Society*, *381*(1), 52-58. doi: 10.1111/j.1365-2966.2007.12254.x

Goodson, A. P., Winglee, R. M., & Böhm, K.-H. (1997). Time-dependent Accretion by Magnetic Young Stellar Objects as a Launching Mechanism for Stellar Jets. *Astrophysical Journal*, *489*(1), 199-209. doi: 10.1086/304774

Gotthelf, E. V., Halpern, J. P., & Alford, J. (2013). The Spin-down of PSR J0821-4300 and PSR J1210-5226: Confirmation of Central Compact Objects as Anti-magnetars. *Astrophysical Journal*, *765*(1), 58. doi: 10.1088/0004-637X/765/1/58

Göğüş, E., Lin, L., Kaneko, Y., Kouveliotou, C., Watts, A. L., Chakraborty, M., ... van der Horst, A. J. (2016). Magnetar-like X-Ray Bursts from a Rotation-powered Pulsar, PSR J1119-6127. *Astrophysical Journal, Letters*, *829*(2), L25. doi: 10.3847/2041-8205/829/2/L25

Gullón, M., Miralles, J. A., Viganò, D., & Pons, J. A. (2014). Population synthesis of isolated neutron stars with magneto-rotational evolution. *Monthly Notices of the Royal Astronomical Society*, *443*(3), 1891-1899. doi: 10.1093/mnras/stu1253

Guo, Y.-J., Dai, S., Li, Z.-S., Liu, Y., Tong, H., & Xu, R.-X. (2015). Understanding the X-ray spectrum of anomalous X-ray pulsars and soft gamma-ray repeaters. *Research in Astronomy and Astrophysics*, *15*(4), 525. doi: 10.1088/1674-4527/15/4/006

Haberl, F. (2004). AXPs and X-ray-dim isolated neutron stars: recent XMM-Newton and Chandra results. *Advances in Space Research*, *33*(4), 638-644. doi: 10.1016/j.asr.2003.07.022

Haberl, F. (2005). The Magnificent Seven: Nearby Isolated Neutron Stars with strong Magnetic Fields. In U. G. Briel, S. Sembay, & A. Read (Eds.), *5 years of science with xmm-newton* (p. 39-44). doi: 10.48550/arXiv.astro-ph/0510480

Haberl, F. (2007). The magnificent seven: magnetic fields and surface temperature distributions. *Astrophysics and Space Science*, *308*(1-4), 181-190. doi: 10.1007/s10509-007-9342-x

Haberl, F., Motch, C., Zavlin, V. E., Reinsch, K., Gänsicke, B. T., Cropper, M., ... Zane, S. (2004). The isolated neutron star X-ray pulsars <ASTROBJ>RX J0420.0-5022</ASTROBJ> and <ASTROBJ>RX J0806.4-4123</ASTROBJ>: New X-ray and optical observations. *Astronomy and Astrophysics*, *424*, 635-645. doi: 10.1051/0004-6361:20040440

Halpern, J. P., & Gotthelf, E. V. (2010). Spin-Down Measurement of PSR J1852+0040 in Kesteven 79: Central Compact Objects as Anti-Magnetars. *Astrophysical Journal*, *709*(1), 436-446. doi: 10.1088/0004-637X/709/1/436

Hambaryan, V., Suleimanov, V., Haberl, F., Schwope, A. D., Neuhäuser, R., Hohle, M., & Werner, K. (2017). The compactness of the isolated neutron star RX J0720.4-3125. *Astronomy and Astrophysics*, *601*, A108. doi: 10.1051/0004-6361/201630368

Harding, A. K. (2013). The neutron star zoo. *Frontiers Phys.*, *8*(6), 679-692. doi: 10.1007/s11467-013-0285-0

Hayashi, M. R., Shibata, K., & Matsumoto, R. (1996). X-Ray Flares and Mass Outflows Driven by Magnetic Interaction between a Protostar and Its Surrounding Disk. *Astrophysical Journal, Letters*, *468*, L37. doi: 10.1086/310222

Hemphill, P. B., Schulz, N. S., Marshall, H. L., & Chakrabarty, D. (2021).

Chandra/LETGS studies of the collisional plasma in 4u 1626–67. *Astrophysical Journal*, *920*(2), 142. Retrieved from https://doi.org/10.3847/1538-4357/ac0ade doi: 10.3847/1538-4357/ac0ade

Hewish, A., Bell, S. J., Pilkington, J. D. H., Scott, P. F., & Collins, R. A. (1968). Observation of a Rapidly Pulsating Radio Source. *Nature*, *217*, 709-713. doi: 10.1038/217709a0

Hu, C.-P., Ng, C. Y., Takata, J., Shannon, R. M., & Johnston, S. (2017). Chandra Phase-resolved Spectroscopy of the High Magnetic Field Pulsar B1509-58. *Astrophysical Journal*, *838*(2), 156. doi: 10.3847/1538-4357/aa67e3

Hulleman, F., van Kerkwijk, M. H., & Kulkarni, S. R. (2000). An optical counterpart to the anomalous X-ray pulsar 4U0142+61. *Nature*, *408*(6813), 689-692. doi: 10.1038/35047024

Hulleman, F., van Kerkwijk, M. H., & Kulkarni, S. R. (2004). The Anomalous X-ray Pulsar 4U 0142+61: Variability in the infrared and a spectral break in the optical. *Astronomy and Astrophysics*, *416*, 1037-1045. doi: 10.1051/0004-6361:20031756

Hurley, K., Li, P., Kouveliotou, C., Murakami, T., Ando, M., Strohmayer, T., ... Smith, I. (1999). ASCA Discovery of an X-Ray Pulsar in the Error Box of SGR 1900+14. *Astrophysical Journal, Letters*, *510*(2), L111-L114. doi: 10.1086/311820

Hurley-Walker, N., Rea, N., McSweeney, S. J., Meyers, B. W., Lenc, E., Heywood, I., ... Williams, A. (2023). A long-period radio transient active for three decades. *Nature*, *619*(7970), 487-490. doi: 10.1038/s41586-023-06202-5

Hurley-Walker, N., Zhang, X., Bahramian, A., McSweeney, S. J., O'Doherty, T. N., Hancock, P. J., ... Galvin, T. J. (2022). A radio transient with unusually slow periodic emission. *Nature*, *601*(7894), 526-530. doi: 10.1038/s41586-021-04272-x

Illarionov, A. F., & Siuniaev, R. A. (1975). X-ray variability through accretion by a black hole in a detached binary system. *Soviet Astronomy Letters*, *1*, 73.

İnam, S. Ç., Şahiner, Ş., & Baykal, A. (2009). Recent torque reversal of 4U 1907+09. *Monthly Notices of the Royal Astronomical Society*, *395*(2), 1015-1020. Retrieved from https://doi.org/10.1111/j.1365-2966.2009.14596.x doi: 10.1111/j.1365-2966.2009.14596.x

Inutsuka, S.-i., & Sano, T. (2005). Self-sustained Ionization and Vanishing Dead Zones in Protoplanetary Disks. *Astrophysical Journal, Letters*, *628*, L155-L158. doi: 10.1086/432796

Jaodand, A., Archibald, A. M., Hessels, J. W. T., Bogdanov, S., D'Angelo, C. R., Patruno, A., ... Deller, A. T. (2016). Timing Observations of PSR J1023+0038 During a Low-mass X-Ray Binary State. *Astrophysical Journal*, *830*, 122. doi: 10.3847/0004-637X/830/2/122

Jawor, J. A., & Tauris, T. M. (2022). Modelling spin evolution of magnetars. *Monthly Notices of the Royal Astronomical Society*, *509*(1), 634-657. doi: 10.1093/mnras/stab2677

Johnston, S., & Karastergiou, A. (2017). Pulsar braking and the P-dot{P} diagram. *Monthly Notices of the Royal Astronomical Society*, *467*(3), 3493-3499. doi: 10.1093/mnras/stx377

Kaplan, D. L., Chakrabarty, D., Wang, Z., & Wachter, S. (2009). A Mid-Infrared Counterpart to the Magnetar 1E 2259+586. *Astrophysical Journal*, *700*(1),

149-154. doi: 10.1088/0004-637X/700/1/149

Kaplan, D. L., Esposito, P., Chatterjee, S., Possenti, A., McLaughlin, M. A., Camilo, F., ... Slane, P. O. (2009). Upper limits on X-ray emission from two rotating radio transients. *Monthly Notices of the Royal Astronomical Society*, *400*, 1445-1450. doi: 10.1111/j.1365-2966.2009.15541.x

Kaplan, D. L., & van Kerkwijk, M. H. (2005). A Coherent Timing Solution for the Nearby Isolated Neutron Star RX J1308.6+2127/RBS 1223. *Astrophysical Journal, Letters*, *635*(1), L65-L68. doi: 10.1086/499241

Kaplan, D. L., & van Kerkwijk, M. H. (2009a). Constraining the Spin-down of the Nearby Isolated Neutron Star RX J0806.4-4123, and Implications for the Population of Nearby Neutron Stars. *Astrophysical Journal*, *705*(1), 798-808. doi: 10.1088/0004-637X/705/1/798

Kaplan, D. L., & van Kerkwijk, M. H. (2009b). Constraining the Spin-Down of the Nearby Isolated Neutron Star RX J2143.0+0654. *Astrophysical Journal, Letters*, *692*(1), L62-L66. doi: 10.1088/0004-637X/692/1/L62

Kaplan, D. L., & van Kerkwijk, M. H. (2011). A Coherent Timing Solution for the Nearby, Thermally Emitting Isolated Neutron Star RX J0420.0-5022. *Astrophysical Journal, Letters*, *740*(1), L30. doi: 10.1088/2041-8205/740/1/L30

Kaplan, D. L., van Kerkwijk, M. H., Marshall, H. L., Jacoby, B. A., Kulkarni, S. R., & Frail, D. A. (2003). The Nearby Neutron Star RX J0720.4-3125 from Radio to X-Rays. *Astrophysical Journal*, *590*(2), 1008-1019. doi: 10.1086/375052

Kaspi, V. M., & Beloborodov, A. M. (2017). Magnetars. *Annual Review of Astron and Astrophysis*, *55*(1), 261-301. doi: 10.1146/annurev-astro-081915-023329

Kaspi, V. M., & Kramer, M. (2016). Radio Pulsars: The Neutron Star Population & Fundamental Physics. *arXiv e-prints*, arXiv:1602.07738.

Kaspi, V. M., Manchester, R. N., Siegman, B., Johnston, S., & Lyne, A. G. (1994). On the Spin-down of PSR B1509-58. *Astrophysical Journal, Letters*, *422*, L83. doi: 10.1086/187218

Kaspi, V. M., & McLaughlin, M. A. (2005). Chandra X-Ray Detection of the High Magnetic Field Radio Pulsar PSR J1718-3718. *Astrophysical Journal, Letters*, *618*(1), L41-L44. doi: 10.1086/427628

Keane, E. F., & Kramer, M. (2008). On the birthrates of Galactic neutron stars. *Monthly Notices of the Royal Astronomical Society*, *391*(4), 2009-2016. doi: 10.1111/j.1365-2966.2008.14045.x

Keane, E. F., Kramer, M., Lyne, A. G., Stappers, B. W., & McLaughlin, M. A. (2011). Rotating Radio Transients: new discoveries, timing solutions and musings. *Monthly Notices of the Royal Astronomical Society*, *415*, 3065-3080. doi: 10.1111/j.1365-2966.2011.18917.x

Keane, E. F., McLaughlin, M. A., Kramer, M., Stappers, B. W., Bassa, C. G., Purver, M. B., & Weltevrede, P. (2013). PSR j1840–1419: A VERY COOL NEUTRON STAR. *Astrophysical Journal*, *764*(2), 180. Retrieved from `https://doi.org/10.1088/0004-637X/764/2/180` doi: 10.1088/0004-637x/764/2/180

Koliopanos, F., & Gilfanov, M. (2016). Luminosity-dependent change of the emission diagram in the X-ray pulsar 4U 1626-67. *Monthly Notices of the Royal Astronomical Society*, *456*(4), 3535-3541. Retrieved from `https://doi.org/10.1093/mnras/stv2873` doi: 10.1093/mnras/stv2873

Kouveliotou, C., Dieters, S., Strohmayer, T., van Paradijs, J., Fishman, G. J.,

Meegan, C. A., ... Murakami, T. (1998). An X-ray pulsar with a superstrong magnetic field in the soft γ-ray repeater SGR1806 - 20. *Nature*, *393*(6682), 235-237. doi: 10.1038/30410

Kuiper, L., & Hermsen, W. (2009). High-energy characteristics of the schizophrenic pulsar PSR J1846-0258 in Kes 75. Multi-year RXTE and INTEGRAL observations crossing the magnetar-like outburst. *Astronomy and Astrophysics*, *501*(3), 1031-1046. doi: 10.1051/0004-6361/200811580

Kylafis, N. D., Trümper, J. E., & Ertan, Ü. (2014). Spectral formation in a radiative shock: application to anomalous X-ray pulsars and soft gamma-ray repeaters. *Astronomy and Astrophysics*, *562*, A62. doi: 10.1051/0004-6361/201322303

Lai, D. (2014). Theory of Disk Accretion onto Magnetic Stars. In *European physical journal web of conferences* (Vol. 64, p. 01001). doi: 10.1051/epjconf/20136401001

Lamb, F. K., Pethick, C. J., & Pines, D. (1973). A Model for Compact X-Ray Sources: Accretion by Rotating Magnetic Stars. *Astrophysical Journal*, *184*, 271-290. doi: 10.1086/152325

Levine, A., Ma, C. P., McClintock, J., Rappaport, S., van der Klis, M., & Verbunt, F. (1988). 4U 1626-67: The Binary with the Smallest Known Mass Function. *Astrophysical Journal*, *327*, 732. doi: 10.1086/166230

Lin, D. N. C., Woosley, S. E., & Bodenheimer, P. H. (1991). Formation of a planet orbiting pulsar 1829-10 from the debris of a supernova explosion. *Nature*, *353*(6347), 827-829. doi: 10.1038/353827a0

Livingstone, M. A., Ng, C. Y., Kaspi, V. M., Gavriil, F. P., & Gotthelf, E. V. (2011). Post-outburst Observations of the Magnetically Active Pulsar J1846-0258. A New Braking Index, Increased Timing Noise, and Radiative Recovery. *Astrophysical Journal*, *730*(2), 66. doi: 10.1088/0004-637X/730/2/66

Lorimer, D. R., Faulkner, A. J., Lyne, A. G., Manchester, R. N., Kramer, M., McLaughlin, M. A., ... Crawford, F. (2006). The Parkes Multibeam Pulsar Survey - VI. Discovery and timing of 142 pulsars and a Galactic population analysis. *Monthly Notices of the Royal Astronomical Society*, *372*(2), 777-800. doi: 10.1111/j.1365-2966.2006.10887.x

Lovelace, R. V. E., Romanova, M. M., & Bisnovatyi-Kogan, G. S. (1995). Spin-up/spin-down of magnetized stars with accretion discs and outflows. *Monthly Notices of the Royal Astronomical Society*, *275*(2), 244-254. Retrieved from `https://doi.org/10.1093/mnras/275.2.244` doi: 10.1093/mnras/275.2.244

Lovelace, R. V. E., Romanova, M. M., & Bisnovatyi-Kogan, G. S. (1999). Magnetic propeller outflows. *Astrophysical Journal*, *514*(1), 368–372. Retrieved from `https://doi.org/10.1086\/306945` doi: 10.1086/306945

Lynden-Bell, D., & Boily, C. (1994). Self-Similar Solutions up to Flashpoint in Highly Wound Magnetostatics. *Monthly Notices of the Royal Astronomical Society*, *267*, 146. doi: 10.1093/mnras/267.1.146

Lyne, A. G., Graham-Smith, F., & Stappers, B. (2022). *Pulsar astronomy* (5th edition.. ed.).

Makishima, K., Ohashi, T., Sakao, T., Dotani, T., Inoue, H., Koyama, K., ... Tawara, Y. (1988). Spin-down of the X-ray pulsar GX1 +4 during an extended low state. *Nature*, *333*(6175), 746-748. doi: 10.1038/333746a0

Manchester, R. N., Hobbs, G. B., Teoh, A., & Hobbs, M. (2005). The australia

telescope national facility pulsar catalogue. *Astrophysical Journal*, *129*(4), 1993–2006. Retrieved from https://doi.org/10.1086/428488 doi: 10.1086/428488

Marsden, D., Lingenfelter, R. E., & Rothschild, R. E. (2001). Does Pulsar B1757-24 Have a Fallback Disk? *Astrophysical Journal, Letters*, *547*(1), L45-L48. doi: 10.1086/318881

Marsden, D., Lingenfelter, R. E., Rothschild, R. E., & Higdon, J. C. (2001). Nature versus Nurture: The Origin of Soft Gamma-Ray Repeaters and Anomalous X-Ray Pulsars. *Astrophysical Journal*, *550*(1), 397-409. doi: 10.1086/319701

McLaughlin, M. A., Lyne, A. G., Lorimer, D. R., Kramer, M., Faulkner, A. J., Manchester, R. N., ... O'Brien, J. T. (2006). Transient radio bursts from rotating neutron stars. *Nature*, *439*, 817-820. doi: 10.1038/nature04440

Menou, K., Perna, R., & Hernquist, L. (2001a). Disk-assisted Spin-down of Young Radio Pulsars. *Astrophysical Journal, Letters*, *554*(1), L63-L66. doi: 10.1086/320927

Menou, K., Perna, R., & Hernquist, L. (2001b). Stability and Evolution of Supernova Fallback Disks. *Astrophysical Journal*, *559*(2), 1032-1046. doi: 10.1086/322418

Merloni, A., Predehl, P., Becker, W., Böhringer, H., Boller, T., Brunner, H., ... German eROSITA Consortium, t. (2012). eROSITA Science Book: Mapping the Structure of the Energetic Universe. *arXiv e-prints*, arXiv:1209.3114.

Michel, F. C. (1988). Neutron star disk formation from supernova fall-back and possible observational consequences. *Nature*, *333*(6174), 644-645. doi: 10.1038/333644a0

Michel, F. C., & Dessler, A. J. (1981). Pulsar disk systems. *Astrophysical Journal*, *251*, 654-664. doi: 10.1086/159511

Middleditch, J., Mason, K. O., Nelson, J. E., & White, N. E. (1981). 4U 1626-67 : A prograde spinning X-ray pulsar in A 2500 S binary system. *Astrophysical Journal*, *244*, 1001-1021. doi: 10.1086/158772

Mignani, R. P., Bagnulo, S., De Luca, A., Israel, G. L., Lo Curto, G., Motch, C., ... Zane, S. (2007). Studies of neutron stars at optical/IR wavelengths. *Astrophysics and Space Science*, *308*(1-4), 203-210. doi: 10.1007/s10509-007-9340-z

Mignani, R. P., Vande Putte, D., Cropper, M., Turolla, R., Zane, S., Pellizza, L. J., ... Treves, A. (2013). The birthplace and age of the isolated neutron star RX J1856.5-3754. *Monthly Notices of the Royal Astronomical Society*, *429*(4), 3517-3521. doi: 10.1093/mnras/sts627

Miller, K. A., & Stone, J. M. (1997). Magnetohydrodynamic Simulations of Stellar Magnetosphere-Accretion Disk Interaction. *Astrophysical Journal*, *489*(2), 890-902. doi: 10.1086/304825

Mineshige, S., Nomura, H., Hirose, M., Nomoto, K., & Suzuki, T. (1997). Black Hole Disk Accretion in Supernovae. *Astrophysical Journal*, *489*(1), 227-233. doi: 10.1086/304776

Morii, M., Kawai, N., Kataoka, J., Yatsu, Y., Kobayashi, N., & Terada, H. (2005). Near-infrared, optical, and X-ray observations of the anomalous X-ray pulsar 4U 0142 + 61. *Adv. Space Res.*, *35*(6), 1177-1180. doi: 10.1016/j.asr.2005.04.051

Motch, C., Pires, A. M., Haberl, F., Schwope, A., & Zavlin, V. E. (2009). Proper

motions of thermally emitting isolated neutron stars measured with Chandra. *Astronomy and Astrophysics*, *497*(2), 423-435. doi: 10.1051/0004-6361/200811052

Muno, M. P., Gaensler, B. M., Nechita, A., Miller, J. M., & Slane, P. O. (2008). A Search for New Galactic Magnetars in Archival Chandra and XMM-Newton Observations. *Astrophysical Journal*, *680*(1), 639-653. doi: 10.1086/527316

Nelson, R. W., Bildsten, L., Chakrabarty, D., Finger, M. H., Koh, D. T., Prince, T. A., ... Wilson, R. B. (1997). On the Dramatic Spin-up/Spin-down Torque Reversals in Accreting Pulsars. *Astrophysical Journal, Letters*, *488*(2), L117-L120. doi: 10.1086/310936

Ng, C. Y., Kaspi, V. M., Ho, W. C. G., Weltevrede, P., Bogdanov, S., Shannon, R., & Gonzalez, M. E. (2012). Deep X-Ray Observations of the Young High-magnetic-field Radio Pulsar J1119-6127 and Supernova Remnant G292.2-0.5. *Astrophysical Journal*, *761*(1), 65. doi: 10.1088/0004-637X/761/1/65

Olausen, S. A., & Kaspi, V. M. (2014). The McGill Magnetar Catalog. *ApJs*, *212*, 6. doi: 10.1088/0067-0049/212/1/6

Orlandini, M., Dal Fiume, D., Frontera, F., Del Sordo, S., Piraino, S., Santangelo, A., ... Parmar, A. N. (1998). BEPPOSAX Observation of 4U 1626-67: Discovery of an Absorption Cyclotron Resonance Feature. *Astrophysical Journal, Letters*, *500*(2), L163-L166. doi: 10.1086/311404

Ostriker, E. C., & Shu, F. H. (1995). Magnetocentrifugally Driven Flows from Young Stars and Disks. IV. The Accretion Funnel and Dead Zone. *Astrophysical Journal*, *447*, 813. doi: 10.1086/175920

Özcan, Ş., Gençali, A. A., & Ertan, Ü. (2020). Is PSR J0726-2612 a dim isolated neutron star progenitor? *Monthly Notices of the Royal Astronomical Society*, *498*(1), 674-679. doi: 10.1093/mnras/staa2493

Özsükan, G., Ekşi, K. Y., Hambaryan, V., Neuhäuser, R., Hohle, M. M., Ginski, C., & Werner, K. (2014). The Vela Pulsar with an Active Fallback Disk. *Astrophysical Journal*, *796*(1), 46. doi: 10.1088/0004-637X/796/1/46

Pacini, F. (1967). Energy Emission from a Neutron Star. *Nature*, *216*, 567-568. doi: 10.1038/216567a0

Page, D. (2009). Neutron Star Cooling: I. In W. Becker (Ed.), *Astrophysics and space science library* (Vol. 357, p. 247). doi: 10.1007/978-3-540-76965-1_11

Page, D., Geppert, U., & Weber, F. (2006). The cooling of compact stars. *Nuclear Physics A*, *777*, 497-530. doi: 10.1016/j.nuclphysa.2005.09.019

Page, D., Lattimer, J. M., Prakash, M., & Steiner, A. W. (2009). Neutrino Emission from Cooper Pairs and Minimal Cooling of Neutron Stars. *Astrophysical Journal*, *707*(2), 1131-1140. doi: 10.1088/0004-637X/707/2/1131

Palmer, D. M., Barthelmy, S., Gehrels, N., Kippen, R. M., Cayton, T., Kouveliotou, C., ... Tueller, J. (2005). A giant γ-ray flare from the magnetar SGR 1806 - 20. *Nature*, *434*(7037), 1107-1109. doi: 10.1038/nature03525

Papitto, A., & de Martino, D. (2020). Transitional millisecond pulsars. *arXiv e-prints*, arXiv:2010.09060.

Papitto, A., de Martino, D., Belloni, T. M., Burgay, M., Pellizzoni, A., Possenti, A., & Torres, D. F. (2015). X-ray coherent pulsations during a sub-luminous accretion disc state of the transitional millisecond pulsar XSS J12270-4859. *Monthly Notices of the Royal Astronomical Society*, *449*(1), L26-L30. Retrieved from `https://doi.org/10.1093/mnrasl/slv013` doi: 10.1093/mnrasl/slv013

Papitto, A., Ferrigno, C., Bozzo, E., Rea, N., Pavan, L., Burderi, L., ... Wong, G. F. (2013). Swings between rotation and accretion power in a binary millisecond pulsar. *Nature*, *501*(7468), 517-520. Retrieved from `https://doi.org/10.1038/nature12470` doi: 10.1038/nature12470

Parent, D., Kerr, M., den Hartog, P. R., Baring, M. G., DeCesar, M. E., Espinoza, C. M., ... Smith, D. A. (2011). Observations of Energetic High Magnetic Field Pulsars with the Fermi Large Area Telescope. *Astrophysical Journal*, *743*(2), 170. doi: 10.1088/0004-637X/743/2/170

Parfrey, K., Spitkovsky, A., & Beloborodov, A. M. (2016). Torque Enhancement, Spin Equilibrium, and Jet Power from Disk-Induced Opening of Pulsar Magnetic Fields. *Astrophysical Journal*, *822*(1), 33. doi: 10.3847/0004-637X/822/1/33

Parfrey, K., Spitkovsky, A., & Beloborodov, A. M. (2017). Simulations of the magnetospheres of accreting millisecond pulsars. *Monthly Notices of the Royal Astronomical Society*, *469*(3), 3656-3669. doi: 10.1093/mnras/stx950

Parthasarathy, A., Johnston, S., Shannon, R. M., Lentati, L., Bailes, M., Dai, S., ... Weltevrede, P. (2020). Timing of young radio pulsars - II. Braking indices and their interpretation. *Monthly Notices of the Royal Astronomical Society*, *494*(2), 2012-2026. doi: 10.1093/mnras/staa882

Parthasarathy, A., Shannon, R. M., Johnston, S., Lentati, L., Bailes, M., Dai, S., ... Weltevrede, P. (2019). Timing of young radio pulsars - I. Timing noise, periodic modulation, and proper motion. *Monthly Notices of the Royal Astronomical Society*, *489*(3), 3810-3826. doi: 10.1093/mnras/stz2383

Pavlov, G. G., Kargaltsev, O. Y., Sanwal, D., & Garmire, G. P. (2001). Variability of the Vela Pulsar Wind Nebula Observed with Chandra. *ApJL*, *554*, L189–L192. doi: 10.1086/321721

Perna, R., Bozzo, E., & Stella, L. (2006). On the Spin-up/Spin-down Transitions in Accreting X-Ray Binaries. *Astrophysical Journal*, *639*(1), 363-376. doi: 10.1086/499227

Perna, R., Duffell, P., Cantiello, M., & MacFadyen, A. I. (2014). The Fate of Fallback Matter around Newly Born Compact Objects. *Astrophysical Journal*, *781*(2), 119. doi: 10.1088/0004-637X/781/2/119

Perna, R., Hernquist, L., & Narayan, R. (2000). Emission Spectra of Fallback Disks around Young Neutron Stars. *Astrophysical Journal*, *541*(1), 344-350. doi: 10.1086/309404

Phinney, E. S., & Blandford, R. D. (1981). Analysis of the pulsar P-P-prime distribution. *Monthly Notices of the Royal Astronomical Society*, *194*, 137-148. doi: 10.1093/mnras/194.1.137

Pires, A. M., Schwope, A. D., & Motch, C. (2017). Follow-up of isolated neutron star candidates from the eROSITA survey. *Astronomische Nachrichten*, *338*(213), 213-219. doi: 10.1002/asna.201713333

Popov, S. B. (2023). The Zoo of Isolated Neutron Stars. *Universe*, *9*(6), 273. doi: 10.3390/universe9060273

Popov, S. B., Turolla, R., & Possenti, A. (2006). A tale of two populations: rotating radio transients and X-ray dim isolated neutron stars. *Monthly Notices of the Royal Astronomical Society*, *369*, L23-L26. doi: 10.1111/j.1745-3933.2006.00166.x

Posselt, B., Pavlov, G. G., Ertan, Ü., Çalışkan, S., Luhman, K. L., & Williams,

C. C. (2018). Discovery of extended infrared emission around the neutron star RXJ0806.4–4123. *Astrophysical Journal*, *865*(1), 1. Retrieved from `https://doi.org/10.3847/1538-4357/aad6df` doi: 10.3847/1538-4357/aad6df

Potekhin, A. Y., & Chabrier, G. (2018). Magnetic neutron star cooling and microphysics. *Astronomy and Astrophysics*, *609*, A74. doi: 10.1051/0004-6361/201731866

Potekhin, A. Y., Zyuzin, D. A., Yakovlev, D. G., Beznogov, M. V., & Shibanov, Y. A. (2020). Thermal luminosities of cooling neutron stars. *Monthly Notices of the Royal Astronomical Society*, *496*(4), 5052-5071. doi: 10.1093/mnras/staa1871

Predehl, P., Andritschke, R., Arefiev, V., Babyshkin, V., Batanov, O., Becker, W., ... Granato, S. (2020). The eROSITA X-ray telescope on SRG. *arXiv e-prints*, arXiv:2010.03477.

Pringle, J. E., & Rees, M. J. (1972). Accretion Disc Models for Compact X-Ray Sources. *Astronomy and Astrophysics*, *21*, 1.

Qiao, G. J., Xue, Y. Q., Xu, R. X., Wang, H. G., & Xiao, B. W. (2003). An accretion disk model for periodic timing variations of pulsars. *Astronomy and Astrophysics*, *407*, L25-L28. doi: 10.1051/0004-6361:20031055

Rappaport, S., Markert, T., Li, F. K., Clark, G. W., Jernigan, J. G., & McClintock, J. E. (1977). Discovery of a 7.68 second X-ray periodicity in 3U 1626-67. *Astrophysical Journal, Letters*, *217*, L29-L33. doi: 10.1086/182532

Rea, N., Coti Zelati, F., Dehman, C., Hurley-Walker, N., de Martino, D., Bahramian, A., ... Galvin, T. J. (2022). Constraining the Nature of the 18 min Periodic Radio Transient GLEAM-X J162759.5-523504.3 via Multiwavelength Observations and Magneto-thermal Simulations. *Astrophysical Journal*, *940*(1), 72. doi: 10.3847/1538-4357/ac97ea

Rea, N., & McLaughlin, M. (2008). Rotating radio transients: multiwavelength observations. *AIP Conference Proceedings*, *968*(1), 151-158. Retrieved from `https://aip.scitation.org/doi/abs/10.1063/1.2840387` doi: 10.1063/1.2840387

Rea, N., McLaughlin, M. A., Gaensler, B. M., Slane, P. O., Stella, L., Reynolds, S. P., ... Chatterjee, S. (2009). Discovery of Extended X-Ray Emission Around the Highly Magnetic RRAT J1819-1458. *Astrophysical Journal, Letters*, *703*(1), L41-L45. doi: 10.1088/0004-637X/703/1/L41

Rea, N., Torres, M. A. P., Jonker, P. G., Mignani, R. P., Zane, S., Burgay, M., ... Steeghs, D. (2007). Accurate X-ray position and multiwavelength observations of the isolated neutron star RBS1774. *Monthly Notices of the Royal Astronomical Society*, *379*(4), 1484-1490. doi: 10.1111/j.1365-2966.2007.12029.x

Ronchi, M., Rea, N., Graber, V., & Hurley-Walker, N. (2022). Long-period Pulsars as Possible Outcomes of Supernova Fallback Accretion. *Astrophysical Journal*, *934*(2), 184. doi: 10.3847/1538-4357/ac7cec

Rozwadowska, K., Vissani, F., & Cappellaro, E. (2021). On the rate of core collapse supernovae in the milky way. *New Astronomy*, *83*, 101498. doi: 10.1016/j.newast.2020.101498

Schulz, N. S., Chakrabarty, D., Marshall, H. L., Canizares, C. R., Lee, J. C., & Houck, J. (2001). Double-peaked X-Ray Lines from the Oxygen/Neon-rich Accretion Disk in 4U 1626-67. *Astrophysical Journal*, *563*(2), 941-949. doi: 10.1086/323988

Schwope, A. D., Schwarz, R., & Greiner, J. (1999). Zeeman lines and a single cyclotron line in the low-accretion rate polar 1RXS J012851.9-233931 (RBS0206). *Astronomy and Astrophysics*, *348*, 861-867. doi: 10.48550/arXiv.astro-ph/9905392

Shakura, N. I., & Sunyaev, R. A. (1973). Black holes in binary systems. Observational appearance. *Astronomy and Astrophysics*, *24*, 337-355.

Takagi, T., Mihara, T., Sugizaki, M., Makishima, K., & Morii, M. (2016). Application of the Ghosh & Lamb relation to the spin-up/down behavior in the X-ray binary pulsar 4U 1626-67. *Publications of the ASJ*, *68*(SP1). Retrieved from `https://doi.org/10.1093/pasj/psw010` (S13) doi: 10.1093/pasj/psw010

Tam, C. R., Kaspi, V. M., van Kerkwijk, M. H., & Durant, M. (2004). Correlated Infrared and X-Ray Flux Changes Following the 2002 June Outburst of the Anomalous X-Ray Pulsar 1E 2259+586. *Astrophysical Journal, Letters*, *617*(1), L53-L56. doi: 10.1086/426963

Taylor, G. B., Stovall, K., McCrackan, M., McLaughlin, M. A., Miller, R., Karako-Argaman, C., ... Schinzel, F. K. (2016). Observations of Rotating Radio Transients with the First Station of the Long Wavelength Array. *Astrophysical Journal*, *831*, 140. doi: 10.3847/0004-637X/831/2/140

Tetzlaff, N., Neuhäuser, R., Hohle, M. M., & Maciejewski, G. (2010). Identifying birth places of young isolated neutron stars. *Monthly Notices of the Royal Astronomical Society*, *402*(4), 2369-2387. doi: 10.1111/j.1365-2966.2009.16093.x

Thompson, C., & Duncan, R. C. (1995). The soft gamma repeaters as very strongly magnetized neutron stars - I. Radiative mechanism for outbursts. *Monthly Notices of the Royal Astronomical Society*, *275*(2), 255-300. doi: 10.1093/mnras/275.2.255

Tiengo, A., & Mereghetti, S. (2007). XMM-Newton Discovery of 7 s Pulsations in the Isolated Neutron Star RX J1856.5-3754. *Astrophysical Journal, Letters*, *657*(2), L101-L104. doi: 10.1086/513143

Tong, H. (2022). Discussions on the nature of GLEAM-X J162759.5-523504.3. *arXiv e-prints*, arXiv:2204.01957.

Trümper, J. E., Dennerl, K., Kylafis, N. D., Ertan, Ü., & Zezas, A. (2013). An Accretion Model for the Anomalous X-Ray Pulsar 4U 0142+61. *Astrophysical Journal*, *764*, 49. doi: 10.1088/0004-637X/764/1/49

Trümper, J. E., Zezas, A., Ertan, Ü., & Kylafis, N. D. (2010). The energy spectrum of anomalous X-ray pulsars and soft gamma-ray repeaters. *Astronomy and Astrophysics*, *518*, A46. doi: 10.1051/0004-6361/200911834

Türkoğlu, M. M., Özsükan, G., Erkut, M. H., & Ekşi, K. Y. (2017). Constraints on the disc–magnetosphere interaction in accreting pulsar 4U 1626-67. *Monthly Notices of the Royal Astronomical Society*, *471*(1), 422-430. Retrieved from `https://doi.org/10.1093/mnras/stx1593` doi: 10.1093/mnras/stx1593

Turolla, R. (2009). Isolated Neutron Stars: The Challenge of Simplicity. In W. Becker (Ed.), *Astrophysics and space science library* (Vol. 357, p. 141). doi: 10.1007/978-3-540-76965-1_7

Ustyugova, G. V., Koldoba, A. V., Romanova, M. M., & Lovelace, R. V. E. (2006). "Propeller" Regime of Disk Accretion to Rapidly Rotating Stars. *Astrophysical Journal*, *646*(1), 304-318. doi: 10.1086/503379

Uzdensky, D. A. (2002). Partial Field Opening and Current Sheet Formation

in the Disk Magnetosphere. *Astrophysical Journal*, *572*(1), 432-444. doi: 10.1086/340308

van Ballegooijen, A. A. (1994). Magnetic fine structures in coronal loops. *Space Sci. Rev.*, *70*(1-2), 31-35. doi: 10.1007/BF00777838

van Kerkwijk, M. H., Chakrabarty, D., Pringle, J. E., & Wijers, R. A. M. J. (1998). Warped Disks as a Possible Origin of Torque Reversals in Accretion-powered Pulsars. *Astrophysical Journal, Letters*, *499*(1), L27-L30. doi: 10.1086/311346

van Kerkwijk, M. H., & Kaplan, D. L. (2008). Timing the Nearby Isolated Neutron Star RX J1856.5-3754. *Astrophysical Journal, Letters*, *673*(2), L163. doi: 10.1086/528796

Vaughan, B. A., & Kitamoto, S. (1997). Correlation Between Luminosity and Accretion Torque in 4U 1626-67 and GX 301-2. *arXiv e-prints*, astro-ph/9707105.

Viganò, D., Rea, N., Pons, J. A., Perna, R., Aguilera, D. N., & Miralles, J. A. (2013). Unifying the observational diversity of isolated neutron stars via magneto-thermal evolution models. *Monthly Notices of the Royal Astronomical Society*, *434*(1), 123-141. doi: 10.1093/mnras/stt1008

Vivekanand, M., & Narayan, R. (1981). A new look at pulsar statistics - Birthrate and evidence for injection. *Journal of Astrophysics and Astronomy*, *2*, 315-337. doi: 10.1007/BF02714556

Vranesevic, N., Manchester, R. N., Lorimer, D. R., Hobbs, G. B., Lyne, A. G., Kramer, M., ... McLaughlin, M. A. (2004). Pulsar Birthrates from the Parkes Multibeam Survey. *Astrophysical Journal, Letters*, *617*(2), L139-L142. doi: 10.1086/427208

Wang, Y. M. (1987). Disc accretion by magnetized neutron stars : a reassessment of the torque. *Astronomy and Astrophysics*, *183*, 257-264.

Wang, Z., Chakrabarty, D., & Kaplan, D. L. (2006). A debris disk around an isolated young neutron star. *Nature*, *440*(7085), 772-775. doi: 10.1038/nature04669

Weltevrede, P., Johnston, S., & Espinoza, C. M. (2011). The glitch-induced identity changes of PSR J1119-6127. *Monthly Notices of the Royal Astronomical Society*, *411*(3), 1917-1934. doi: 10.1111/j.1365-2966.2010.17821.x

Wijers, R. A. M. J., & Pringle, J. E. (1999). Warped accretion discs and the long periods in X-ray binaries. *Monthly Notices of the Royal Astronomical Society*, *308*(1), 207-220. Retrieved from `https://doi.org/10.1046/j.1365-8711.1999.02720.x` doi: 10.1046/j.1365-8711.1999.02720.x

Woosley, S. E., Heger, A., & Weaver, T. A. (2002). The evolution and explosion of massive stars. *Reviews of Modern Physics*, *74*(4), 1015-1071. doi: 10.1103/RevModPhys.74.1015

Yan, T., Perna, R., & Soria, R. (2012). The influence of fallback discs on the spectral and timing properties of neutron stars. *Monthly Notices of the Royal Astronomical Society*, *423*(3), 2451-2463. doi: 10.1111/j.1365-2966.2012.21051.x

Yi, I., & Vishniac, E. T. (1999). Spectral Transition and Torque Reversal in X-Ray Pulsar 4U 1626-67. *Astrophysical Journal, Letters*, *516*(2), L87-L90. doi: 10.1086/311997

Yi, I., Wheeler, J. C., & Vishniac, E. T. (1997). Torque Reversal in Accretion-powered X-Ray Pulsars. *Astrophysical Journal, Letters*, *481*(1), L51-L54. doi: 10.1086/310639

Zel'dovich, Y. B., Ivanova, L. N., & Nadezhin, D. K. (1972). Nonstationary Hydrodynamical Accretion onto a Neutron Star. *Soviet Ast.*, *16*, 209.

Zezas, A., Trümper, J. E., & Kylafis, N. D. (2015). Broad-band X-ray spectra of anomalous X-ray pulsars and soft γ-ray repeaters: pulsars in a weak-accretion regime? *Monthly Notices of the Royal Astronomical Society*, *454*(4), 3366-3375. doi: 10.1093/mnras/stv1918